DEREGULATION OF SELECTIVE AUTOPHAGY & SIRTUIN 3 EXPRESSION IN LUNG AGING AND PULMONARY FIBROSIS

AN ABSTRACT

SUBMITTED ON THE TWENTY-FIRST DAY OF MARCH 2016

TO THE DEPARTMENT OF MEDICINE

IN PARTIAL FULFILLMENT OF THE REQUIREMENTS

OF THE GRADUATE SCHOOL

OF TULANE UNIVERSITY

FOR THE DEGREE OF DOCTOR

OF

PHILOSOPHY BY

MEREDITH L. SOSULSKI

APPROVED:

Cecilia G. Sanchez, Ph.D.
Director

Joseph Lasky, M.D.

Deborah Sullivan, Ph.D.

Gilbert Morris, Ph.D.

Erik Flemington, Ph.D.

ABSTRACT

Accumulation of intracellular damage by reactive oxygen species accelerates biological aging, leading to the development of age-related lung diseases such as idiopathic pulmonary fibrosis (IPF). Mitochondrial dysfunction and mitochondria-related oxidative stress has been implicated in the pathogenesis of many age-related diseases. Selective autophagic degradation of mitochondria (mitophagy) is critical to maintain a proper pool of the organelle and preserve cellular energy homeostasis. Oxidative stress resulting from age-dependent defects in the quality of proteins and degradation of mitochondria promotes alveolar epithelial cell damage potentiating lung injury. Our research found diminished autophagy corresponding with elevated levels of oxidized proteins and lipofuscin in response to lung injury in old and middle-aged mice compared to younger animals. More importantly, older mice exposed to lung injury are characterized by deficient mitophagic responses. The pro-fibrotic cytokine transforming growth factor beta 1 (TGFβ1) plays a pivotal role in driving fibroblast-to-myofibroblast differentiation (FMD), an important feature of pulmonary fibrosis. TGFβ1-mediated FMD is characterized by reduced autophagy flux, altered mitophagy and defects in mitochondrial function. In accordance, PINK1 expression is reduced in the aging murine lung and biopsies from IPF patients compared to controls.

Our research also revealed a decline in mitochondrial protein deacetylase sirtuin 3 (SIRT3) expression in the lungs of aging mice. Low levels of SIRT3 transcripts were

observed in two different animal models of pulmonary fibrosis. SIRT3 expression was reduced in fibrotic regions of lung tissues from patients with fibrotic diseases. We demonstrated that down-regulation of SIRT3 by TGFβ1 promotes acetylation of major oxidative stress response regulators, such as superoxide dismutase 2 (SOD2) and isocitrate dehydrogenase 2 (IDH2), and that resveratrol induced SIRT3 expression and ameliorated acetylation changes induced by TGFβ1. Knockdown of SIRT3 expression by siRNA exacerbated TGFβ1-induced FMD. By contrast, promotion of SIRT3 expression attenuated the effect of TGFβ1 on myofibroblast differentiation. Finally, SIRT3-deficient mice were more susceptible to pulmonary fibrosis in response to bleomycin and had increased collagen deposition compared to control mice. Collectively, our research indicates that an age-related decline in autophagy, SIRT3 expression, and mitochondrial homeostasis may contribute to the promotion and/or perpetuation of pulmonary fibrosis.

DEREGULATION OF SELECTIVE AUTOPHAGY & SIRTUIN 3 EXPRESSION IN LUNG AGING AND PULMONARY FIBROSIS

A DISSERTATION

SUBMITTED ON THE TWENTY-FIRST DAY OF MARCH 2016

TO THE DEPARTMENT OF MEDICINE

IN PARTIAL FULFILLMENT OF THE REQUIREMENTS

OF THE GRADUATE SCHOOL

OF TULANE UNIVERSITY

FOR THE DEGREE OF DOCTOR

OF

PHILOSOPHY BY

MEREDITH L. SOSULSKI

APPROVED:

Cecilia G. Sanchez, Ph.D.
Director

Joseph Lasky, M.D.

Deborah Sullivan, Ph.D.

Gilbert Morris, Ph.D.

Erik Flemington, Ph.D.

This dissertation is dedicated to my parents Richard and Elizabeth Sosulski.

ACKNOWLEDGMENTS

I would like to first and foremost thank my advisor and mentor, Cecilia Sanchez. I am extremely grateful for your constant support, patience, and guidance throughout my time at Tulane. You have been a great advisor and your passion for science has always inspired me. I am thankful to have had the opportunity to study research in your lab as I know you were committed to giving me the best education I could receive which I know will be quite valuable wherever I end up. Without you, this dissertation would not have been possible.

To my committee members Dr. Joseph Lasky, Dr. Deborah Sullivan, Dr. Gilbert Morris and Dr. Erik Flemington: thank you all for serving on my committee. All the encouragement and guidance has been invaluable during the development of my thesis.

I would like to thank all the past and present members of the laboratory group: Dr. Mark Sides, Dr. Fayong (Frank) Luo, Svitlana Danchuk, Chunmin Dong, Dr. Beibei Xu, Yan Zhuang, Dr. Qinyan Yin, Rafael Gongora, and Brian Deskin. I extend my deepest gratitude for your patience and friendship. I would also like to thank Miriam Ruiz for her help and support.

I want to send out special thanks to my family, Mom, Dad, Dara, Amanda, Lauren, and Rick for their continued support and love throughout my life. I would like to thank my friends in New Orleans, Monica, Nicki, Erin, Doug, Mallory, and Dan.

Last but not least, I would like to thank the Liverpool supporters crew at Finns for taking me in and for your continued friendship. YNWA.

TABLE OF CONTENTS

LIST OF TABLES

LIST OF FIGURES

CHAPTER 1. INTRODUCTION

1.1 Idiopathic Pulmonary Fibrosis

Idiopathic pulmonary fibrosis (IPF) is an interstitial lung disease in which normal lung architecture and function is compromised by excessive collagen deposition ultimately resulting in respiratory failure[1-5]. A confident histological pattern of usual interstitial pneumonia (UIP) and reticular pattern on high-resolution computed tomography are most often used to diagnose IPF. The characteristic pathological features of IPF occur in a consistent manner with fibrosis initially located along the lower, posterior and subpleural portions of the lungs progressing over time continually reducing the area of functional lung tissue[5-7]. Symptoms of IPF, which include slowly progressive dyspnea, consistent dry hacking cough, and finger clubbing, usually present in patients 50-70 years of age and typically result in mortality[1-4, 6]. This disease primarily affects individuals of middle-age or older commonly with a history of cigarette smoking and men at a rate more often than women[6]. Common comorbidities of IPF include gastroesophageal reflux disease, obstructive sleep apnea and depression worsening the quality of life for most affected persons[5, 6].

Due to variability in diagnostic criteria, most recent studies in the USA have estimated IPF has an incidence and prevalence of 16.3 and 42.7 cases per 100,000 persons respectively, making this disease the most common form of the idiopathic interstitial pneumonias[5, 6, 8-10]. Additionally, with an aging population the incidence of

IPF is predicted to double in the USA between 2005 and 2030[11]. IPF is a highly progressive and lethal disease with a median survival time of 3 years from diagnosis and a 5-year survival rate that is worse than most forms of cancer[1-4, 6]. Recently, two compounds, pirfenidone and nintedanib, have been FDA-approved for the treatment of IPF. Both pirfenidone, an anti-fibrotic and anti-inflammatory compound, and nintedanib, an inhibitor of multiple tyrosine kinase pathways involved in the pathogenesis of IPF, have been effective in reducing the decline in lung function in patients with IPF[6, 12-14]. Even so, continuing research is necessary to find a real cure for this devastating disease.

1.2 Aging & Other Risk Factors in IPF

An abnormal and sustained wound healing process following an injury to the alveolar epithelium of the lung is believed to be the underlying cause of idiopathic pulmonary fibrosis[5, 6, 15]. Wound repair processes are driven by myofibroblasts that accumulate at the site of injury and produce excessive amounts of collagen and other extracellular matrix (ECM) components[6]. Although myofibroblasts may be derived from multiple cell types including circulating fibrocytes, endothelial cells, and epithelial cells, resident fibroblasts are responsible for most differentiated myofibroblasts in pulmonary fibrosis[16]. Indeed, for IPF patients two important prognostic factors are the abundance of myofibroblasts and the extent of collagen deposition demonstrating the importance of understanding myofibroblast differentiation in the development of novel therapeutic approaches which ultimately prevent pulmonary fibrosis.

Despite the fact that the cause of IPF remains unknown, aging is the predominant factor as evidenced by the fact that IPF rarely affects persons under 50 years of age. Aging is a complex process accompanied by a number of molecular modifications including net shortening of telomeres, accumulation of oxidative stress, epigenetic changes, mitochondrial dysfunction and weakened immune responses[2]. As the lung is a unique organ under a constant barrage of insults from the environment, the accumulation of environmental stressors over time may cause the chronic epithelial injury underlying this disease. Several identified risk factors discussed below may only contribute to the development of fibrosis insomuch as natural aging alterations may induce susceptibility to damage and deficient mechanisms to cope with stress[2, 6].

For instance, genetic studies in familial forms of IPF, estimated to account for 10% of cases, have identified mutations in two main processes: telomere maintenance and surfactant homeostasis[17]. Consistent with the observation that IPF patients have shortened telomeres, mutations identified in telomere maintenance genes, *TERT*, *TERC*, *DKC1*, *TINF2*, *RTEL1*, and *PARN*, all contribute to the shortening of telomeres[5, 17, 18]. Similarly, patients with dyskeratosis congenita, a premature aging disease, also develop pulmonary fibrosis suggesting mutations in age-related genes may predispose persons to IPF[5].

Aging also increases susceptibility to and accumulation of endoplasmic reticulum (ER) stress[19]. Mutations in *SFTPA1, SFTPA2*, *SFTPC*, *SFTPD,* and *ABCA3* genes, which all disrupt surfactant processing & trafficking have also been shown to induce endoplasmic reticulum (ER) stress in the lung[5, 17]. In response to ER stress, the cell initiates the process of the unfolded protein response (UPR) to reduce the imbalance

between cellular demand and protein synthesis. Alveolar type II cells from IPF patients have been reported to have elevated levels of UPR markers. Additionally, activation of the UPR may drive cells to undergo epithelial-to-mesenchymal transition (EMT) furthering pro-fibrotic cellular mechanisms. This finding correlates with mouse models of fibrosis which found that chronic activation of the UPR promotes the epithelium to respond to injury in a pro-fibrotic phenotype[5].

Other risk factors such as smoking and environmental exposures may be linked with IPF due to their chronic irritation over time[2]. A history of cigarette smoking is a strongly correlated factor for patients who may develop pulmonary fibrosis, with an even higher risk associated for smokers with a history of 21-40 pack-years[2, 6]. In terms of environmental or occupational agents, epidemiologic studies have found exposures to metal and wood dust particularly associated with IPF[5, 6]. Cigarette smoke and other exogenous factors have been proven to increase MUC5B expression, a gel-forming mucin associated with clearance in the lung and improved macrophage function[17]. Similarly, genome-wide studies identified a minor allele in the promoter of *MUC5B* associated with increased expression correlated with incidence of IPF, although carriage is correlated with slower progression and better prognosis[6, 18]. Indeed, IPF patients have greatly increased expression of MUC5B compared to controls assumed as an attempt to improve mucociliary transport[17]. However, it has been hypothesized that the abundance of MUC5B levels may lead to impaired clearance of inhaled particles or micro-organisms over time resulting in an overall deficient mucosal host defense[18, 20, 21]. During aging, this susceptibility of an impaired immune response may be exploited upon injury.

Lastly, viral infections have been identified as a risk factor for the development of pulmonary fibrosis. IPF, in particular, been linked to the infection of human herpes viruses (HHV) including cytomegalovirus (CMV), herpes simplex virus type 1 (HSV-1) and most notably Epstein-Barr virus (EBV)[2, 6, 22, 23]. A recent study found evidence of a previous infection with at least one HHV in 32 of 33 patients with IPF compared to previous infection in only 9 of 25 controls[24]. Recent studies have shown HHV infection to induce ER stress and increase the expression of transforming growth factor beta 1 (TGFβ1) in alveolar cells potentially prompting epithelial injury and myofibroblast differentiation[23, 25]. Additionally, chronic reactivation of HHV in elderly patients has been detected suggesting that viral control by aged immune systems is lacking at best[26]. Still, mechanisms for how viruses contribute to the development of fibrosis are only just becoming understood and require further investigation. Overall, it is likely that the decline of an individual's immune system during aging leaves the lung particularly susceptible to viral-induced fibrosis.

1.3 Animal Models of Pulmonary Fibrosis

In order to understand molecular mechanisms involved in the pathogenesis of pulmonary fibrosis, a number of experimental rodent models have been employed in the literature. Commonly used models include exposures to asbestos, silica, irradiation, bleomycin and viral vector expression of TGFβ1 to induce lung injury[27, 28]. Here we will discuss the use of bleomycin and adenovirus-TGFβ1 overexpression in more detail.

Bleomycin is a chemotherapeutic agent widely used for experimentally induced pulmonary fibrosis models[27, 29]. To induce pulmonary fibrosis, bleomycin has been delivered either directly into the airway by intranasal, intratracheal or oropharyngeal aspiration routes or systemically by intravenous, subcutaneous or intraperitoneal injection[27, 28]. Regardless the route of administration, bleomycin results in direct DNA strand breakage as well as oxidative stress to cause lung damage. Additionally, the lung is more prone to bleomycin-induced toxicity due to naturally low expression of its inactivating enzyme bleomycin hydrolase[27, 28]. Most frequently, a single instillation of bleomycin in the U/kg range is given directly into the airway before sacrificing animals two or four weeks following the exposure. Recently, detailed time-course studies of bleomycin-induced lung fibrosis have shown an inflammatory phase (< 7 days) after administration followed by an active fibrotic phase (7-14 days) and a late fibrosis phase (21-35 days) post exposure[28, 30]. Previous studies have shown the most suitable time point for assessing lung fibrosis was 14 days after bleomycin exposure. This time point ensures diffuse fibrosis with less variability or mortality when compared to a time point at 21 days after exposure[29]. Coinciding with this time point, peak gene expression changes were detected in response to bleomycin during the active fibrosis phase (14 days). These changes were also significantly induced in expression profiles from patients with aggressive IPF demonstrating the relevance of this model[30]. Additionally, histopathological changes that occur in response to bleomycin are similar to those in patients with IPF[27]. Still, bleomycin-induced lung fibrosis resolves in mice by six weeks, limiting the usefulness of this model[28]. However, recent studies have shown that older mice had higher levels of TGFβ1 pathway activation and show worse fibrosis after

bleomycin-induced lung injury[31]. Older mice also had increased recruitment and retention of fibrocytes which may prohibit the resolution of fibrosis suggesting that aging mice display a pathology more representative of the human disease[31, 32]. Overall, the use of the bleomycin-induced lung injury model has been essential in elucidating molecular mechanisms in pulmonary fibrosis.

Another method for the study of fibrosis is the use of adenovirus vectors to express inflammatory or fibrotic cytokines. Previous studies have employed adenoviral vectors expressing tumor necrosis factor alpha (TNFα), interleukin-1 beta (IL-1β), or TGFβ1[27, 28, 33]. Although, the most commonly studied model is overexpression of pro-fibrotic cytokine TGFβ1 by non-replicating adenovirus vector, which is typically administered in a single instillation directly to the airways to ensure damage to the lung. Assessment of the adenovirus-TGFβ1 (AdTGFβ1)-induced damage proved that infection with 10^8 & 10^9 plaque-forming units (PFU) was effective in causing severe fibrosis for studies, although this fibrosis mostly resolved by 28 days. Histochemical analysis found expression of AdTGFβ1 to be localized predominantly along the epithelium of both the bronchiolar and alveolar regions of the lung with elevated levels of active TGFβ1 between 3 and 10 days, ultimately peaking 7 days after administration[27, 33]. Time-course studies have also shown an initial inflammatory phase (up to 7 days) followed by a fibrotic phase with maximal collagen concentrations at 14 days post infection in response to AdTGFβ1-induced lung injury[27, 28, 33]. Changes in soluble mediators and epithelial cell senescence that occurs in response to AdTGFβ1 are consistent with those which occur in IPF patients[27]. Overall, use of this model has been effective in elucidating downstream signaling pathways involved in pulmonary fibrosis.

1.4 TGFβ1 Signaling and Propagation of Pulmonary Fibrosis

A key pathological feature of IPF is the formation of fibroblastic foci formed by local TGFβ1 expression that drives resident fibroblasts to undergo fibroblast-to-myofibroblast differentiation (FMD)[3, 31, 32, 34, 35]. Under normal tissue healing circumstances, activation of myofibroblasts initiates the synthesis of extracellular matrix (ECM) proteins such as collagen and alpha-smooth muscle actin (α-SMA) resulting in increased contractibility necessary for wound closure. However, failure of these responses to terminate results in excessive connective tissue deposition, proliferation of myofibroblasts, and stiff scar tissue which fails to function like normal organ tissue[36-38].

Although three isoforms of TGFβ (TGFβ1, TGFβ2, and TGFβ3) exist in mammals, TGFβ1 is most frequently associated with pulmonary fibrosis. In the lung, TGFβ1 is produced by a variety of cell types including fibroblasts, neutrophils, alveolar macrophages, and myofibroblasts[39]. During normal homeostatic conditions, secreted TGFβ1 is kept in an inactivated form by latency-associated peptides (LAPs) and latent TGFβ-binding proteins (LTBPs) in the ECM[39, 40]. However, during wound healing TGFβ1 is activated by proteolytic cleavage and released from LAPs permitting engagement with its receptors. Importantly, release of TGFβ1 from its large latent complex can occur by a myriad of mediators including changes in pH, reactive oxygen species (ROS), matrix metalloproteinases MMP9 or MMP2, and binding of integrins under mechanical stress[39, 40]. Once freed, TGFβ1 signaling proceeds through the interaction of a TGFβ1 homodimer with pairs of type I and type II receptors resulting in phosphorylation of the type I receptor.

In canonical TGFβ1 signaling, this activated receptor complex then phosphorylates regulatory Smads, Smad2 or Smad3, which then interact and complex with co-activator Smad4 in order to enter the nucleus and initiate gene transcription via interaction with p300 and Creb-binding-protein (CBP)[37, 39, 40]. These genes targeted by TGFβ1 signaling include connective tissue growth factor (CTGF), fibronectin EDA (FnEDA), α-SMA and collagen type I (Col1) as well as other pro-fibrotic cytokines such as platelet-derived growth factor (PDGF) and epidermal growth factor (EGF) furthering the fibrotic response[36, 39].

TGFβ1 signaling can also proceed via non-cononical pathways including various branches of MAP kinases, Rho-like GTPase signaling and phosphatidylinositol-3-kinase (PI3K)/AKT pathways[41]. Focusing on the role of the PI3K/AKT pathway, TGFβ1 can activate this pathway through its phosphorylation of Akt independent of Smad2/3 activation. The activated PI3K/Akt can then initiate multiple downstream effectors including mammalian target of rapamycin (mTOR) which acts as a nutrient sensor and is a key regulator of protein synthesis through phosphorylation of S6 kinase (S6K)[41]. Interestingly, activation of the PI3K/AKT pathway has also been implicated in the induction of EMT and FMD contributing to excessive myofibroblast formation[41]. However, PI3K/AKT signaling can also modulate and antagonize TGFβ1 signaling through the sequestration of Smad3 by Akt in the cytoplasm demonstrating the complex intertwining of these two pathways in mediating myofibroblast activation.

Similarly, it is important to note that TGFβ1-mediated myofibroblast differentiation lays the foundation for the formation of stiff scar tissue and that this increased matrix stiffening induces the activation of latent TGFβ1 thus initiating a pro-fibrotic feedback loop. Indeed, fibroblasts cultured on stiff ECM matrices produce more α-SMA suggesting

a phenotypic shift to a more myofibroblast-like cell type typical of IPF fibroblasts[5, 38]. Interestingly, in the model organism, *Caenorhabditis elegans* (*C. elegans*), the TGFβ pathway has been shown to reduce longevity by its upregulation of insulin/IGF1 signaling (IIS) pathway highlighting its role in accelerated aging diseases[42]. Lastly, it is highly significant that the expression of TGFβ1 is known to increase with aging which may drive fibrotic mechanisms in the lung as well as further explain the susceptibility of older individuals to the development of IPF.

1.5 Autophagy

Autophagy is an intracellular degradation and recycling process that is evolutionarily conserved. The process of autophagy is activated in response to nutrient deprivation, ER stress, and cellular damage and has been shown to be essential for cellular stress recognition, survival and longevity[43-45].

Autophagy generally refers to three pathways of lysosomal degradation: macroautophagy, microautophagy and chaperone-mediated autophagy. Our focus is primarily on macroautophagy so we will quickly discuss the two other pathways. Briefly, microautophagy occurs in a typically non-selective process through random invagination of the lysosomal membrane. Cytoplasmic material enclosed is then degraded by the resident hydrolases in the vesicle[46]. Chaperone-mediated autophagy (CMA) occurs independent of vesicles via direct delivery of single proteins to the lysosome for degradation. In the cytosol, proteins containing a KFERQ motif are recognized by chaperones, most often heat shock cognate protein of 70 kDa (hsc70), and delivered to

the lysosome. The protein-chaperone complex then binds to the specific lysosomal receptor LAMP-2A whereupon the protein is unfolded and translocated into the lysosome for subsequent degradation[46].

Macroautophagy (from here on simply referred to as autophagy) is the process in which cargo, that can be made up of damaged proteins, aggregates or organelles, is isolated in double membrane vesicles known as autophagosomes prior to fusion of these vesicles with lysosomes. More than 30 genes have been identified that participate in autophagy which is typically described in four steps: initiation, elongation, completion and cargo degradation. Autophagy is executed during initiation with the formation of the nucleation complex which gives rise to the limiting membrane of the autophagosome. The limiting membrane may come from a variety of sources including the plasma membrane, ER, Golgi or mitochondria. Elongation of the membrane proceeds through two ubiquitin-like conjugation systems, both regulated by autophagy related 7 (Atg7), in order to develop the autophagosome: formation of the Atg5-12 complex and conversion of microtubule-associated protein 1 light chain 3 (LC3) to phosphotidylethanolamine. LC3 acts as a site to which selective adaptor proteins, such as sequestosome 1 (p62/SQSTM1), can bind for specific cargo degradation. Additionally, the lipidation of LC3 contributes to the completion of the autophagosome. The sealed autophagosome then fuses with a lysosome whereupon acidification of the vesicle take place via the infusion of hydrolases resulting in complete cargo degradation[46, 47]. Multiple signaling mechanisms keep autophagy in check, of which the best characterized is mTOR, the nutrient sensor complex which negatively regulates autophagy at the initiation step.

Due to the fact that autophagy is a dynamic process, multiple markers or methods are required to properly monitor autophagic progress[47]. Here we will discuss some commonly employed approaches including immunoblotting for autophagy markers, electron microscopy and fluorescence microscopy to measure autophagy or autophagic flux (actual degradation activity). Firstly, the most frequently studied marker for autophagy is LC3. The lipidation of LC3-I to LC3-II is easily measured by western blotting (WB) and trends in autophagy can be observed, such as a lack of LC3-II suggesting inhibition of complete autophagosome formation. However, in order to measure autophagy flux, an inhibitor of autophagosome-lysosome fusion such as chloroquine (CQ) must be employed to properly assess the degradation of autophagosomes[47]. Similarly, the accumulation of the marker p62/SQSTM1 by WB analysis must be observed in the presence of lysosome inhibitors to conclusively indicate reduced autophagy. Electron microscopy, the method by which autophagy was first detected, can also be used to identify autophagosomes by their unique double membraned appearance[47]. Lastly, immunofluorescence microscopy for the detection of LC3 may be used to monitor autophagy by the quantification of punctae staining. Additionally, detection of other proteins of interest may be used in conjunction to determine whether or not they can be targeted by autophagy observed by colocalization with LC3 punctae[47].

Within the lung, autophagy may be useful in combating ROS, epithelium ER stress and microbial infection thereby regulating the pathogenic processes that drive pulmonary disease[48]. However, recent studies have observed an age-related decline in autophagic flux and clearance leading to increased levels of damaged organelles and misfolded proteins in various tissues[49, 50]. As such, impaired autophagy has been

implicated in the progression of multiple chronic and age-related human diseases, suggesting deficient autophagy may contribute to IPF[51-53]. In contrast, activation of autophagy by inhibition of mTOR has been shown to delay aging mechanisms and extend lifespan; a beneficial course which may be applicable to slowing the progression of pulmonary fibrosis[54-56].

1.6 Selective Degradation of Mitochondria

Mitochondria are dynamic organelles involved in various cellular functions including calcium regulation, metabolite synthesis, and cell fate decisions, in addition to the production of adenosine triphosphate (ATP)[57, 58]. Due to their participation in oxidative phosphorylation and ensuing ROS production, mitochondria are constantly under stress to preserve cellular energy homeostasis making selective autophagic degradation of mitochondria (mitophagy) critical to maintaining a proper pool of the organelle and avoid cell death[59, 60].

The process of targeting specific mitochondria for autophagy typically proceeds via two sensors of mitochondrial dysfunction: PTEN-induced putative kinase 1 (PINK1), a serine/threonine kinase, and Parkin RBR E3 ubiquitin protein ligase (PARK2/Parkin)[57, 59, 60]. Upon depolarization of the mitochondrial membrane potential ($\Delta\Psi m$), PINK1 is translocated to the outer mitochondrial membrane whereupon its accumulation leads to the recruitment and activation of Parkin. Once phosphorylated, Parkin is converted into an activated phospho-Ub-dependent E3 ligase resulting in the ubiquitinylation of multiple substrates, including mitofusin 2 (Mfn2), located on the outer mitochondrial membrane[57,

[59, 60]. PINK1 can also phosphorylate the ubiquitin tagged proteins initiating further cycles of Parkin recruitment and activation resulting in a positive feedback loop controlling mitophagy[60]. Autophagy receptors, such as p62/SQSTM1 and gamma-aminobutyric acid receptor-associated protein (GABARAP), are thereby recruited by ubiquitinated organelle allowing the damaged mitochondria to be sequestered within an autophagosome via interaction with LC3[57, 59, 60]. Mitophagy can also occur independent of PINK1 through outer mitochondrial membrane-localized mediators such as BCL2/Adenovirus E1B 19kDa Interacting protein 3-like (Bnip3L/Nix). Under stress conditions, Bnip3L phosphorylation promotes binding to LC3 thereby inducing mitophagic activity[57].

Most recently, mitochondrial dysfunction has been implicated in the pathogenesis of nearly all chronic and age-related diseases[55, 57]. The decline in mitophagy during aging may leave the lung particularly susceptible to the development of pulmonary fibrosis. It has therefore been suggested that induction of mitophagy may reduce mitochondria-related oxidative stress and provide a potential therapeutic target for opposing aging-associated diseases.

1.7 Sirtuins

Silent information regulator (SIR) genes, also known as sirtuins, are a highly conserved family of proteins identified in almost all species from bacteria to mammals. Sirtuins belong to class III histone deacetylases are dependent upon oxidized nicotinamide adenine dinucleotide (NAD+) for their enzymatic activity. Seven sirtuins

genes (SIRT1 to SIRT7) are encoded by the mammalian genome[61, 62]. Considered to play an important role in controlling other genes, sirtuins enact modifications in an organism's response to stress via posttranslational modifications (PTMs). Indeed, sirtuins have been implicated in certain biological aspects of aging[61]. The seven sirtuin isoforms vary in their subcellular location, enzymatic activity and substrates. SIRT1, SIRT6 and SIRT7 primarily reside in the nucleus whereas SIRT3, SIRT4, and SIRT5 are localized to mitochondria and SIRT2 resides mostly within the cytoplasm[61, 62].

Sirtuin 3 (SIRT3) is the major mitochondrial deacetylase and particularly involved in regulating mitochondrial functions including metabolism and cell fate decisions[63]. Lysine acetylation is the most abundant protein posttranslational modification in the mitochondrion[64]. SIRT3 deacetylation regulates many cellular functions including ATP synthesis, production of ROS, antioxidant mechanisms, and apoptosis[65]. SIRT3 also controls the flow of the mitochondrial oxidative phosphorylation (OXPHOS) pathway demonstrating its critical role regulating energy metabolism as mice deficient in SIRT3 show reduced ATP levels in metabolically active tissues[63]. Deacetylation of mitochondrial proteins induces mitophagy which allows SIRT3 to control the switch between mitophagy or cell survival and cell death[66]. At this moment, SIRT3 is the only sirtuin confirmed to be linked to human lifespan and longevity making it a promising target for therapeutic compounds[67, 68]. Thus far, the most reliable compound to influence the expression of sirtuins is resveratrol, a plant derivative extracted from the skin of red wine grapes. Resveratrol has been shown to induce and activate SIRT1 & SIRT3[61].

Two possible roles of SIRT3 that may be of particular importance to lung fibrosis are its regulation of oxidative stress and regulation of Akt signaling[62, 69]. Recent studies have shown that overexpression of SIRT3 can prevent cardiac hypertrophy in mice via inhibition of mitochondrial ROS and inactivation of the PI3K/Akt pathway[62]. Since TGFβ1 signaling in the lung has been linked to activate both these pathways, it may be that activation of SIRT3 can slow the differentiation of fibroblasts to myofibroblasts and potentially delay the development of pulmonary fibrosis.

CHAPTER 2. TGFβ1 MODULATES AUTOPHAGY AND MITOCHONDRIAL HOMEOSTASIS DURING MYOFIBROBLAST DIFFERENTIATION

2.1 Introduction

Although an age-related decline in autophagic flux and clearance has been observed in various tissues, cigarette smoking (CS) has been reported to induce autophagy in lung epithelial cells and fibroblasts[49, 50,70-72]. In recent years, although smoking is a risk factor for IPF, CS-induced autophagy has been associated more closely with the pathogenesis of chronic obstructive pulmonary disease (COPD), another aging-related lung disease, since COPD patients are reported to have higher levels of autophagy markers[73]. In contrast, patients with IPF display low levels of autophagy markers, despite high levels of ER stress previously shown to induce autophagy[48, 73, 74]. To further understand this apparent ambiguity in pulmonary fibrosis, we investigated the mechanisms by which TGFβ1 may alter autophagy. We hypothesized that non-canonical activation of the mTOR pathway by TGFβ1 inhibits autophagy in fibroblasts driving the process of myofibroblast differentiation.

Defects in mitochondrial homeostasis and turnover are associated with late-onset pathologies, the accumulation of defective mitochondria in aging tissues, and advanced oxidative stress[75, 76]. As such, induction of mitochondrial turnover and recycling through autophagy is thus a legitimate pharmacological target in age-related lung diseases. In recent years, evidence has been accumulating implicating TGFβ1 in the regulation of

mitochondrial bioenergetics and oxidative stress responses characteristic of chronic aging diseases[77, 78]. In spite of this recognition, little research has been done to explore TGFβ1 effects on mitochondrial dynamics including mitochondrial biogenesis and fusion/fission events in fibroblasts. We hypothesized that TGFβ1 may alter mitochondrial homeostasis via inhibition of mitophagy and mitochondrial biogenesis inducing oxidative stress and mitochondrial dysfunction promoting myofibroblast differentiation.

2.2 Results

TGFβ1 inhibits autophagy during myofibroblast differentiation in a time-dependent manner

To investigate the role of autophagy in pulmonary fibrosis, we tested the effect of TGFβ1 in normal human lung fibroblasts (NHLF) and examined autophagic markers. RNA transcripts from NHLF untreated and treated with TGFβ1 for 24 h were first screened using a gene expression array for 84 key genes involved in autophagy as components of the molecular machinery and regulators in order to determine if autophagy-related genes are regulated at the mRNA level by TGFβ1. The results showed that 21 different autophagy-related mRNAs were significantly regulated by TGFβ1 in NHLF (Fig. 1.1A-B). These results were confirmed by quantitative real-time polymerase chain reaction (qRT-PCR) with an independent set of primers (Fig. 1.1B). The complete list of gene expression changes is shown in Table 1.1. Interestingly, TGFβ1 repressed genes involved in the processes of autophagosome formation and maturation as well as co-regulators of autophagy/apoptosis and regulators of autophagy in response to intracellular pathogens and other intracellular signals (Fig. 1.1B). Only one gene, IGF1,

was significantly up-regulated (>30 fold change) by TGFβ1 (Fig. 1.1B). Importantly, TGFβ1 repressed p62/SQSTM1 by 50% (Fig. 1.1B).

To determine the effect of TGFβ1 upon autophagy flux in NHLF, cells were treated for 12, 24, and 48 h with 1 ng/ml of TGFβ1, alone or with 30 μM chloroquine (CQ) treatment 4 h prior to collection. The purpose was to observe time dependent differences in the autophagy flux during the process of myofibroblast differentiation. Western blot (WB) analysis confirmed that TGFβ1 reduced autophagy at 24 h (determined as the increase in LC3-II levels upon addition of CQ) but no significant differences were noticed after 48 h (Fig. 1.1C). p62/SQSTM1 protein levels assessed by western blot declined in TGFβ1-treated fibroblasts which CQ treatment failed to increase to the same levels observed in control fibroblasts (Fig. 1.1C). The measurement of p62/SQSTM1 expression as a marker of autophagic flux is controversial and misinterpreted; this protein is subject to regulation at both transcriptional and post-translational levels. Analyses by qRT-PCR previously shown in Fig. 1.1B showed that TGFβ1 inhibited p62/SQSTM1 gene expression, which indicates that p62/SQSTM1 cannot be used as an autophagy flux marker in this context. We next evaluated the time-dependent regulation of mTOR during the process of myofibroblast differentiation after TGFβ1 treatment. Western blots using antibodies specific for the active (phosphorylated) forms of AKT and a downstream target of mTOR, p70 S6-Kinase 1, indicated that TGFβ1 induced the AKT/mTOR pathway in a time-dependent manner with an activation peak at 24 h (Fig. 1.1D). The lysosome inhibitor CQ promoted accumulation of collagen type I (Col1) but not α-smooth muscle actin (α-SMA), even in absence of TGFβ1, suggesting that in normal human lung fibroblasts Col1 is targeted for lysosomal

Figure 1.1

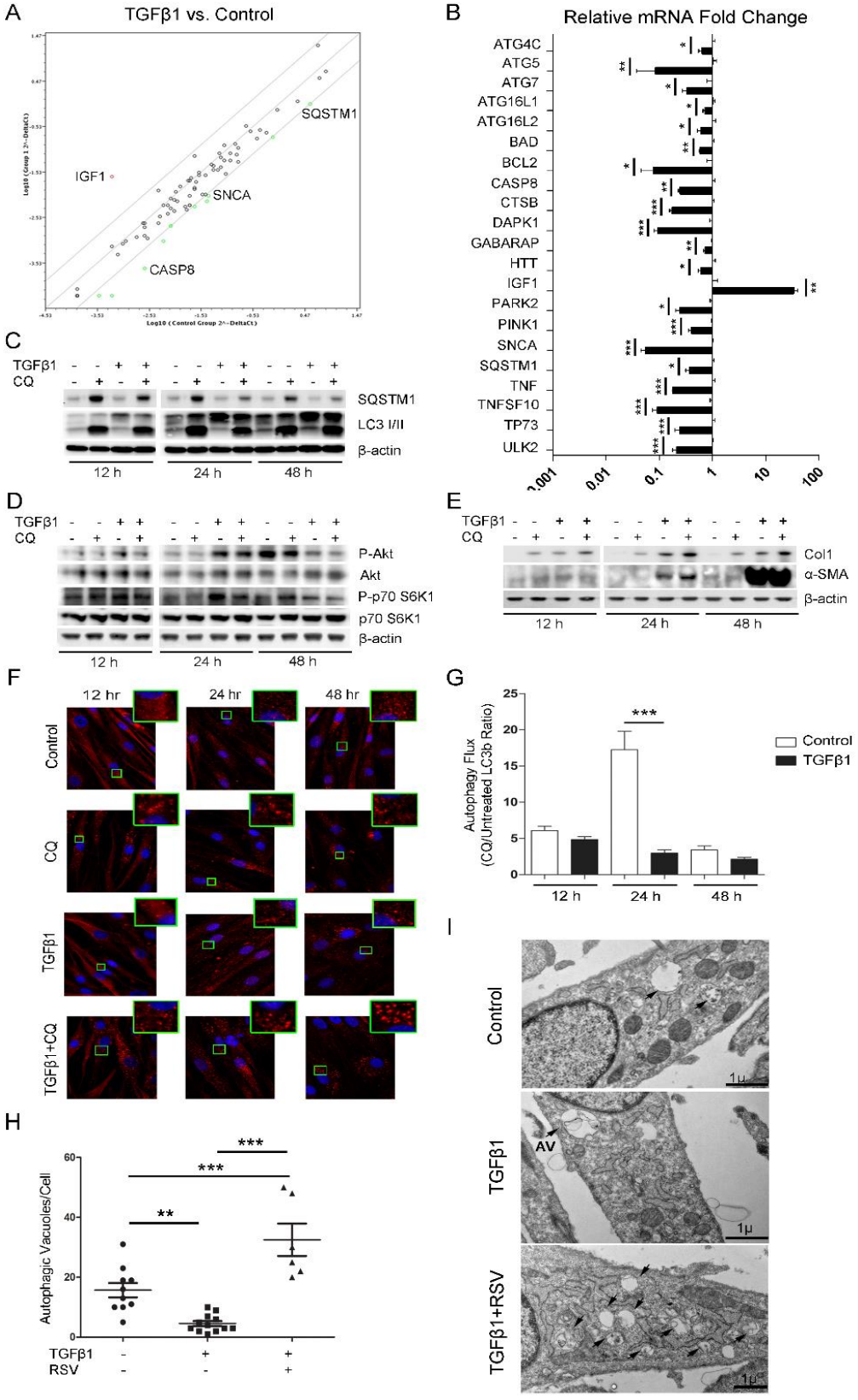
A
TGFβ1 vs. Control
SQSTM1
IGF1
SNCA
CASP8
B
Relative mRNA Fold Change
ATG4C
ATG5
ATG7
ATG16L1
ATG16L2
BAD
BCL2
CASP8
CTSB
DAPK1
GABARAP
HTT
IGF1
PARK2
PINK1
SNCA
SQSTM1
TNF
TNFSF10
TP73
ULK2
C
TGFβ1
CQ
SQSTM1
LC3 I/II
β-actin
12 h
24 h
48 h
D
TGFβ1
CQ
P-Akt
Akt
P-p70 S6K1
p70 S6K1
β-actin
12 h
24 h
48 h
E
TGFβ1
CQ
Col1
α-SMA
β-actin
12 h
24 h
48 h
F
12 hr
24 hr
48 hr
Control
CQ
TGFβ1
TGFβ1+CQ
G
Autophagy Flux
(CQ/Untreated LC3b Ratio)
Control
TGFβ1
12 h
24 h
48 h
H
Autophagic Vacuoles/Cell
TGFβ1
RSV
I
Control
TGFβ1
TGFβ1+RSV
AV
1μ

Figure 1.1. Repression of autophagy during FMD in lung fibroblasts by TGFβ1. A) Gene expression array for autophagy related genes comparing NHLF treated with or without TGFβ1 for 24 h. B) Real time RT-PCR analysis with independent primers for indicated genes to confirm significant fold changes detected in expression. A base-10 log scale is used for the X-axis of graph. C) NHLF cultured for 12, 24, and 48 h with and without TGFβ1 and/or chloroquine (CQ) added 4 h prior to collection for western blot (WB) analysis. Representative WB for autophagic markers with the indicated antibodies and β-actin loading control. D) Representative WB for mTOR pathway activation with the indicated antibodies and β-actin loading control. E) Representative WB for fibrotic markers collagen type I (Col1), α-smooth muscle actin (α-SMA) and β-actin loading control. F) Representative immunofluorescence images for LC3 punctae in NHLF treated for 12, 24, and 48 h with TGFβ1 and 4 h with chloroquine (CQ) to investigate the autophagy flux. G) Quantification of LC3 punctae immunofluorescence indicates differences in the autophagic flux after 24 h treatment with TGFβ1. H) Quantification of autophagic vacuoles (AV) in electron microscopy images in (I) performed on control (10 cells), TGFβ1 treated (12 cells), and TGFβ1 and RSV co-treatment (6 cells). I) Confirmatory electron microscopy (TEM) for autophagosome analysis. Resveratrol (RSV) co-treatment is used as a tool to induce autophagosome formation. Arrows show autophagic vacuoles or are labelled AV. Arbitrary Units abbreviated as AU. *P<0.05, **P<0.01, ***P<0.005.

degradation, but not α-SMA (Fig. 1.1E).

Changes in the autophagy flux were confirmed by an increase in the immunofluorescence of the LC3b punctae upon CQ treatment (Fig. 1.1F-G). Analysis of the CQ treatment confirms that the maximum inhibition of the autophagy flux (CQ treated/untreated) corresponds temporally with the peak in mTOR activity (Fig. 1.1D, G). Finally, we confirmed the inhibitory effects of TGFβ1 on autophagy in human lung fibroblasts by semi-quantitative analysis of number of autophagic vacuoles (AV) detected by electron microcopy, as presented in Figure 1.1H-I.

TGFβ1 modulates PINK1 expression, mitophagy & mitochondrial homeostasis during FMD

qRT-PCR analysis confirmed TGFβ1-induced reduced mRNA levels for p62/SQSTM1 and PINK1 in dose-dependent manner (Fig. 1.2A). These results suggest that deficient mitochondrial targeting for degradation could occur during FMD through

TGFβ1-induced deregulation of the PINK1/PARKIN/p62 pathway. In order to determine if the TGFβ1-induced reduction in PINK1 expression altered the selective targeting of mitochondria for autophagic degradation, NHLF were cultured with or without CQ after TGFβ1 treatment. CQ increased the accumulation of PINK1 and TOM20 as a result of the active autophagy flux in NHLF, however this process was impaired in presence of TGFβ1. By contrast, resveratrol (RSV), a hormetic compound that promotes autophagy promoted active mitophagy (Fig. 1.2B).

Mitochondria isolation was performed in NHLF treated with or without TGFβ1 and/or RSV in order to determine if the reduction in PINK1 and p62/SQSTM1 expression observed is reflected in the level of recruitment of mitochondria for degradation. Western blot analysis demonstrated that the TGFβ1-mediated decline in p62/SQSTM1 in total cell protein was also observed in the isolated mitochondria (Fig. 1.2C). Similarly, the levels of PINK1 and Bnip3L/Nix, a receptor for mitophagy, declined in the isolated mitochondria from TGFβ1-treated cells compared to controls as mitochondrial protein levels were normalized with TOM20 (Fig. 1.2C). In contrast, co-treatment with RSV maintained the expression levels of PINK1, p62/SQSTM1 and Bnip3L in mitochondria (Fig. 1.2C).

Due to reduced degradation of mitochondria, which has been associated with increased mitochondrial dysfunction, superoxide levels were measured. Assessment of ROS levels using the DCFH-DA assay demonstrated an increase in ROS consequent to TGFβ1 that was ameliorated by RSV treatment (Fig. 1.2D). To demonstrate the functional relevance of these results, we performed western blot analyses of the relative levels of the oxidative phosphorylation (OXPHOS) complexes in mitochondrial

Figure 1.2

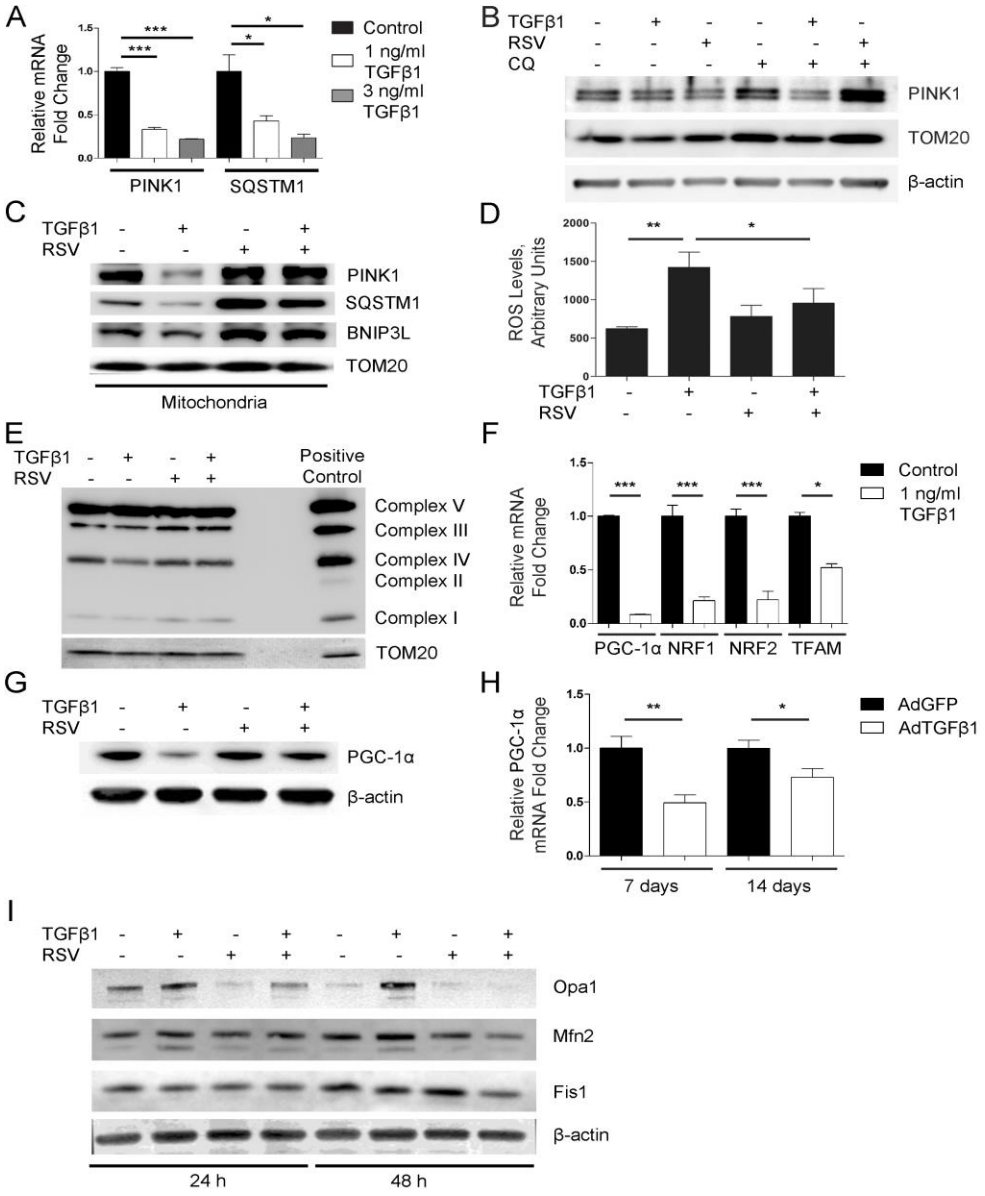

Figure 1.2. Deregulated mitochondrial homeostasis and PINK1 expression in FMD. A) qRT-PCR analysis for TGFβ1 dose dependent changes in the transcriptional levels of PINK1 and p62/SQSTM1 in NHLF after 24 h. B) NHLF control or treatment with TGFβ1 and/or resveratrol (RSV) for 24 h. Chloroquine (CQ) added 4 h prior to collection for autophagic flux analysis. Representative western blots (WB) for PINK1 and TOM20 expression. β-actin used as a loading control. C) Representative WB of mitochondria isolated from NHLF treated or untreated with TGFβ1 and/or resveratrol (RSV) probed for indicated antibodies. TOM20 used as loading control. D) Quantification of reactive oxygen species from NHLF treated with or without TGFβ1 and/or RSV. E) Representative WB for OXPHOS complexes from NHLF treated or untreated with TGFβ1 and/or RSV. TOM20 used as loading control. F) qRT-PCR analysis for TGFβ1 changes in the transcriptional levels of PGC-1α, NRF-1, NRF-2, and TFAM in NHLF after 24 h. G) Representative WB for PGC-1α from NHLF treated or untreated with TGFβ1 and/or RSV. H) qRT-PCR analysis for mRNA expression levels of PGC-1α, at 7 and 14 days post oropharyngeal aspiration of control Adenovirus-GFP (AdGFP) or Adenovirus-TGFβ1 (AdTGFβ1) in mice (n=5 per treatment). I) Representative WB for mitochondrial dynamics markers Opa1, Mfn2, and Fis1 from NHLF treated or untreated with TGFβ1 and/or RSV at 24 and 48 h. β-actin used as loading control. *P<0.05, **P<0.01, ***P<0.005.

preparations from these cells. Levels of complex III and IV declined in mitochondria from TGFβ1-treated cells, which were reversed by co-treatment with RSV (Fig. 1.2E).

With the knowledge that TGFβ1 altered mitochondrial degradation, we aimed to study overall effects on mitochondrial homeostasis via mitochondrial biogenesis and dynamics factors. qRT-PCR analysis showed TGFβ1 significantly downregulated the expression of several mitochondrial biogenesis factors peroxisome proliferator-activated receptor gamma co-activator 1-alpha (PGC-1α), nuclear respiratory factor-1 (NRF-1), nuclear respiratory factor-2 (NRF-2/GABP), and transcription factor A, mitochondrial (TFAM) at 24 h (Fig. 1.2F). This downregulation was confirmed at the protein level for PGC-1α by WB, which was improved upon co-treatment with RSV (Fig. 1.2G). We further confirmed the deregulation of PGC-1α by TGFβ1 *in vivo* using a non-replicating adenovirus transducing either GFP (AdGFP) or active TGFβ1 (AdTGFβ1) to model pulmonary injury in mice. Real-time RT-PCR analyses from whole lung extracts were performed at 7 and 14 days post-infection. The results demonstrated a TGFβ1-associated reduction in PGC-1α in the lung at both time-points post-infection (Fig. 1.2H). Lastly, we explored possible effects of TGFβ1 in mitochondrial fusion & fission dynamics. In NHLF treated with TGFβ1 and/or RSV for 24 or 48 h, WB analysis showed an upregulation of mitochondrial fusion factors, optic atrophy 1 (Opa1) and mitofusin 2 (Mfn2) without changes in the expression of mitochondrial fission 1 protein (Fis1) (Fig. 1.2I). These changes, which were detectable at 24 h, were even more evident at 48 h (Fig. 1.2I) suggesting TGFβ1 treatment induces mitochondrial elongation and morphological changes contributing to overall mitochondrial dysfunction.

Fibroblasts undergoing active autophagy resist the remodeling effects of TGFβ1

Since myofibroblasts are key players in pulmonary fibrosis and the major source of interstitial collagen deposition, we explored possible therapeutic implications of autophagy induction relative to FMD in cell culture. NHLF were treated with mTOR-dependent and –independent inducers of autophagy in the presence or absence of TGFβ1 and the FMD response was evaluated by western blot for Col1 and α-SMA. Selective inhibition of mTOR with Torin 1 repressed TGFβ1-mediated induction of Col1 and α-SMA, while increasing the LC3b-II/LC3b-I ratio (Fig. 1.3A-D). Calorie-restriction decelerates mTOR-driven aging in cells as well as in organisms. NHLF were pretreated with complete media or HBSS media to induce nutrient restriction for 24 h followed by treatment with TGFβ1 for an additional 24 h. The results from western blots (and qRT-PCR, data not shown) demonstrated that preconditioning with nutrient restriction promoted resistance to induction of fibrotic markers, Col1 and α-SMA expression shown here, by TGFβ1 (Fig. 1.3E-G). Non-specific hormetic compounds such as RSV promoted autophagy and also prevented FMD in a dose-dependent manner (Fig. 1.3H-J). To more directly implicate autophagy in repression of TGFβ1-mediated FMD we used Tat-beclin 1, a membrane permeable peptide that selectively induces autophagy. Treatment with Tat-beclin 1 peptide reduced the expression of fibrotic markers in a dose-dependent manner (Fig. 1.3K-M). Finally, to determine if autophagy induction after myofibroblast formation can still be beneficial, we differentiated NHLF into myofibroblasts by treating cells with TGFβ1 for 48 h before treating cells with or without RSV for an additional 24 h. WB analysis showed that RSV treated differentiated myofibroblasts had lower levels of Col1 which were able to be restored in the presence of CQ suggesting Col1

Figure 1.3

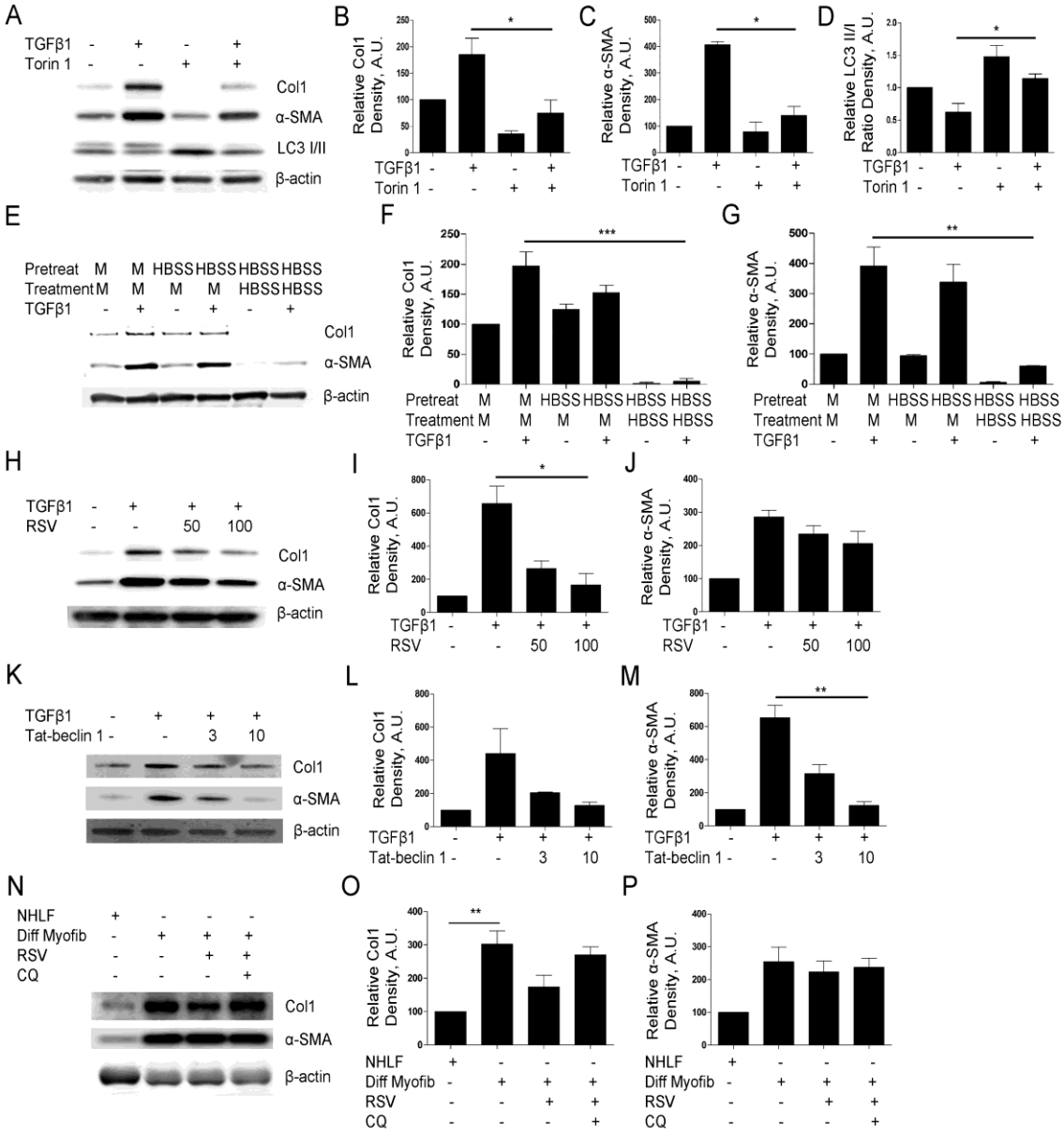

Figure 1.3. Fibroblasts undergoing active autophagy resist remodeling effects of TGFβ1. Inhibition of FMD is demonstrated by western blot from total extracts derived from NHLF treated with TGFβ1 and autophagy inducers. Densitometry analysis for representative WBs shown probed with antibodies to fibrotic markers collagen type I (Col1) and α-Smooth Muscle Actin (α-SMA) using β-actin as protein loading control. A-D) NHLF cultured in the presence of TGFβ1 and Torin 1 for 24 h. E-G) NHLF pre-cultured in nutrient-restricted conditions (HBSS) or complete media (M) then co-treated with TGFβ1 for an additional 24 h. H-J) TGFβ1 alone or co-treatment with TGFβ1 plus resveratrol (RSV) at multiple doses for 24 h. K-M) NHLF were cultured in presence of TGFβ1 and doses of Tat-beclin 1 peptide for 24 h. N-P) Differentiated myofibroblasts from culturing NHLF in TGFβ1 for 48 h prior to co-treatment with TGFβ1 plus RSV for an additional 24 h in the presence or absence of chloroquine (CQ) for 4 h. Arbitrary Units abbreviated as AU. *P<0.05, **P<0.01, ***P<0.005.

degradation is targeted by autophagy in differentiated myofibroblasts (Fig. 1.3N-O). However, again the levels of α-SMA remained unchanged in the presence or absence of RSV, signifying autophagic degradation of fibrotic markers in myofibroblasts is specific to collagen type I (Fig. 1.3N-P).

Moreover, using a genetic approach, we confirmed that inhibition of autophagy by knockdown of ATG5 and ATG7 in NHLF promoted expression of α-SMA and Col1 (Fig. 1.4A-B). Taken together, these results indicate that active autophagy prevents FMD and that promotion of autophagy may be necessary and sufficient to maintain normal lung fibroblasts.

Figure 1.4

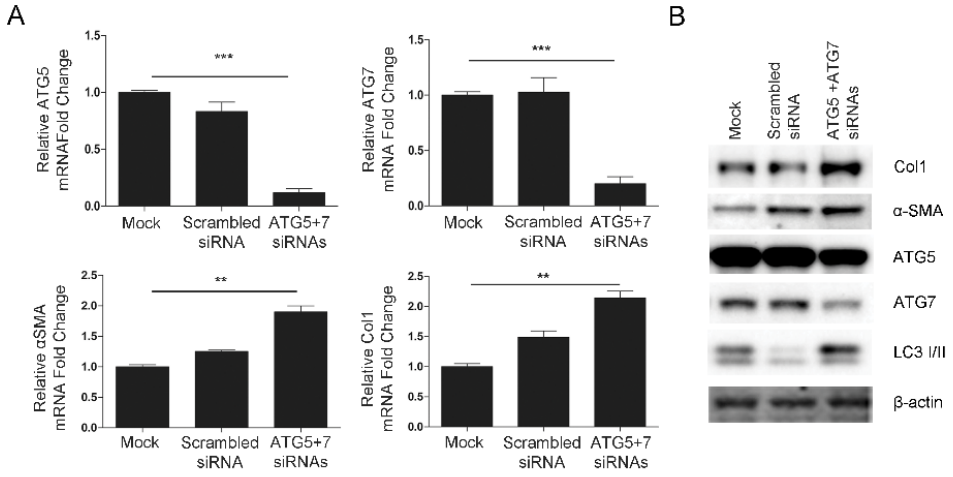

Figure 1.4. Autophagy inhibition induces expression of fibrotic markers. A) qRT-PCR analysis from NHLF transfected with siRNA for ATG5 and ATG7 to evaluate transcriptional changes in ATG5, ATG7, and fibrotic markers collagen type I (Col1) and α-SMA expression. B) Representative western blots for Col1, α-SMA, ATG5, ATG7, and LC3 in NHLF deficient in ATG5 and ATG7. **P<0.01, ***P<0.005.

2.3 Discussion

Our data support the role of autophagy and mitophagy, as protective mechanisms, against fibrogenesis. We found that TGFβ1 represses autophagy, mitochondrial recycling and homeostasis, and inhibits PINK1 expression in normal human lung fibroblasts during FMD. Autophagy is a stress response and a quality control mechanism that protects against cellular stress and injury[79, 80]. Thus, impaired autophagic activity and mitophagy in response to injury may contribute to the onset of age-related lung diseases.

Previous studies using lung biopsies from IPF patients reported a diminution in autophagy[48, 74]. Herein, we impart an appreciation for TGFβ1-mediated regulation of the autophagic response during lung aging as part of the normal and pathological response to injury and fibrogenesis. Our findings demonstrate that autophagy may restrain trans-differentiation of normal human lung fibroblasts. A proposed model of these events is shown in Figure 1.5A. TGFβ1 reduces autophagy, in part, by selectively repressing expression of autophagy mediators in normal lung fibroblasts. As shown in our studies, TGFβ1 reduces the expression of p62/SQSTM1. p62/SQSTM1 serves as multifunctional regulator of cell signaling involved in selective autophagy, intracellular trafficking and the nuclear factor erythroid 2-related factor 2 (NFE2L2/Nrf2) antioxidant response[81, 82]. Relative to the latter activity, defects in p62/SQSTM1 may contribute to the deregulation in NFE2L2/Nrf2 activity seen in myofibroblasts and pulmonary fibrosis[81, 83]. Thus, p62/SQSTM1 could provide dual protection to stressed cells by facilitating both autophagy and the NFE2L2/Nrf2-mediated antioxidant response. The relevance of p62/SQSTM1 function to pulmonary fibrosis is further supported by studies describing accelerated aging and age-related pathologies associated with loss of p62/SQSTM1[84].

Figure 1.5

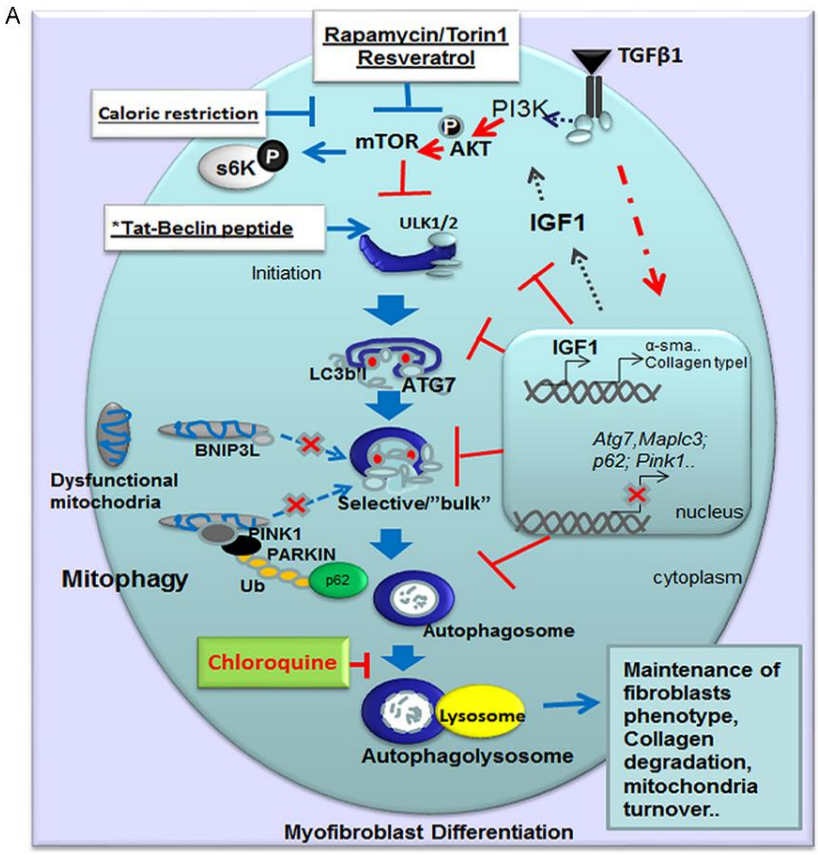

Figure 1.5. Proposed model for TGFβ1 repression of autophagy during myofibroblast differentiation. A) TGFβ1 activates the PI3K/AKT/mTOR pathway which inhibits the initiation of the autophagosome formation. TGFβ1 will impart, directly or indirectly, deregulation of autophagy related genes that will inhibit autophagy at different levels of the process, including autophagosome formation, selectivity and degradation. Furthermore, TGFβ1 inhibits the expression and recruitment of PINK1/PARKIN/p62 to the mitochondria, promoting accumulation of dysfunctional mitochondria. Fibroblasts, as well as myofibroblasts, use autophagy as a means to control the levels of intracellular Col1. Deficient autophagy promotes Col1 and Hsp47 accumulation. Induction of autophagy in an mTOR-dependent (Rapamycin, Torin 1, caloric restriction or RSV) or mTOR-independent manner (LiCl, Tat-beclin 1), inhibits FMD. Contrary, inhibition of autophagy promotes myofibroblast differentiation independently of TGFβ1.

Our research demonstrates a clear role for TGFβ1 in altering mitochondrial homeostasis at multiple levels. Firstly, it was observed here that TGFβ1 induced the fusion and elongation of mitochondria contributing to the increased production of ROS observed in TGFβ1-treated cells. Mitochondrial specific ROS has recently been shown to

be necessary for TGFβ1 signaling and that inhibition of complex III generated ROS can prevent fibrotic marker induction[85]. TGFβ1 also reduced PINK1/p62 dependent mitochondrial recycling as well as mitochondrial oxidative phosphorylation. Finally, TGFβ1 inhibited mitochondrial biogenesis in NHLF by reducing PGC-1α expression in fibroblasts and murine models of pulmonary fibrosis. Interestingly, PGC-1α is a known controller of the main mitochondrial deacetylase, sirtuin 3 (SIRT3), suggesting TGFβ1 may also play a role in altering mitochondrial protein acetylation status.

We found that TGFβ1 stimulates the expression of the cytokine IGF1, an inhibitor of autophagy and a marker of aging in healthy adults[86]. In some organisms, mutations that reduce the activity of the IGF1/AKT pathway increase longevity[87]. Like TGFβ1, IGF1 is elevated in the lungs of patients with IPF as well as in animal models of pulmonary fibrosis. IGF1 and TGFβ1 can act synergistically to promote changes in cell metabolism, survival, and cytoskeletal reorganization[88].

Overall, our studies connect autophagy and mitochondrial homeostasis to cell fate during fibrogenesis. Nevertheless, a cell-type specific genetic approach and the redundancy of mechanisms that regulate mitochondrial homeostasis need to be investigated, as pulmonary fibrosis is a complex disease that involves multiple interacting signaling pathways[83].

2.4 Materials & Methods

Cell culture & Reagents. Normal Human Lung Fibroblasts (NHLF) were obtained from ATCC and maintained in Fibroblast Growth Medium-2 (FGM-2, Lonza,

Walkersville, MD, USA) before serum starving cells in Fibroblast Basal Medium (FBM, Lonza) supplemented with 0.2% bovine serum albumin (BSA, Gemini Bio-Products Inc., Woodland, CA, USA). During treatments NHLF were cultured in FBM plus 0.2% BSA. For experiments, recombinant TGFβ1 (R&D Systems, Minneapolis, MN, USA) was used at a concentration of 1 ng/ml. For autophagy flux experiments, chloroquine (CQ) (Sigma, St. Louis, MO, USA) was added at least 4 h prior to harvesting at a concentration of 30 μM. Resveratrol (Sigma) was used at concentrations of 50 and 100 μM, the latter concentration being used for most experiments. Torin 1 obtained from Selleck Chemicals (Houston, TX, USA) was used at a concentration of 250 nM. Hank's Balanced Salt Solution (HBSS, Life Technologies, Grand Island, NY, USA) was used for nutrient restriction experiments. Tat-beclin 1 peptide was obtained from Phoenix Pharmaceuticals, Inc. (Burlingame, CA, USA) and used at concentrations of 3 and 10 μM.

RNA isolation & qRT-PCR & Gene Expression Array. Total RNA was isolated using Trizol® Reagent (Invitrogen, Carlsbad, CA, USA) according to manufacturer's instructions. RNA concentration was measured using a NanoDrop spectrophotometer (Thermo Scientific Nanodrop, Nanodrop Technologies, Wilmington, DE, USA). The gene expression profile was evaluated using RT^2 Profiler^{TM} PCR array for autophagy (PAHS-084A, SABiosciences, Frederick, MD, USA) according to standard protocol. For gene expression array studies, 1 μg of total RNA was reverse transcribed using the RT^2 First Strand Kit (SABiosciences) and resulting cDNA was added to RT2qPCR Mastermix (SABiosciences) at correct dilutions and aliquoted to PCR array. The real-time PCR reaction was performed using the MyiQ iCycler (Bio-Rad). Analysis

of the PCR array profile was performed using web-based software RT^2 Profiler PCR Array Data Analysis version 3.5 provided at the SABiosciences website (http://pcrdataanalysis.sabiosciences.com/pcr/arrayanalysis.php). Genes that demonstrated a fold change >3 were selected for further study.

For quantitative real-time PCR (qRT-PCR) analysis, 1 μg of total RNA was reverse transcribed using iScript™ cDNA Synthesis Kit (Bio-Rad Laboratories Inc., Hercules, CA, USA) according to manufacturer's protocol. Quantitative real-time PCR reactions were performed using iQ™SYBR® Green Supermix (Bio-Rad) in the Bio-Rad MyiQ iCycler (Hercules, CA). Relative expression levels were calculated using the $2^{-\Delta\Delta C(T)}$ method and normalized to 36b4 expression. All primer information given in Table 1.1.

Western blots. Cells were harvested in 1x RIPA Buffer (Cell Signaling, Danvers, MA, USA), sonicated, and quantified using the Bradford Method (Bio-Rad). Protein samples combined with 4x NuPAGE LDS Sample Buffer and 10x NuPAGE Sample Reducing Agent (Invitrogen) for a final concentration of 1x for both buffers and boiled for 5 minutes. 20-25 micrograms of each protein sample was separated on NuPage SDS 4-12% Bis-Tris gradient gels (Invitrogen) and transferred onto PVDF membranes (Invitrogen). For time-dependent cell lysates, protein samples were separated on 15% Acrylamide 1.5M Tris/10% SDS gel. Membranes were blocked in 5% BSA in TBST or 5% nonfat dry milk (Blotting-Grade Blocker, Bio-Rad) in TBST for 1 h at RT then probed with primary antibody overnight at 4°C while shaking.

For immunoblot detection, antibodies to Collagen-1, BNIP3L, PGC-1α, PINK1 and p62/SQSTM1 were purchased from Abcam (Western blot, 1:1000; Cambridge, MA, USA). Antibodies to ATG7, Phospho-AKT (S473), AKT, Phospho-p70 S6 Kinase (T389), p70 S6 Kinase, Phospho-Smad2 (S465/467), Smad2, Phospho-Smad3 (S423/425), Smad3 and β-actin were purchased from Cell Signaling (1:1000; Danvers, MA, USA). Antibodies to Fis1, Mfn2, Opa1 and TOM20 were purchased from Santa Cruz Biotechnology (1:500; Dallas, TX, USA). Antibody to α-Smooth Muscle Actin (SMA) was purchased from Sigma (1:10,000). Antibodies to ATG5 and LC3 were purchased from MBL International (1:500; Woburn, MA, USA).

Western blots were imaged using ImageQuant LAS 4000 (GE Healthcare, Pittsburgh, PA, USA) or LiCor imaging systems. Anti-mouse IgG, HRP-linked, anti-rabbit IgG, HRP-linked (1:15,000; Cell Signaling) for chemiluminescent detection and IRDye 800CW goat anti-rabbit IgG or IRDye 680 goat anti-mouse IgG (1:15,000; LiCor, Lincoln, NE, USA) for fluorescent detection. Densitometry analysis was performed using National Institutes of Health (NIH) ImageJ 1.48d (Wayne Rasband NIH, USA, http:imagej.nih.gov/ij) software.

Immunofluorescence & Image Analysis. For immunofluorescence samples, slides were permeabilized in 0.2% Trition-X in TBS buffer for 45 m at RT and washed in TBS after blocking with 10% BSA in TBS (blocking serum) for 1 h, the primary antibody was added. Antibody to LC3 (rabbit) was used at a dilution of 1:200 and incubated overnight at 4°C in a humidified chamber. Secondary antibodies AlexaFluor 594 goat anti-rabbit IgG (Invitrogen) and AlexaFluor 488 goat anti-mouse IgG (Invitrogen) were employed for immunofluorescence detection at a dilution of 1:1000. Nuclei were

counterstained using DAPI (Invitrogen) before mounting in Prolong Gold antifade media (Invitrogen). For quantification of LC3 punctae, images were captured with an Olympus BX60 microscope equipped with epifluorescence optics (Olympus, Melville, NY) and coupled device camera Magnafire (MagnaFire 2.6; Olympus) with a barrier filter equipped for simultaneous detection of FITC, Texas red and DAPI. TIFF files were normalized, merged and analyzed with Image J. The number of LC3 dots was counted in at least five independent visual fields at 100x oil objective of magnification. The results were expressed as puncta per cell.

Electron microscopy. NHLF cultured on 10 cm2 plates were fixed in 2.5% glutaraldehyde in 0.1 M sodium cacodylate buffer pH 7.4 for 1 h at room temperature. Samples were washed three times for 5 m in 0.1 M sodium cacodylate buffer and sent to the Electron Microscopy Core Facility of the Department of Cell Biology at Yale University School of Medicine (New Haven, CT). The Yale core facility provides images and grids for subsequent analysis with the Tecnai G2 F30 TWIN 300 kV/FEG Transmission Electron Microscope (FEI, Hillsboro, OR, USA) at Tulane University. For electron microscopy analysis, the number of autophagic vacuoles (AV) per cell body were counted using EM images at direct magnification of 4500x and 12,000x for the various treatment conditions. Electron micrographs (control n=10, TGFβ1=12, TGFβ1+RSV=6) were examined, and values are expressed as AVs per field. All numerical values are expressed as mean ± SEM.

Mitochondria Isolation & OXPHOS Screen. Mitochondria were isolated from NHLF post-treatment using the Thermo Scientific (Rockford, IL, USA) Mitochondrial Isolation Kit for Cultured Cells according to the manufacturer's protocol. Mitochondria

samples were combined for a final concentration of 1x LDS sample buffer and separated on aforementioned gels without boiling to prevent reduced expression levels due to protein aggregation. Rat heart mitochondria provided with OXPHOS antibody (MitoSciences, Abcam, Cambridge, MA, USA) was used as a positive control. MitoProfile total OXPHOS rodent WB antibody cocktail (MitoSciences) was used for immunodetection of the 5 OXPHOS complexes at a dilution of 1:250.

Oxidative Stress Assay. ROS levels were measured in cells by detection of DCF, the fluorescent product formed from the oxidation of 2,7-dichlorodihydrofluorescein diacetate (DCFH-DA, Sigma, St. Louis, MO, USA).

Mice & Tissue Samples. All animal protocols were performed as approved by the Tulane University Institutional Animal Care and Use Committee. C57BL/6 male mice were obtained from the Jackson Laboratory (Bar Harbor, ME, USA). Animals were anesthetized with 2% isoflurane vapor (VetOne, Meridian, ID, USA) in oxygen. Treatments were administered in 50 μl of sterile PBS by oropharyngeal aspiration. C57Bl/6 mice aged 6-8 weeks were treated with 3 x 108 PFU of replication-deficient adenovirus encoding either GFP (control group, AdGFP, n=5) or active TGF-β1 (AdTGF-β1, n=5). Animals were anesthetized with 80 mg/kg ketamine plus 8 mg/kg xylazine and euthanized by exsanguination 14 or 7 days after adenovirus treatments respectively. The right lungs were snap-frozen in liquid nitrogen and stored at -80°C for RNA or protein isolation.

Transfections. For siRNA knockdown experiments, NHLF were transfected using the Neon Transfection System (Invitrogen). $1x10^6$ cells per transfection were

harvested and washed once in PBS (Invitrogen) then resuspended in 100 µl of resuspension buffer R with 5 µM siGENOME SMARTpool ATG5 (M-004374-04) & ATG7 (M-020112-01) targeted siRNA (Dharmacon RNAi Technologies Inc., Lafayette, CO, USA), 5 µM control non-silencing siRNA (D-001210-01) or sterile water for mock transfection. This mix was transfected in 100 µl using two pulses of 1400 V input pulse voltage and 20ms input pulse width. Transfected NHLF were plated on 60 mm tissue culture dishes in 5 ml of FGM-2 medium for 48 h.

Statistical analysis. All data is expressed as mean values ± SEM. Comparisons between two groups were made using unpaired, two-tailed Student's t test. Analysis of variance (ANOVA) followed by Bonferroni's multiple comparison test was used for multiple groups. Statistical significance was assigned at a value of $p < 0.05$. All experiments were repeated at least twice.

CHAPTER 3: DEFICIENCY OF AUTOPHAGIC AND MITOPHAGIC RESPONSES IN THE AGING LUNG

3.1 Introduction

The predisposition for disrepair during aging coincides with increases in TGFβ1 signaling[31, 32]. Here, we sought to explore whether changes that have heretofore been considered age-related in response to bleomycin can be detected or promoted in fibrotic lungs of young and late middle-aged, as well as old mice, and whether these changes were progressive. Age-related changes in mitochondria are associated with increased production of reactive oxygen species, reduced ATP production and decreased functionality[89]. Thus, sufficient mitophagic processes are essential to aging-associated diseases such as IPF. We hypothesized that a decline in efficient autophagy and selective autophagic degradation of mitochondria during aging is implicated in the pathogenesis of fibrosis.

3.2 Results

Deficient autophagic response and increase in lipofuscin deposits are concomitant with disrepair in the aging lung

The autophagic response in vivo was evaluated by microtubule-associated protein 1 light chain 3 β (LC3B) punctae, the lipidated form of LC3, immunostaining in

bleomycin-exposed lungs from young (2-month-old), middle-aged (14-month-old) and old (22-month-old) mice. The analysis revealed more punctae in younger mice (2-month-old) when compared to older mice (14- and 22-month-old) exposed to bleomycin (Fig. 2.1A-C). Additionally, young mice had higher levels of LC3b punctae in both the interstitium and the respiratory epithelium (Fig. 2.1C). The deficient autophagic response in older mice exposed to bleomycin compared to young mice was also confirmed by autophagosome detection in electron microscopy (Fig. 2.1D). Compared to 2-month-old mice, the lungs of the older mice also exhibited severe interstitial and intra-alveolar pneumonia and fibrosis with the presence of myofibroblasts, as well as an increase in collagen fibers (Fig. 2.1D). No significant differences were detected between 14- and 22-month-old mice after lung injury.

After bleomycin exposure, an age-dependent increase in the expression of fibrotic markers, Col1, connective tissue growth factor (CTGF/CCN2) and plasminogen activator inhibitor-1 (PAI1) were confirmed by qRT-PCR (Fig. 2.1E). Interestingly, untreated 22-month-old mice had enlarged alveolar spaces compared to 2-month-old mice with higher levels of MMP9 expression (Fig. 2.1E). Collagen deposition was detected by Masson's trichrome staining analysis. An increase in collagen deposition in the 14- and 22-month-old mice compared to young mice was observed (Fig. 2.1F-G). Tissues were immunostained for heat shock protein 47 (Hsp47), a collagen-binding glycoprotein localized in the endoplasmic reticulum and a biomarker of early stages of fibrogenesis. Higher levels of Hsp47-positive cells (myofibroblast-type cells) appeared in 22- and 14-month-old mice compared to 2-month-old mice subjected to bleomycin (Fig. 2.1H-I).

We studied bleomycin-exposed lungs from young mice (2-month-old) and older

Figure 2.1

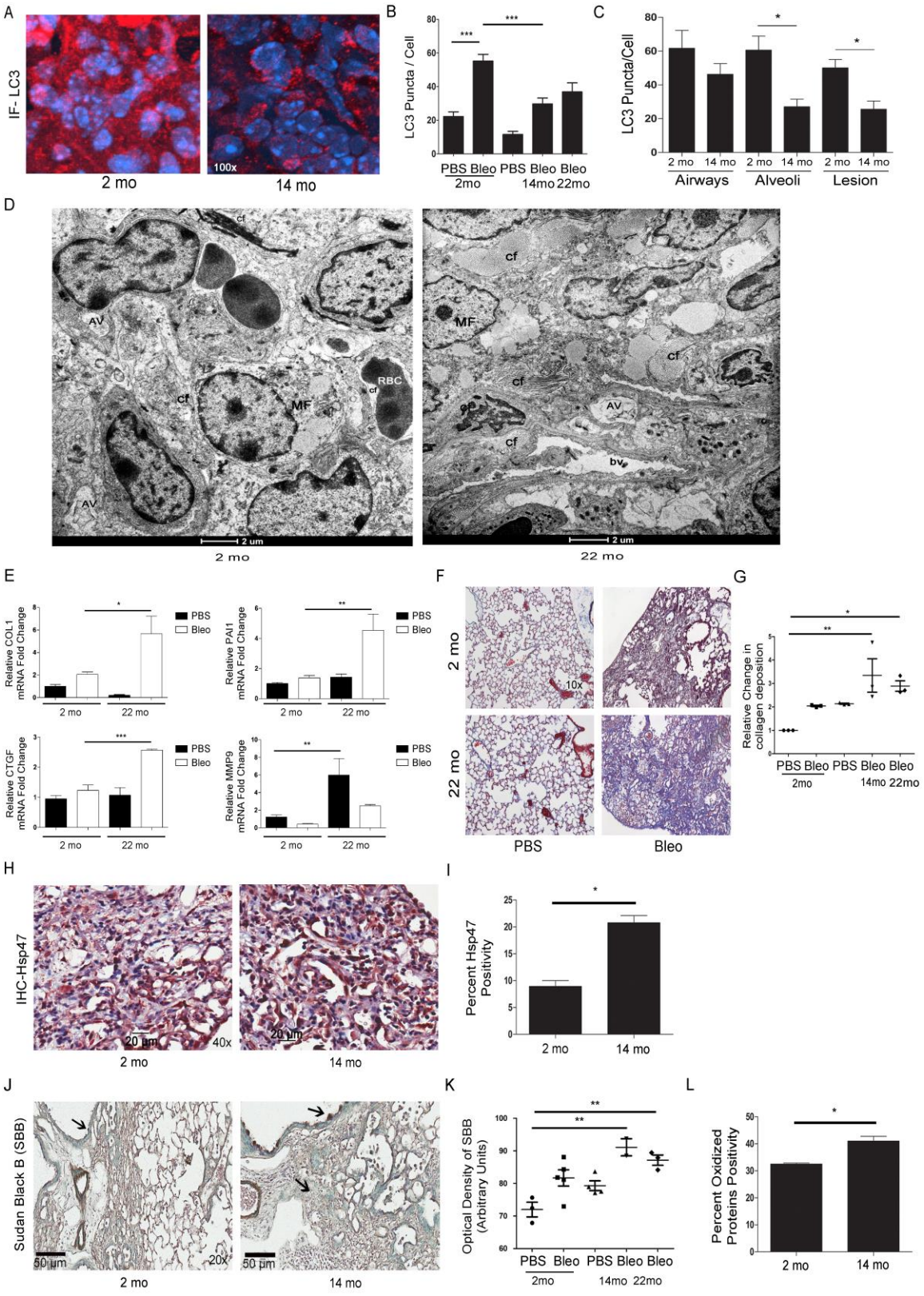
A
IF- LC3
100x
2 mo
14 mo
B
LC3 Puncta / Cell
PBS Bleo PBS Bleo Bleo
2mo 14mo 22mo
C
LC3 Puncta/Cell
2 mo 14 mo 2 mo 14 mo 2 mo 14 mo
Airways Alveoli Lesion
D
AV
cf
MF
RBC
bv
2 um
2 mo
22 mo
E
Relative COL1 mRNA Fold Change
Relative PAI1 mRNA Fold Change
Relative CTGF mRNA Fold Change
Relative MMP9 mRNA Fold Change
PBS
Bleo
2 mo
22 mo
F
2 mo
22 mo
10x
PBS
Bleo
G
Relative Change in collagen deposition
PBS Bleo PBS Bleo Bleo
2mo 14mo 22mo
H
IHC-Hsp47
20 um
40x
2 mo
14 mo
I
Percent Hsp47 Positivity
2 mo
14 mo
J
Sudan Black B (SBB)
50 um
20x
2 mo
14 mo
K
Optical Density of SBB (Arbitrary Units)
PBS Bleo PBS Bleo Bleo
2mo 14mo 22mo
L
Percent Oxidized Proteins Positivity
2 mo
14 mo

Figure 2.1. Bleomycin exposure exacerbates age-dependent differences in lipofuscin content, collagen deposition, Hsp47 and the autophagic marker LC3. A-B) Representative images and quantification of LC3b staining show the autophagic response to injury in 2-, 14- and 22-month-old mouse lung. Positive LC3b appears as red punctae. Nuclei counterstained with DAPI (blue). C) Quantification of LC3 punctae in 2-month-old and 14-month-old mice in different sections of the lung tissue, including airways, alveolar epithelium, and fibrotic tissue. D) Representative electron microscopy images in 2-month-old and 22-month-old mice post Bleo exposure showing collagen fibrils. Collagen fibrils labeled as cf, blood vessels as bv, myofibroblasts as MF, red blood cells as RBC, capillaries as c and autophagic vesicles as AV. E) qRT-PCR analysis for fibrotic markers COL1, PAI1, CTGF and MMP9 expression in 2-month-old (n=5) and 22-month-old mice (n=4) after Bleo exposure. F-G) Representative images and quantification of Masson's trichrome staining to evaluate collagen deposition in 2- and 22-month-old lung. Positive collagen deposition appears blue. H-I) Representative images and quantification of Hsp47 staining/cell demonstrate fibrogenesis in middle-aged lung. Positive cells stain red (NovaRed stain). Nuclei counterstained with haematoxylin. J) Representative images of Sudan Black B (SBB) staining for lipofuscin during fibrogenesis in 2- and 14-month-old lung. Positive SBB appears dark brown-black. Nuclei counterstained with methyl green (blue-green). Arrows show SBB positive lipofuscin. K) Quantification of SBB staining in 2-, 14- and 22-month-old mouse lung sections. L) Quantification of accumulated oxidized proteins in 2- and 14-month-old lung after oropharyngeal aspiration of Bleo or PBS vehicle only, at 14 days post exposure. *P<0.05, **P<0.01, ***P<0.005.

mice, including 14-month-old and 22-month-old, for lipofuscin content, a non-degradable intralysosomal polymeric substance that accumulates during aging. This was in order to determine whether what have heretofore been considered age-related changes in lipofuscin can be detected in fibrotic lungs of young and late middle-aged mice. Assessment of Sudan Black B (SBB) staining and quantification by ImageJ revealed more lipofuscin aggregates in the lungs of 14-month-old mice versus 2-month-old mice after oropharyngeal aspiration of bleomycin indicative of lysosome damage and reduced lysosomal degradation (Fig. 2.1J-K). No significant differences were detected between 14-month-old and 22-month-old mice. Additionally, the OxyIHC™ Oxidative Stress system for protein oxidation showed increased levels of oxidized proteins suggesting age-related changes in degradation processes result in higher levels of fibrosis and damaged proteins (Fig. 2.1L).

Age-related changes in the mitophagic response to bleomycin

In accordance with the increase in collagen deposition in aging lung (Fig. 2.1F-G) and mitochondrial dysfunction observed in age-related diseases[31, 75], we chose to further evaluate changes in mitophagy in old mice (22-month-old) and young mice (2-month-old) treated with bleomycin. qRT-PCR analysis demonstrated PINK1 expression was reduced in 22-month-old compared to 2-month-old mice (Fig. 2.2A). Sequestration of mitochondria inside autophagic vacuoles was determined by colocalization of TOM20 (mitochondria) and LC3B (autophagosome) by immunofluorescence in lung tissue from control (PBS) and bleomycin-exposed young and old mice (Fig. 2.2B-C). Quantification of mitophagy events demonstrated that higher levels of mitochondria inside autophagic vacuoles were induced in the young mice as compared to older mice after bleomycin exposure suggesting a deficient mitophagic response after lung injury in aging mice (Fig. 2.2B-C).

To demonstrate if the reduced PINK1 expression by TGFβ1 in normal human lung fibroblasts is recapitulated in animal models of pulmonary fibrosis, we exposed mice to 3 x 10^8 PFU of replication-deficient adenovirus encoding either GFP (AdGFP) or active TGFβ1 (AdTGFβ1). Real-time RT-PCR and western blot analyses from whole lung extracts were performed 7 days post-infection. The results demonstrated a TGFβ1-associated reduction in PINK1 in the lung 7 days post-infection (Fig. 2.2D). A corresponding reduction in PINK1 protein levels was confirmed by western blots and densitometry (Fig. 2.2E-F). Finally, immunohistochemistry performed on human IPF

Figure 2.2

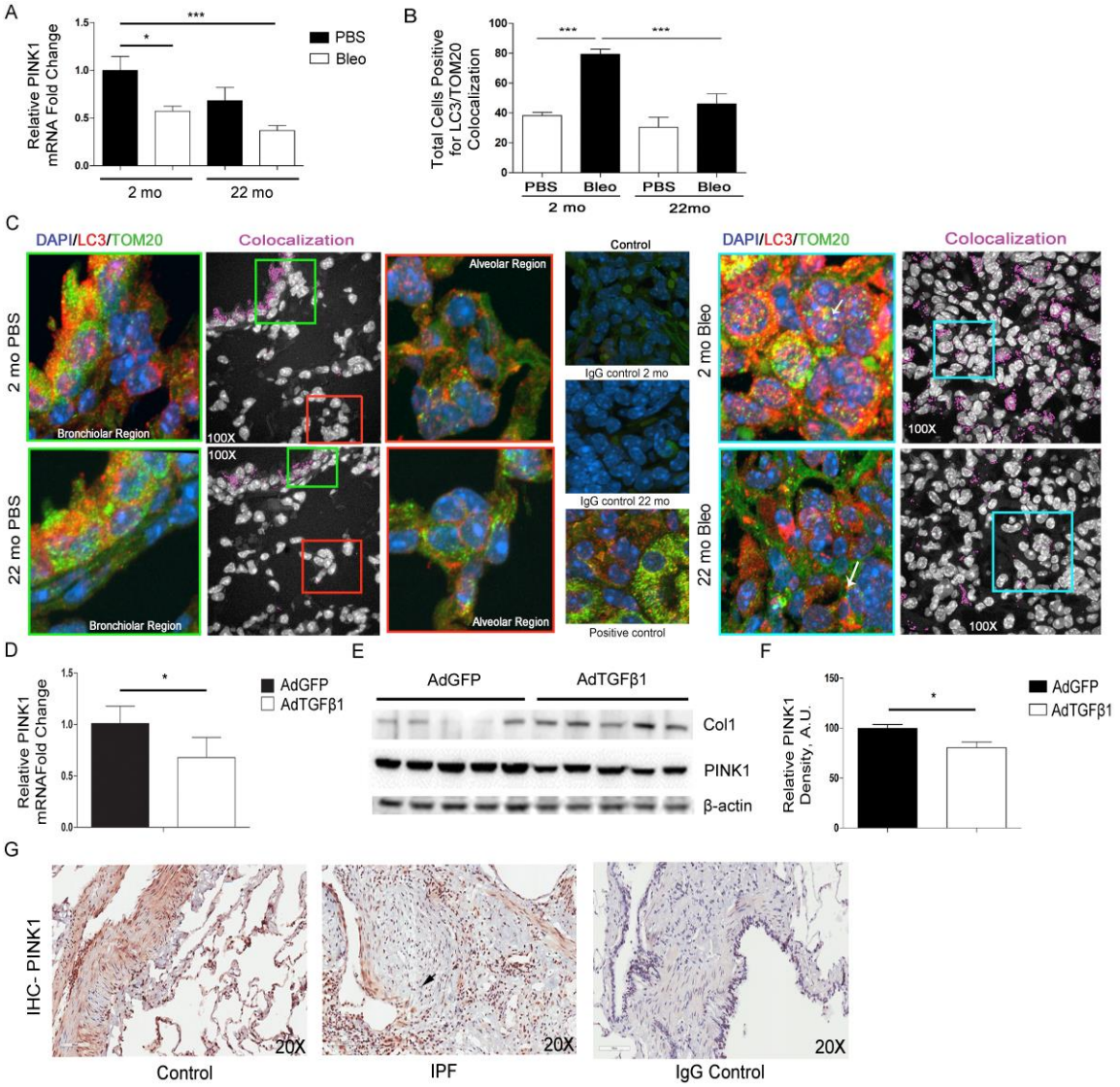

Figure 2.2. Deregulated mitophagy and PINK1 expression in pulmonary fibrosis. A) qRT-PCR analysis for PINK1 expression in 2-month-old (n=5) and 22-month-old mice (n=5) after oropharyngeal aspiration of bleomycin (Bleo) or PBS vehicle only, at 14 days post exposure. B) Quantification of number of mitochondria inside autophagic compartments in young and old mice exposed with vehicle (PBS) or bleomycin. C) Representative images of the basal level of colocalization of LC3 punctae and TOM20, a mitochondria marker, in young (2-month-old) and old (22-month-old) mouse lung tissue. Yellow points indicate mitochondria inside autophagosomes in merged color images as positive LC3 staining appears as red punctae and TOM20 green. Colocalization points appear pink in black and white image. Nuclei counterstained with DAPI appears blue. *Row 1*: Highlighted green square focuses on bronchiolar region of lung in PBS exposed (control) mouse. *Row 2*: Colocalization points in PBS exposed (control) mouse lung. *Row 3*: Highlighted red square focuses on alveolar region of lung in PBS exposed (control) mouse. *Row 4*: IgG-only controls in lung tissues used as negative controls. Kidney stained for LC3 and TOM20 used as positive control. *Row 5*: Highlighted blue square focuses on fibrotic region of lung in bleomycin (Bleo) exposed mouse lung. *Row 6*: Colocalization points in Bleo exposed mouse lung. D) qRT-PCR analysis for mRNA expression levels of PINK1, at 7 days post oropharyngeal aspiration of control Adenovirus-GFP (AdGFP) or Adenovirus-TGFβ1 (AdTGFβ1) in mice (n=5 per treatment). E) Representative western blot (WB) for collagen type I (Col1) and PINK1 expression from AdTGFβ1 or AdGFP control infection in mouse

lung, at 7 days post infection. β-actin used as loading control. F) Densitometry analysis of PINK1 expression shown in Figure 3.2E. G) IHC in lung tissue samples from an IPF patient and a control patient show differential expression of PINK1. Positive cells appear red (NovaRed stain). Nuclei counterstained with haematoxylin appear blue. Arrow shows fibrotic lesion. IgG only used as negative control. Arbitrary Units abbreviated as AU. *P<0.05, ***P<0.005.

lung and control lung samples confirmed low levels of PINK1 in the IPF tissue and non-detectable PINK1 staining in the fibrotic foci (Fig. 2.2G).

3.3 Discussion

In accord, our studies in animal models of pulmonary fibrosis demonstrated that susceptibility to pulmonary fibrosis during aging correlates with reduced autophagy, measured by the number of autophagosomes and mitochondria associated with autophagosomes, an increase in lipofuscin deposits and age-dependent decline in PINK1 expression. Also, lung tissues from IPF patients express reduced levels of PINK1. Our research identified an inverse correlation between the number of autophagosomes and the accumulation of lipofuscin and collagen deposits in bleomycin-treated mice. We propose that deficient autophagy can exacerbate lung injury by promoting oxidative stress, dysfunctional mitochondria and lipofuscin deposits. The accumulation of lipofuscin further limits autophagic turnover, exacerbating fibrosis. Interestingly, neutralization of IL-17A by autophagy was able to protect against bleomycin-induced pulmonary fibrosis in mice[90]. Here, we propose a model for how insufficient responses of autophagic and mitophagic processes after lung injury may contribute to the development of pulmonary fibrosis (Fig. 2.3A).

Our finding that repressed autophagic responses during aging contributes to lung fibrosis contrasts with the excessive autophagy that underlies the pathogenesis of emphysema[91]. Our results support the possibility that autophagy may be a critical determinant of the response to lung injury by settling the development of fibrosis or emphysema.

Our findings indicate PINK1 is another target repressed by TGFβ1. Studies demonstrating that TGFβ1 regulates phosphatase and tensin homolog (PTEN), a driver of PINK1 expression, are consistent with this finding[92]. PTEN deficiency promotes fibrogenesis[93, 94]. The relevance of our findings was further confirmed by our recent observation that PINK1 knock-out mice have a pro-inflammatory environment characterized by increased levels of IL-6 (data not shown). In fact, recent studies in PINK1 null mice demonstrated high levels of TGFβ1 and susceptibility to pulmonary fibrosis[95, 96]. The TGFβ1–PINK1 interaction could constitute a feed forward cycle that favors the perpetuation of fibrosis that is characteristic of the IPF lung. Further analyses of PINK1 knock-out mice will better define the role of PINK1 in lung aging and pulmonary fibrosis.

It is still unclear if or how TGFβ1 influences human aging. In *C. elegans*, the TGFβ signaling pathway represses lifespan[97]. In humans, a correlation between a polymorphism in the TGFβ1 gene and longevity suggests a similar function[98]. The aging lung displays a profibrotic phenotype characterized by enhanced TGFβ1 expression and signaling[31, 99, 100]. Our data describe the influence of TGFβ1 upon aging through changes in autophagy, mitochondrial homeostasis and promotion of aberrant responses to lung injury.

At the cellular level, reduction of autophagy and mitophagy could abet myofibroblast differentiation and assist adaptation to metabolic changes and thereby prevent apoptosis. However, deregulated cellular proteostasis and mitochondria recycling may contribute to other features of interstitial lung diseases, such as disrupted cellular redox, chronic inflammation, and increased vulnerability of the lung epithelia to second hit injury[83, 101]. Conversely, moderate induction of autophagy promotes resistance to oxidative stress and extension of lifespan[56]. In fact, we and others have found that hormetic compounds like resveratrol promote autophagy and mitochondrial homeostasis, while inhibiting FMD and pulmonary fibrosis in animal models[102, 103]. Finally, we propose promoting autophagy and mitochondrial homeostasis to intervene against age-related lung diseases like pulmonary fibrosis.

Figure 2.3

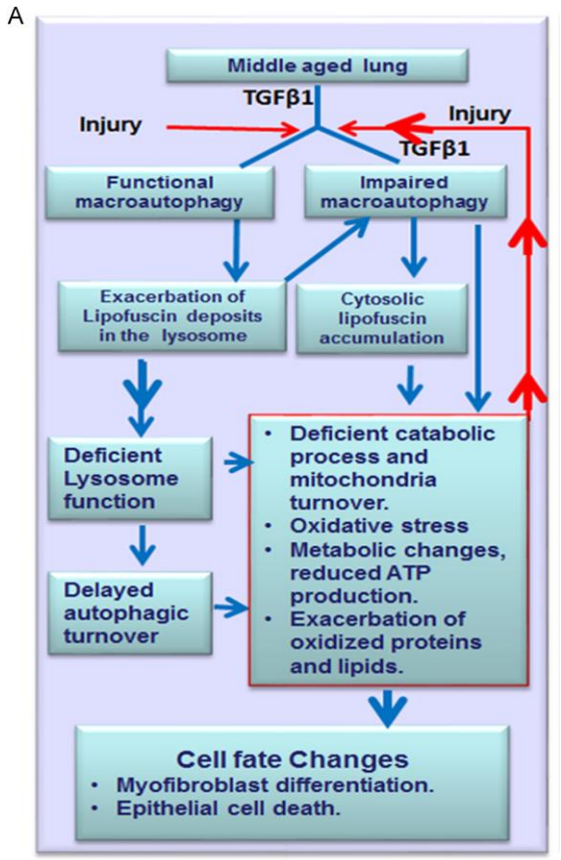

Figure 2.3. Schematic representation of a proposed model for fibrosis. During aging, TGFβ1 expression increases in the lung. Upon injury in an aging lung, autophagy is induced to cope with the elevated cellular stress. Lysosomal degradation of large amounts of damaged or oxidized proteins results in accumulation of lipofuscin promoting lysosome dysfunction. In consequence, autophagic and thereby mitophagic turnover is delayed exacerbating oxidative stress and mitochondrial homeostasis in cells. Induced levels of oxidative stress and mitochondrial dysfunction initiates further tissue damage inducing a positive feedback loop ultimately promoting myofibroblast differentiation and epithelial cell death driving the development of fibrosis.

3.4 Materials & Methods

Mice & Tissue Samples. All animal protocols were performed as approved by the Tulane University Institutional Animal Care and Use Committee. C57BL/6 male mice

were obtained from the Jackson Laboratory (Bar Harbor, ME, USA). Animals were anesthetized with 2% isoflurane vapor (VetOne, Meridian, ID, USA) in oxygen. Treatments were administered in 50 μl of sterile PBS by oropharyngeal aspiration. C57Bl/6 mice aged young (2-month-old, n=5 per treatment), middle-aged (14-month-old, n=5) and old (22-month-old, n=5 per treatment) received 2 U/kg Bleomycin (Teva Parenteral Medicines, Irvine, CA, USA) or vehicle only (PBS) for control. C57Bl/6 mice aged 6-8 weeks were treated with 3 x 108 PFU of replication-deficient adenovirus encoding either GFP (control group, AdGFP, n=5) or active TGF-β1 (AdTGF-β1, n=5). Animals were anesthetized with 80 mg/kg ketamine plus 8 mg/kg xylazine and euthanized by exsanguination 14 or 7 days after bleomycin or adenovirus treatments respectively. The right lungs were snap-frozen in liquid nitrogen and stored at -80°C for RNA or protein isolation. The left lungs were inflation-fixed with 10% neutral buffered formalin (Sigma-Aldrich, Sigma-Aldrich Corp., St. Louis, MO, USA) through the trachea at 25 cm H2O pressure for 15 min, excised from the mice, and stored in fresh 10% neutral buffered formalin at 4°C for histology. At least two independent experiments were performed and analyzed. Sections from Human IPF and control lung specimens were obtained from the NIH Lung Tissue Research Consortium (LTRC).

RNA Isolation & qRT-PCR. Total RNA was isolated using Trizol® Reagent (Invitrogen, Carlsbad, CA, USA) according to manufacturer's instructions. RNA concentration was measured using a NanoDrop spectrophotometer (Thermo Scientific Nanodrop, Nanodrop Technologies, Wilmington, DE, USA). For quantitative real-time PCR (qRT-PCR) analysis, 1 μg of total RNA was reverse transcribed using iScript™ cDNA Synthesis Kit (Bio-Rad Laboratories Inc., Hercules, CA, USA) according to

manufacturer's protocol. Quantitative real-time PCR reactions were performed using iQ^{TM}SYBR® Green Supermix (Bio-Rad) in the Bio-Rad MyiQ iCycler (Hercules, CA). Relative expression levels were calculated using the $2^{-\Delta\Delta C(T)}$ method and normalized to 36b4 expression. All primer information given in Table 1.1.

Histology, Immunohistochemistry & Immunofluoresence. Histologic sections of lung tissue (4 μm) were deparaffinized and rehydrated according to the standard protocol. Masson's trichrome staining was performed as previously described[31]. For immunohistochemical samples, slides were incubated in BLOXALL™ Blocking solution (Vector Laboratories, Burlingame, CA, USA) for 10 m before proceeding with antigen retrieval. Slides were then incubated for 20 m in 0.5% Ammonium chloride and rinsed in PBS then incubated in 0.3M Glycine for 10 m. Slides were blocked in HEPES NaCl buffer (20 mM HEPES, 1% BSA, 135 mM NaCl) for 5 min then incubated for 30 m with blocking serum. The primary antibody of Hsp47 (H300) was used at a dilution of 1:50 was incubated for 30 m followed by diluted biotinylated secondary antibody for 30 m. Slides were then incubated with NovaRed Vectastain®ABC Reagent (Vector Laboratories) for 30 m then nuclei counterstained with haematoxylin and mounted. For immunofluorescence samples, slides were permeabilized in 0.2% Trition-X in TBS buffer for 45 m at RT and washed in TBS after blocking with 10% BSA in TBS (blocking serum) for 1 h, the primary antibody was added. Antibodies to LC3 (rabbit) and TOM20 (mouse) were used at a dilution of 1:200 and incubated overnight at 4°C in a humidified chamber. Secondary antibodies AlexaFluor 594 goat anti-rabbit IgG (Invitrogen) and AlexaFluor 488 goat anti-mouse IgG (Invitrogen) were employed for

immunofluorescence detection at a dilution of 1:1000. Nuclei were counterstained using DAPI (Invitrogen) before mounting in Prolong Gold antifade media (Invitrogen).

Sudan Black B Staining. Tissue slides were deparaffinized and rehydrated to 70% ethanol. Freshly prepared Sudan Black B (SBB; Fisher Scientific, Pittsburgh, PA, USA) stain was prepared as previously described[104] and slides incubated in SBB for 20 min. Nuclei were counterstained with methyl green.

Electron Microscopy. NHLF cultured on 10 cm2 plates were fixed in 2.5% glutaraldehyde in 0.1 M sodium cacodylate buffer pH 7.4 for 1 h at room temperature. Samples were washed three times for 5 m in 0.1 M sodium cacodylate buffer and sent to the Electron Microscopy Core Facility of the Department of Cell Biology at Yale University School of Medicine (New Haven, CT). The Yale core facility provides images and grids for subsequent analysis with the Tecnai G2 F30 TWIN 300 kV/FEG Transmission Electron Microscope (FEI, Hillsboro, OR, USA) at Tulane University.

Imaging & Quantitative Analysis. For histology and immunohistochemistry analysis, images were captured with a Scan Scope Aperio, version 10.2.0.0 Aperio Technologies (Leica Biosystems, Buffalo Grove, IL, USA) at the same magnification with similar contrast. TIFF file images were then exported and analyzed using ImageJ (imagej.nih.gov). For quantification of Sudan Black B staining, images were inverted, applied threshold and positive areas measured. For quantification of Hsp47 staining, color images were deconvoluted, and positive red color areas measured with the result expressed as the fraction of positive-stained pixels over total area analyzed. For immunofluorescence, images were captured in Z-stacks using Nikon A1+ Inverted

Confocal microscope (Nikon Instruments Inc., Melville, NY, USA). Three-dimensional reconstruction and volume rendering of Z-stacks were carried out with appropriate ImageJ plug-in and NIS element AR 4.30 (Nikon) software. For quantification of LC3 punctae, images were captured with an Olympus BX60 microscope equipped with epifluorescence optics (Olympus, Melville, NY) and coupled device camera Magnafire (MagnaFire 2.6; Olympus) with a barrier filter equipped for simultaneous detection of FITC, Texas red and DAPI. TIFF files were normalized, merged and analyzed with Image J. The number of LC3 dots was counted in at least five independent visual fields at 100x oil objective of magnification. The results were expressed as puncta per cell. For quantification of mitochondria within autophagosomes, the colocalization of autophagosomes (LC3 punctae) and mitochondria (TOM20) was detected using the Colocalization Finder plug-in in Image J.

Statistical analysis. All data is expressed as mean values ± SEM. Comparisons between two groups were made using unpaired, two-tailed Student's t test. Analysis of variance (ANOVA) followed by Bonferroni's multiple comparison test was used for multiple groups. Statistical significance was assigned at a value of $p < 0.05$. All experiments were repeated at least twice.

CHAPTER 4. DOWN-REGULATION OF SIRT3 BY TGFβ1 PROMOTES MYOFIBROBLAST DIFFERENTIATION

4.1 Introduction

Sirtuins, NAD+-dependent protein deacetylases, can modulate the oxidative stress response, metabolism, and lifespan[105-107]. Due to its preferential mitochondrial localization and association with extended lifespan in humans, Sirtuin 3 (SIRT3) emerged in the last few years as a protein of particular interest in aging studies and age-related diseases[108-112].

Promotion of oxidative stress and myofibroblast differentiation by TGFβ1 signaling across tissues is recognized as a critical factor in the pathogenesis of systemic scleroderma (Ssc) and IPF. However, it is unclear whether or how TGFβ1 influences tissue aging or how biological aging promotes the fibrotic response. New evidence demonstrates that impairment of mitochondrial homeostasis and recycling, mediated in part by TGFβ1, may contribute to age-related lung diseases such as IPF. Nevertheless, the cell type-dependent molecular mechanisms of aging that promote fibrogenesis remain unknown.

SIRT3 participates in regulating multiple processes through its effects on the acetylation status of proteins involved in the oxidative stress response, mitochondrial dynamics, and metabolism. Such mechanisms have been shown to be altered in pulmonary fibrosis. For example, SIRT3 promotes deacetylation of forkhead box O3a

(FoxO3a) leading to FoxO3a-dependent gene expression[113]. SIRT3 also deacetylates several components of the mitochondrial antioxidant response and respiratory chain, including the mitochondrial matrix protein isocitrate dehydrogenase 2 (IDH2), a major source of reduced nicotinamide adenine dinucleotide phosphate (NADPH). Additionally, SIRT3 regulates SOD2, glutathione peroxidase-1 (GPX1), adenosine triphosphate (ATP) synthase, and cytochrome c[114-118]. SIRT3 also deacetylates and destabilizes hypoxia-inducible factor-1α (HIF-1α) which is involved in the metabolic reprogramming of mitochondria[119]. Finally, SIRT3 regulates mitochondrial dynamics during stress by activating optic atrophy 1 (OPA1), a dynamin-related guanosine triphosphatase required for the fusion of mitochondria[120]. Therefore, due to the myriad of roles SIRT3 plays in the regulation of mitochondrial function, metabolism, and dynamics, it is expected that changes in SIRT3 expression within the aging lung will result in an altered, and possibly compromised, response to injury. We hypothesized SIRT3 may play a role in preventing TGFβ1-induced myofibroblast differentiation by activation of SOD2 and other antioxidant response substrates.

4.2 Results

Down-regulation of SIRT3 by TGFβ1 promotes acetylation of major oxidative stress response regulators SOD2 and IDH2

We first endeavored to determine if TGFβ1 can regulate SIRT3 expression. At the protein level, WB analysis showed that TGFβ1 reduced the expression of SIRT3 and SOD2 in NHLF at 24 h, which was restored to normal levels in the presence of

resveratrol (RSV), a polyphenol compound that inhibits myofibroblast differentiation and induces SIRT3 RNA expression[121-123] (Fig. 3.1A-D). Analysis of qRT-PCR for NHLF treated with increasing doses of TGFβ1 for 24 h demonstrated a decline in SIRT3 and SOD2 transcript levels in a dose-dependent manner (Fig. 3.1E).

Since SIRT3 is a mitochondrial deacetylase for IDH2 and SOD2, two major components of the mitochondrial antioxidant pathway, we examined their acetylation status in the presence of TGFβ1. We observed an increase in the acetylated form of IDH2 (K413) in NHLF at 24 h with TGFβ1 treatment (Fig. 3.1F-G). Due to decreased SOD2 levels in total cell lysate, the acetylation status of SOD2 in the mitochondria was interrogated to provide a better understanding of SIRT3-mediated deacetylase activity and the type of oxidative stress response during FMD. The WB analysis revealed an increase in acetylated SOD2 (K68) in mitochondria, suggesting that TGFβ1-induced repression of SIRT3 results in less SIRT3-dependent deacetylase activity and antioxidant response mediated by IDH2 and SOD2 (Fig. 3.1H-I). Immunofluorescence and subsequent quantification confirmed the reduction in SIRT3 and SOD2 levels post-TGFβ1 treatment (Fig. 3.1J-M). Our findings correlate with the increase in ROS during FMD, previously reported[124].

Figure 3.1

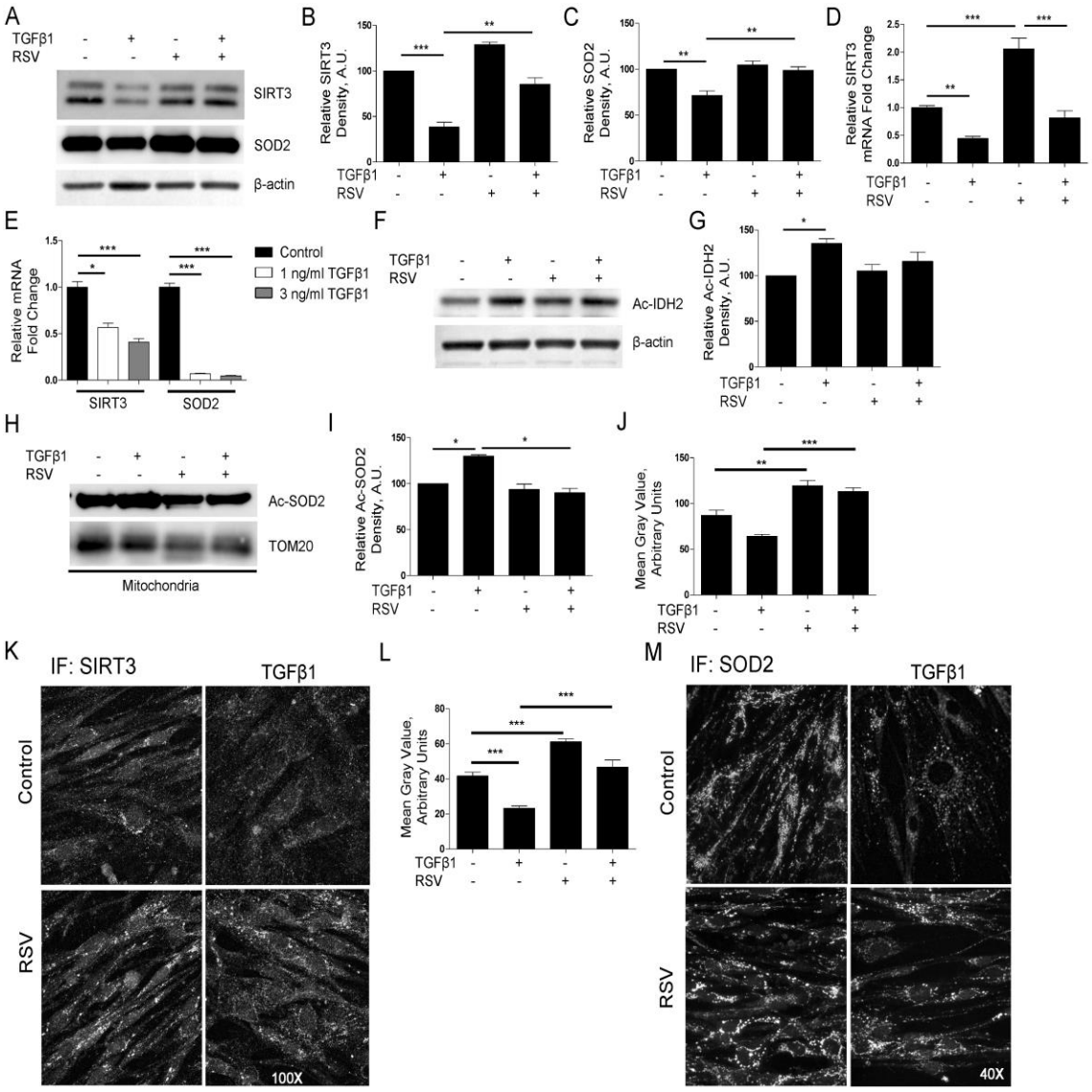

Figure 3.1. TGFβ1 down-regulates SIRT3 concomitant with acetylation of major oxidative stress response regulators. A) Representative WB for SIRT3 and SOD2 expression from NHLF-treated or untreated, with TGFβ1 and/or resveratrol. β-actin was used as a loading control. B-C) Densitometry analysis of WB for SIRT3 and SOD2 expression shown in (A). D) Real-time RT-PCR (qRT-PCR) analysis for SIRT3 mRNA expression in NHLF-treated, with or without TGFβ1 and/or resveratrol, at 24 h. E) qRT-PCR analysis for TGFβ1 dose-dependent changes in the transcriptional levels of SIRT3 and SOD2 mRNA expression in NHLF after 24 h. F) Representative WB for acetylated IDH2 expression from NHLF-treated or untreated, with TGFβ1 and/or resveratrol. β-actin was used as a loading control. G) Densitometry analysis of WB for acetylated IDH2 expression is shown in (F). H) Representative WB of mitochondria isolated from NHLF-treated or untreated, with TGFβ1 and/or resveratrol probed for acetylated SOD2 (Ac-SOD2). TOM20 was used as a loading control. I) Densitometry analysis of WB for acetylated SOD2 expression is shown in (H). J-K) Quantification and representative immunofluorescence (IF) images for SIRT3 in NHLF-treated, with TGFβ1 and/or RSV at 24 h. L-M) Quantification and representative immunofluorescence images for SOD2 in NHLF-treated, with TGFβ1 and/or resveratrol at 24 h. Resveratrol abbreviated as RSV. Arbitrary Units abbreviated as AU. *$p < 0.05$, **$p < 0.01$, ***$p < 0.005$.

Down-regulation of SIRT3 promotes myofibroblast differentiation mediated by TGFβ1

To determine the relevance of the repression of SIRT3 during fibroblast-myofibroblast differentiation (FMD) mediated by TGFβ1, we transfected NHLF with siRNA targeting SIRT3 and evaluated the expression of fibrotic markers. qRT-PCR analyses demonstrated that repression of SIRT3 promoted expression of collagen type I and PAI1 which was significant compared to the non-targeting siRNA control after TGFβ1 treatment (Fig. 3.2A-C). WB analyses confirmed the induction of Col1 and Pai1 expression at the protein level (Fig. 3.2D-G). These results indicate that inhibition of SIRT3 may promote TGFβ1-dependent myofibroblast differentiation.

Figure 3.2

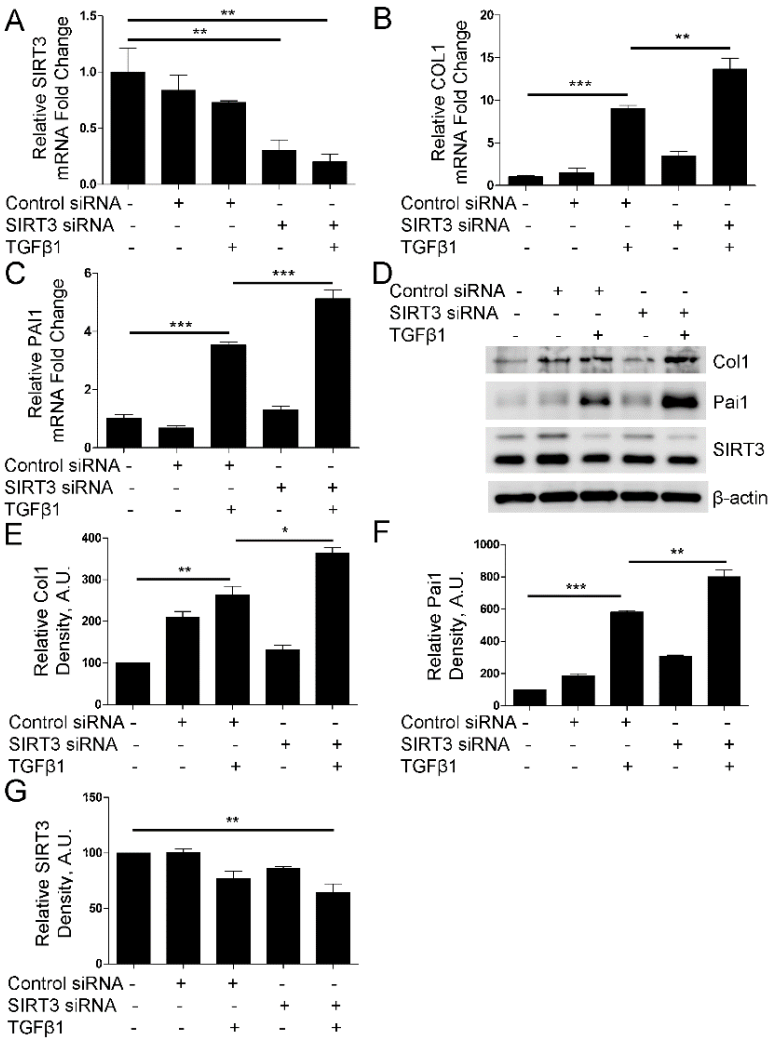

Figure 3.2. Down-regulation of SIRT3 promotes myofibroblast differentiation mediated by TGFβ1. A-C) Real-time qRT-PCR analysis from NHLF, transfected with siRNA targeting SIRT3, treated with or without TGFβ1, to evaluate transcriptional changes in SIRT3 and fibrotic markers collagen type I (COL1) and plasminogen activator inhibitor-1 (PAI1). D) Representative WB for Col1, PAI1 and SIRT3 expression in NHLF-deficient in SIRT3. β-actin was used as a loading control. E-G) Densitometry analysis of WB for fibrotic markers and SIRT3 expression is shown in (D). Arbitrary units are abbreviated as AU. *$p < 0.05$, **$p < 0.01$, ***$p < 0.005$.

Over-expression of SIRT3 decreases myofibroblast differentiation potential mediated by TGFβ1

Since we demonstrated that down-regulation of SIRT3 promotes myofibroblast differentiation mediated by TGFβ1, we further interrogated the possible inhibitory effect of SIRT3 on TGFβ1-induced myofibroblast differentiation. For this experiment, expression of fibrotic markers was analyzed in NHLF transfected with an adenovirus encoding either GFP (AdGFP, control) or SIRT3 (AdSIRT3) in the presence or absence of TGFβ1 and cofactor NAD^+. Analyses by qRT-PCR showed a significant reduction in COL1, α-SMA, and PAI1 expression post-TGFβ1 treatment when SIRT3 was over-expressed (AdSIRT3) compared to control treatment (AdGFP) (Fig. 3.3A-D). We confirmed the statistically significant decrease in the expression of fibrotic markers α-SMA and Pai1 by WB as presented by densitometry analysis (Fig. 3.3E-H). Taken together, these data support the role of SIRT3 in modulating TGFβ1-mediated FMD.

Figure 3.3

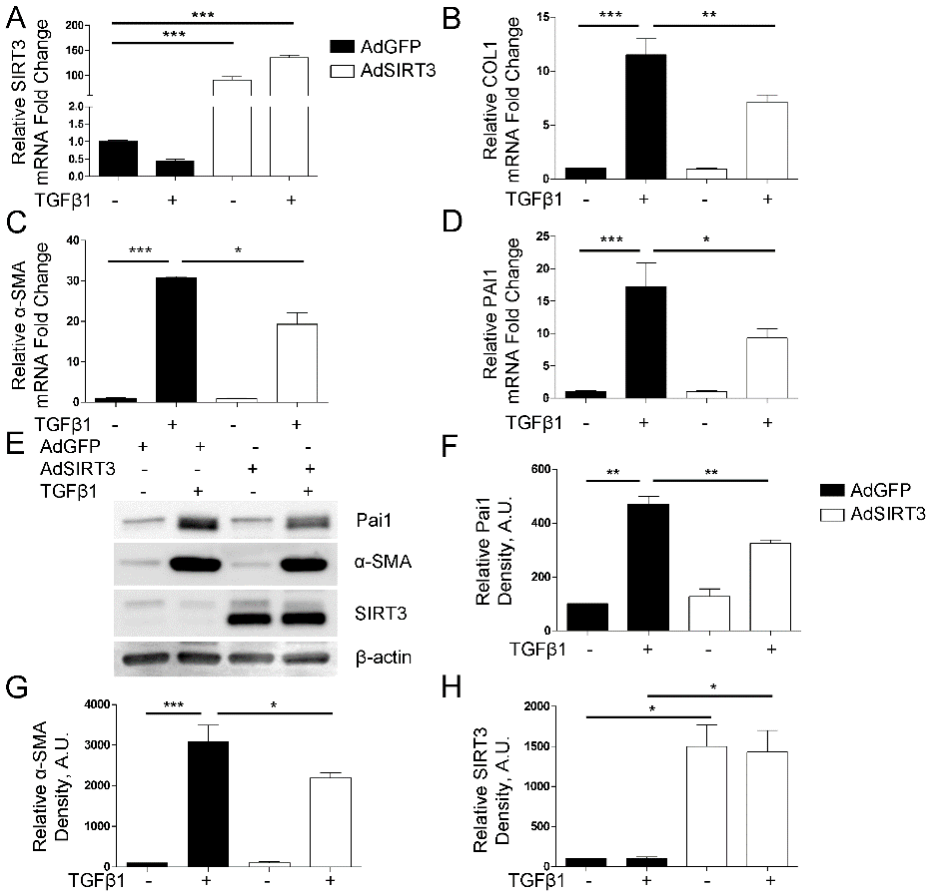

Figure 3.3. Over-expression of SIRT3 decreases myofibroblast differentiation potential mediated by TGFβ1. A-D) Real-time qRT-PCR analysis from NHLF, transfected with adenovirus over-expressing SIRT3, treated with or without TGFβ1, to evaluate transcriptional changes in SIRT3 and fibrotic markers collagen type I (COL1), α-smooth muscle actin (α-SMA), and plasminogen activator inhibitor-1 (PAI1). E) Representative WB for PAI1, α-SMA and SIRT3 expression in NHLF over-expressing SIRT3. β-actin was used as a loading control. F-H) Densitometry analysis of WB for fibrotic markers and SIRT3 expression shown in (E). Arbitrary units are abbreviated as AU. *$p < 0.05$, **$p < 0.01$, ***$p < 0.005$.

4.3 Discussion

Mitochondria play a central role in energy metabolism and age-related diseases. SIRT3, an NAD+-dependent histone deacetylase with preferential localization to the mitochondria, has previously been associated with lifespan[67]. We demonstrated that

TGFβ1 reduces the expression of SIRT3, promoting changes in oxidative stress, and favoring myofibroblast differentiation and the exacerbation of fibrotic tissue. This downregulation by TGFβ1 is presumably Smad3-dependent, although further experiments are necessary to confirm this hypothesis. Our study indicates that SIRT3 deficiency promotes the fibrotic effects of TGFβ1 and over-expression of SIRT3 can diminish the effects of TGFβ1 in FMD, probably through maintenance of an efficient oxidative stress response and promotion of mitochondrial integrity and metabolism during stress.

Several studies previously reported that myofibroblast differentiation, driven by TGFβ1, is characterized by an increase in ROS due in part to unbalanced mitochondria homeostasis, deficient recycling, and deficient oxidative stress responses[124-127]. This process can be inhibited by restoring redox homeostasis using antioxidants or NADPH oxidase 4 (NOX4) inactivation[128, 129]. Other studies have shown that increased cellular superoxide levels are characteristic of stressed SIRT3-deficient mouse embryonic fibroblasts (MEF)[130]. By contrast, promotion of SIRT3 reduces reactive oxygen species in other tissues by deacetylating and activating IDH2, a major source of NADPH, as well as deacetylating and activating SOD2[131]. Thus the ability of SIRT3 to protect cells from oxidative stress has been shown to be dependent on SOD2- and IDH2-induced activity[118, 131, 132]. Our studies indicate that acetylation (deactivation) of SOD2 and IDH2 are characteristic of FMD. We demonstrated that resveratrol promotes SIRT3 expression and SOD2 and IDH2 deacetylation, thereby promoting cellular homeostasis and inhibition of myofibroblast differentiation[121, 124]. Taken together, our studies suggest that the TGFB1/SIRT3 pathway is responsible for altered SOD2 and IDH2 acetylation, the post-

translational modification known to contribute to the promotion of oxidative stress and consequent myofibroblast differentiation in the aging lung. Interestingly, deficiency in SOD2 expression has been associated with premature aging[133, 134]. It is then possible that the deregulation of SOD2 activity by SIRT3 may contribute to accelerated biological aging and progression of age-related lung diseases like IPF and pulmonary fibrosis in SSc[135, 136].

SIRT3 also regulates OPA1, a dynamin-related guanosine triphosphatase required for fusion of mitochondria, thereby altering mitochondrial dynamics during stress[120]. SIRT3 has been shown to interact and deacetylate FoxO3a within mitochondria as well as increase FoxO3a-dependent gene expression[113]. FoxO3a modulates mitochondrial mass, ATP production, oxidative stress response, and clearance of defective mitochondria through transcriptional regulation of autophagy-related genes[137-139]. FoxO3a has been shown to be inactive (phosphorylated) in the fibrotic lungs of IPF patients[140] and deficiency of FoxO3a protects myofibroblasts from undergoing apoptosis[141]. In fact, induction of SIRT3 has been shown to inhibit cardiac hypertrophic response by increasing FoxO3a-dependent antioxidant defense mechanisms in mice[69]. We previously demonstrated that fibrotic lung is characterized by a deficient autophagic response which others have shown is probably due to low FoxO3a expression in lung fibroblasts[124, 142]. In all, our studies support the role of the TGFB1/SIRT3/FoxO3a axis as a major regulator of autophagy and mitochondria dynamics in pulmonary fibrosis.

4.4 Materials & Methods

Cell Culture and Reagents. Normal human lung fibroblasts (NHLF) from the American Type Culture Collection (ATCC, Manassas, VA, USA) were maintained in Fibroblast Growth Medium-2 (FGM-2, Lonza, Walkersville, MD, USA) before serum starving cells in Fibroblast Basal Medium (FBM, Lonza) supplemented with 0.2% bovine serum albumin (BSA, Gemini Bio-Products Inc., Woodland, CA, USA). NHLF were then cultured in FBM plus 0.2% BSA for various treatments. Recombinant human TGFβ1 (R&D Systems, Minneapolis, MN, USA) was used at various concentrations from 1-3 nanogram per milliliter (ng/ml). Resveratrol and NAD+ from Sigma (St. Louis, MO, USA) were used at concentrations of 100 μM and 500 μM respectively.

Western Blots. Cells were harvested in 1× radioimmunoprecipitation assay (RIPA) buffer purchased from Cell Signaling (Danvers, MA, USA), sonicated, and quantified using the Bradford Method (Bio-Rad Laboratories Inc., Hercules, CA, USA). Protein samples combined with 4x NuPAGE LDS Sample Buffer and 10x NuPAGE Sample Reducing Agent (Invitrogen) for a final concentration of 1x for both buffers and boiled for 5 minutes. 20-25 micrograms of each protein sample was separated on NuPage SDS 4-12% Bis-Tris gradient gels (Invitrogen) and transferred onto PVDF membranes (Invitrogen). For time-dependent cell lysates, protein samples were separated on 15% Acrylamide 1.5M Tris/10% SDS gel. Membranes were blocked in 5% BSA in TBST or 5% nonfat dry milk (Blotting-Grade Blocker, Bio-Rad) in TBST for 1 h at RT then probed with primary antibody overnight at 4°C while shaking.

Antibodies were used at 1:1000 to probe for Collagen type I (Col1) and acetylated K68 SOD2 (Ac-SOD2) and were purchased from Abcam (Cambridge, MA, USA). Antibody to acetylated K413 IDH2 (Ac-IDH2) was purchased from GeneTel Laboratories LLC (1:1000, Madison, WI, USA). Antibodies to SIRT3 and β-actin were purchased from Cell Signaling (1:1000; Danvers, MA, USA). The antibody to translocase of outer mitochondrial membranes 20 kDa (TOM20) was purchased from Santa Cruz Biotechnology (1:500; Dallas, TX, USA). Antibody to SOD2 was purchased from EMD Millipore (1:1000; Billerica, MA, USA). Antibody to plasminogen activator inhibitor type 1 (Pai1) was purchased from PeproTech (1:10,000; Rocky Hill, NJ, USA). Antibody to alpha-smooth muscle actin (α-SMA) was purchased from Sigma-Aldrich (1:10,000; St. Louis, MO, USA). Anti-mouse immunoglobulin G (IgG), horseradish peroxidase (HRP)-linked and anti-rabbit IgG, HRP-linked (1:15,000; Cell Signaling) for chemiluminescence detection; and near-infrared dye 800CW (IRDye 800CW)-labeled goat anti-rabbit IgG or IRDye 680-labeled goat anti-mouse IgG (1:15,000) were purchased from LiCor, Lincoln, NE, USA) for fluorescence detection.

RNA Isolation & qRT-PCR. Isolation of total RNA was performed using Trizol® Reagent (Invitrogen) according to manufacturer's instructions. RNA concentration was measured using a NanoDrop spectrophotometer (Thermo Scientific NanoDrop, NanoDrop Technologies, Wilmington, DE, USA). For qRT-PCR analysis, 1 μg of total RNA was reverse transcribed using an iScriptTM cDNA Synthesis Kit (Bio-Rad) according to the manufacturer’s protocol. Reactions were performed using iQ^{TM}SYBR® Green Supermix (Bio-Rad) and a Bio-Rad MyiQ iCycler. Relative

expression levels were calculated using the $2^{-\Delta\Delta C(T)}$ method and normalized to 36b4 expression. All primer information given in Table 1.1.

Mitochondria Isolation. Mitochondria were isolated from NHLF post-treatment using the Thermo Scientific (Rockford, IL, USA) Mitochondrial Isolation Kit for Cultured Cells according to the manufacturer's protocol.

Immunofluorescence Microscopy. NHLF were fixed in 4% paraformaldehyde (Electron Microscopy Sciences, Hatfield, PA, USA), permeabilized in 0.1% TX-100, 0.001% Tween-20, 0.3M Glycine, 0.2% BSA in TBS buffer for 5 min at RT, and washed in TBS after blocking with blocking serum (2.5% BSA, 5% normal goat serum, 0.05% TX-100, 0.0025% Tween-20 in TBS) for 30 min. Antibodies to SOD2 and SIRT3 were used at a dilution of 1:50 and incubated overnight at 4°C in a humidified chamber. AlexaFluor 594-conjugated goat anti-rabbit IgG (Invitrogen) was employed as secondary antibody at a dilution of 1:1000 for immunofluorescence detection. Nuclei were counterstained using 4’,6-diamidino-2-phenylindole (DAPI, Invitrogen) before mounting in Prolong Gold Antifade reagent (Invitrogen).

For image analysis of IF for SOD2 images were captured using an Olympus BX60 microscope equipped with epifluorescence optics (Olympus, Melville, NY) and a charge-coupled device camera (MagnaFire 2.6, Olympus). IF for SIRT3 images were captured using a Nikon A1+ Inverted Confocal microscope (Nikon Instruments Inc., Melville, NY, USA). All captured images were saved as 8-bit files and analyzed using Image J 1.48d (Wayne Rasband, NIH, Bethesda, MD, USA; http:imagei.nih.gov/ij).

Transfections. For small interfering ribonucleic acid (siRNA) knockdown experiments, NHLF were transfected using the Neon Transfection System (Invitrogen, Carlsbad, CA, USA) with siGENOME SMARTpool SIRT3-targeted siRNA (Dharmacon RNAi Technologies Inc., Lafayette, CO, USA), control non-silencing siRNA (Qiagen, Valencia, CA, USA), or sterile water (mock transfection) for a final concentration of 50 nM siRNA. Cells were plated on 60-mm tissue culture dishes in FGM-2 medium for 48 h after electroporation, as previously described[124]. For SIRT3 over-expression experiments, adenoviruses encoding GFP (control virus, Cat. No. 1060) or human SIRT3 (Cat. No. 1499) were purchased from Vector Biolabs (Malvern, PA, USA). NHLF were transfected with 3 x 106 PFU/ml and cultured for 72 h with co-factor NAD+ to assure that transfected SIRT3 would be functional and/or 1 ng/ml TGFβ1.

Statistical Analysis. All data are expressed as mean values ± standard error of the mean (SEM). Comparisons between two groups were made using the unpaired, two-tailed Student's t test. Analysis of variance (ANOVA) and Bonferroni's multiple comparison test were used for multiple groups. Statistical significance was assigned at a value of $p < 0.05$. All experiments were repeated at least twice.

CHAPTER 5. SIRTUIN 3 DEFICIENCY PROMOTES PULMONARY FIBROSIS

5.1 Introduction

At the cellular level, aging begins with the accumulation of molecular damage progressing to tissue and organ dysfunction. This molecular damage is theorized to arise from oxidative stress leading to mitochondrial DNA (mtDNA) mutations and organelle dysfunction[143]. Sirtuin 3 prevents oxidative stress-induced apoptosis through its deacetylation and activation of antioxidant responses. SIRT3 also plays a critical role in regulating mitochondrial functions and overall cell energy metabolism. SIRT3 deacetylates and activates various enzymes involved in the electron transport chain, fatty acid oxidation (FAO), and amino acid metabolism and therefore acts as a mediator in the shift from excess nutrient states to nutrient restriction[110]. This metabolic regulation by SIRT3 thus allows cells to meet energy demands and escape cell death. As such, SIRT3 is considered to be a protector against aging-associated diseases as evidenced by multiple age-related disease models[63, 110]. We hypothesized that inhibition of SIRT3 by TGFβ1 may potentiate lung fibrosis.

Accelerated biological aging as well as increases in TGFβ1 activity are common features of fibrosis in IPF and systemic scleroderma (SSc)[144-147]. Nevertheless, it is unclear if, and how, TGFβ1 influences biological aging. We propose that SIRT3 constitutes a new link between TGFβ1 activity and aging in the progression of pulmonary fibrosis.

5.2 Results

Down-regulation of SIRT3 expression in lung aging and pulmonary fibrosis

Mice lacking SIRT3 develop several diseases related to aging at an accelerated pace[136]. While it is known that the molecular mechanisms of lung aging and fibrosis are related, few studies have been undertaken to show the role of SIRT3 in age-related lung diseases. Here, we aimed to determine the changes in SIRT3 expression during lung aging and pulmonary fibrosis. Young (2-month-old) and old (22-month-old) mice were exposed to bleomycin by oropharyngeal aspiration to induce lung injury leading to the development of fibrosis. qRT-PCR analysis demonstrated a reduction in SIRT3 mRNA levels with age. The group of old mice showed a significant reduction in SIRT3 expression compared to young mice (Fig. 4.1A). Bleomycin treatment also resulted in lower levels of SIRT3 transcripts in young mice, although differences were not statistically significant between age-matched PBS-treated controls (Fig. 4.1A).

Next, we evaluated the expression of SIRT3 in another model of pulmonary fibrosis that is TGFβ1-dependent. C57BL/6 young mice were exposed to a replication-deficient adenovirus encoding active TGFβ1 (AdTGFβ1). The results of qRT-PCR analyses showed a significant reduction in SIRT3 expression in the lung at 14 days post-infection compared to GFP (AdGFP) control infection (Fig. 4.1B). The down-regulation of SIRT3 in aging and the two models of pulmonary fibrosis suggest that SIRT3 plays a role in lung fibrogenesis during aging.

We also evaluated the expression of SIRT3 in primary human lung fibroblasts extracted from the fibrotic lung of SSc patients. We chose SSc lung fibroblasts because

Figure 4.1

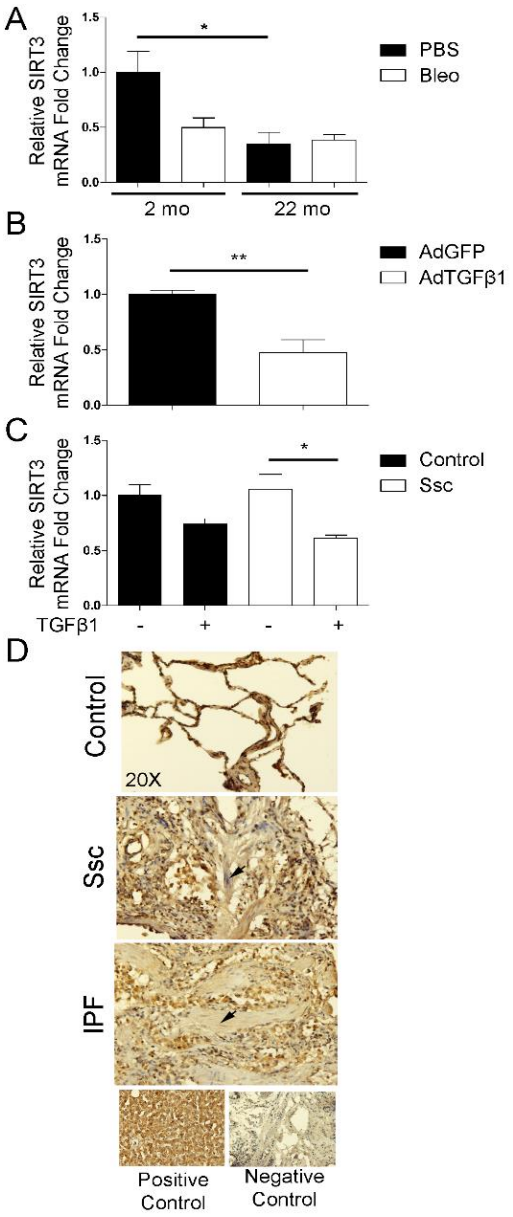

Figure 4.1. Down-regulation of Sirtuin 3 (SIRT3) expression in aging and pulmonary fibrosis. A) Real-time quantitative reverse-transcriptase polymerase chain reaction (qRT-PCR) analysis for SIRT3 mRNA expression in aging (22-month-old) and young (2-month old) mice at 14 days after oropharyngeal aspiration of phosphate buffered saline (PBS) or bleomycin (Bleo) (n = 5 per treatment). B) qRT-PCR analysis for SIRT3 mRNA expression in young mice at 14 days post oropharyngeal aspiration of control Adenovirus-GFP (AdGFP) or Adenovirus-TGFβ1 (AdTGFβ1) (n = 5 per treatment). C) qRT-PCR analysis for SIRT3 mRNA expression in TGFβ1-treated fibroblasts from normal (control) and systemic scleroderma (SSc) patients at 24 h. D) Immunohistochemistry (IHC) in lung tissue samples from control, systemic scleroderma (SSc) and idiopathic pulmonary fibrosis (IPF) patients show differential expression of SIRT3. Positive cells appear brown (DAB Stain). Nuclei counterstained with hematoxylin appear blue. Arrow shows fibrotic lesion. Liver tissue was used as a positive control. IgG only was used as negative control. *$p < 0.05$, **$p < 0.01$.

they have been shown to express high levels of TGFβ receptors and be highly responsive to the effects of TGFβ1[148]. As expected, lung fibroblasts from SSc patients exhibited decreased levels of SIRT3 expression upon treatment with TGFβ1 as compared to control donors (Fig. 4.1C). Similarly, IHC performed on SSc and IPF specimens display low levels of SIRT3 staining within fibrotic areas (Fig. 4.1D).

SIRT3 deficiency promotes pulmonary fibrosis

To confirm the role for SIRT3 in pulmonary fibrosis, SIRT3-deficient (*Sirt3*$^{-/-}$) and wild-type (WT) control mice were exposed to bleomycin. At 14 days post-bleomycin exposure lungs were analyzed for markers of fibrosis. Histological analysis of WT and *Sirt3*$^{-/-}$ lungs using Masson's trichrome staining showed increased collagen deposition in *Sirt3*$^{-/-}$ mice compared to control after bleomycin exposure (Fig. 4.2A-B). qRT-PCR analyses confirmed the lack of SIRT3 transcripts in knockout mice as well as an increase in SMAD3 transcript levels, possibly indicating an activation of the canonical TGFβ1 signaling pathway (Fig. 4.2C-D). Additionally, *Sirt3*$^{-/-}$ mice displayed high levels of IL-6 mRNA transcripts, suggesting an escalation of the inflammatory response post-lung injury (Fig. 4.2E). An increase in transcript levels for the fibrotic marker PAI1 subsequent to injury (Fig. 4.2F). This increase in PAI1 expression was also evident at the protein level by WB analysis as demonstrated by densitometry analysis (Fig. 4.2F-G). Similarly, although little change was detected in α-SMA expression, additional fibrotic markers, such as type V collagen, alpha chain 1 (Col5A1), heat shock protein 47 (Hsp47) and connective tissue growth factor (CTGF/CCN2), also showed increased protein expression in *Sirt3*$^{-/-}$ mice as compared to controls following bleomycin-induced injury

(Fig. 4.2G-L). Taken together, these data suggest that SIRT3 deficiency may contribute to the development of pulmonary fibrosis.

Figure 4.2

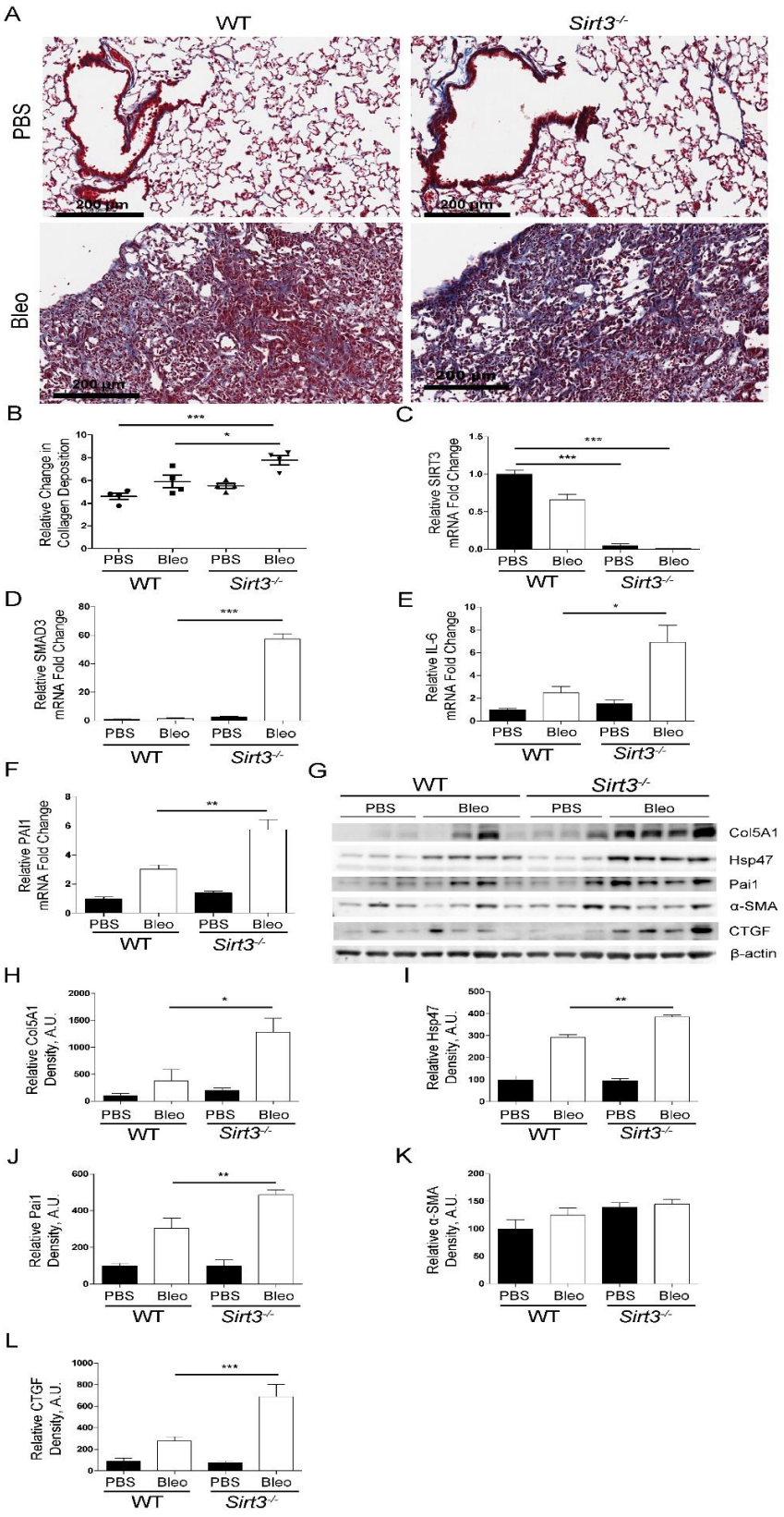
A
WT
Sirt3-/-
PBS
Bleo
200 μm
B
Relative Change in Collagen Deposition
C
Relative SIRT3 mRNA Fold Change
D
Relative SMAD3 mRNA Fold Change
E
Relative IL-6 mRNA Fold Change
F
Relative PAI1 mRNA Fold Change
G
Col5A1
Hsp47
Pai1
α-SMA
CTGF
β-actin
H
Relative Col5A1 Density, A.U.
I
Relative Hsp47 Density, A.U.
J
Relative Pai1 Density, A.U.
K
Relative α-SMA Density, A.U.
L
Relative CTGF Density, A.U.
PBS
Bleo

Figure 4.2. SIRT3 deficiency promotes pulmonary fibrosis. A-B) Representative images and quantification of Masson's trichrome staining to evaluate collagen deposition in SIRT3-deficient (*Sirt3*$^{-/-}$, n = 7 per treatment) and wild-type (WT, n = 5 per treatment) control mice after bleomycin (Bleo) or PBS vehicle, at 14 days post exposure. Positive collagen deposition appears blue. C-F) Real-time qRT-PCR for SIRT3, SMAD3, IL-6 and PAI1 expression. G) Representative WB for fibrotic markers type V collagen, alpha chain 1 (Col5A1), Hsp47, PAI1, α-SMA, and connective tissue growth factor (CTGF) expression in lung tissue extracted from SIRT3-deficient mice. β-actin used as loading control. H-L) Densitometry analysis of WB from SIRT3-deficient or wild-type (WT) control mice exposed to bleomycin (Bleo) or PBS only by oropharyngeal aspiration after 14 days for fibrotic markers, Col5A1, Hsp47, PAI1, α-SMA and CTGF, expression shown in (G). Arbitrary units are abbreviated as AU. *$p < 0.05$, **$p < 0.01$, ***$p < 0.005$.

Glycolytic reprogramming of fibroblasts by TGFβ1

Due to the known role SIRT3 plays in mitochondrial metabolism, we aimed to determine if TGFβ1 treatment may cause an increase in glycolysis due in part to its down-regulation of SIRT3 expression. We first confirmed that TGFβ1 induces glycolysis by qRT-PCR analysis, lactate production assays and glycolytic function tests. In NHLF, expression of three glycolytic enzymes, hypoxia inducible factor 1 alpha (HIF-1α), hexokinase II (HXK2) and lactate dehydrogenase A (LDHA), was found to be induced by TGFβ1 treatment (Fig. 4.3A). The induction of LDHA corresponded to an increase in the production of lactate following TGFβ1, which was ameliorated upon co-treatment with RSV (Fig. 4.3B). We next evaluated the effect of TGFβ1 on metabolism by measuring the extracellular acidification rate (ECAR) using the Seahorse Glycolytic stress test (Seahorse Bioscience). NHLF treated with TGFβ1 exhibited an elevated glycolytic capacity as determined by the extracellular acidification rate (ECAR) upon the addition of oligomycin which was significantly reduced upon RSV co-treatment (Fig. 4.3C). Additionally, TGFβ1 treatment resulted in an increase in the glycolytic reserve percentage which was restored to normal levels upon co-treatment with RSV (Fig. 4.3D).

In order to determine if this induction is dependent upon the down-regulation of SIRT3, we transfected NHLF with siRNA targeting SIRT3 and measured ECAR using the Seahorse Bioscience analyzer. The extracellular acidification rate was not induced by the absence of SIRT3, suggesting this effect is not due to reduced SIRT3 levels only (Fig. 4.3E-F). Instead, inhibition of SIRT3 seems to have diminished any response to glycolytic mediators, either glucose or oligomycin, possibly demonstrating its role in regulating metabolic flexibility. Similarly, overexpression of SIRT3 did not affect glycolysis in NHLF (Fig. 4.3G-H). Overall, our results indicate TGFβ1 increases the glycolytic capacity of cells in a SIRT3-independent manner.

Figure 4.3

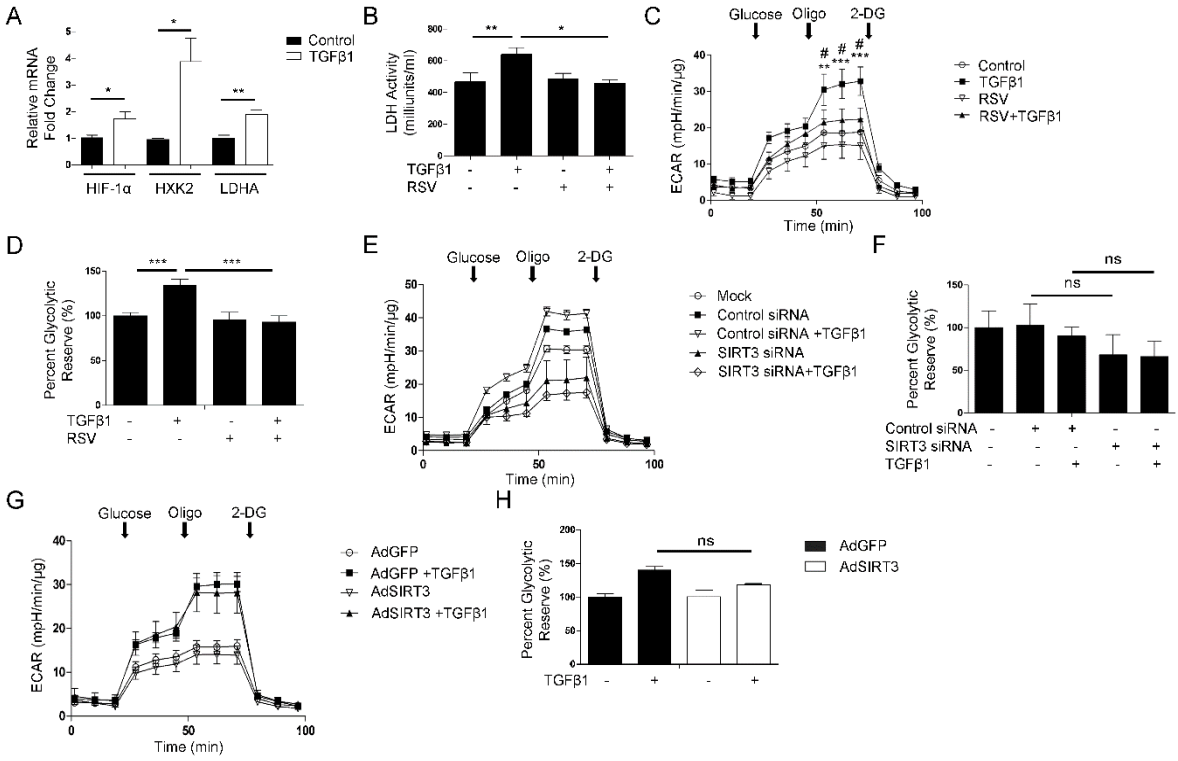

Figure 4.3. Glycolytic reprogramming of fibroblasts by TGFβ1. A) Real-time quantitative reverse-transcriptase polymerase chain reaction (qRT-PCR) analysis for HIF-1α, HXK2, and LDHA mRNA expression in TGFβ1 treated NHLF, 24 h. B) Lactate dehydrogenase activity as measure by lactate production in NHLF treated with TGFβ1 and/or resveratrol (RSV), 24 h. C-D) Measurements of the extracellular acidification rate (ECAR) and glycolytic reserve as a percentage using the Glycolytic Stress Test on Seahorse Bioscience XF^{e}24 analyzer in NHLF treated with TGFβ1 and/or RSV, 24 h. (n = 5 per treatment, mean +/- SEM). E-F) Measurements of ECAR and glycolytic reserve as a percentage using the Glycolytic Stress Test on Seahorse Bioscience XF^{e}24 analyzer in SIRT3 deficient (SIRT3 KD) NHLF treated with or without TGFβ1 for 24 h. (n = 4 per treatment, mean +/- SEM). G-H) Measurements of ECAR and glycolytic reserve as a percentage using the Glycolytic Stress Test on Seahorse Bioscience XF^{e}24 analyzer in SIRT3 overexpressing (AdSIRT3) NHLF treated with or without TGFβ1 for 24 h. (n = 5 per treatment, mean +/- SEM).

5.3 Discussion

Mice lacking SIRT3 (*Sirt3*$^{-/-}$) develop several aging-associated diseases at an accelerated pace, such as cancer, metabolic syndrome, cardiovascular disease, and

neurodegenerative diseases and provide a valuable model of accelerated aging[62, 136, 149, 150]. For example, in hematopoietic stem cells (HSCs), SIRT3 was shown to be suppressed with aging and upregulation of SIRT3 in aged HSCs improved their regenerative capacity[109]. Other studies show that SIRT3 prevents aging in the heart and tissue remodeling and implicate SIRT3 deficiency in cardiac hypertrophy[62, 63, 151, 152]. Here, we demonstrated that the fibrotic lungs from IPF and SSc patients, as well as lungs from animal models of pulmonary fibrosis, are characterized by deficient SIRT3 expression. Finally, we established that SIRT3 expression declines in the aging lung, a tissue previously shown to be pro-fibrotic, characterized by increased TGFβ1 signaling and collagen deposition[31, 153].

Considering the diverse nature of SIRT3 substrates, deficiency in SIRT3 may favor metabolic changes characteristic of myofibroblasts. In fact, recent studies demonstrated TGFβ1 promotes a metabolic switch that is critical for the maintenance of its pro-survival properties[154, 155]. SIRT3 targets many key metabolic enzymes, including acetyl-CoA synthase 2 (ACSS2), ornithine transcarbamylase, and acyl-CoA long-chain dehydrogenase 2 (ACADL). Furthermore, SIRT3 destabilizes hypoxia-inducible factor 1-alpha (HIF-1α), a major player in Warburg reprogramming of cellular metabolism[156, 157]. Consequentially, it will be critical in the near future to truly investigate the role of TGFβ1/SIRT3 in metabolism and its contribution to the establishment and perpetuation of fibrotic tissue during aging.

A loss-of-function SIRT3 single nucleotide polymorphism (SNP) is prevalent in pulmonary arterial hypertension (PAH) and suggests that loss of SIRT3 activity may predispose humans to pulmonary hypertension[158]. PAH in IPF and SSc has been

increasingly acknowledged and contributes to morbidity in these diseases[159]. SIRT3 knockout (*Sirt3*$^{-/-}$) mice develop spontaneous pulmonary hypertension[158]. Resveratrol can prevent the development of PAH and inhibit the development of pulmonary fibrosis in animal models[54, 160-164]. Our studies revealed that SIRT3-deficient mice are more susceptible to the development of pulmonary fibrosis than wild-type (WT) controls. Even though pulmonary hypertension was not evaluated in this study, SIRT3-deficient mice are a good model for future studies aimed to better understand the interplay between pulmonary hypertension in pulmonary fibrosis during aging.

It is highly important to identify the limiting factors that define the persistence of the fibrotic lung and the promotion of biological aging. Our study demonstrated that SIRT3 is a limiting factor in the fibrotic response in aging and that reduced expression of SIRT3 promotes a fibrotic response mediated by TGFβ1. In the future, dissection of the role of mitochondrial post-translational modifications and metabolism during lung aging, as well as during the process of myofibroblast differentiation, needs to be undertaken. Future studies on SIRT3 and the SIRT3-related acetylome could provide a pool of biomarkers and therapeutic discovery program targets in tissue remodeling. The identification of specific SIRT3 modulators is a strong area of research. We expect that small molecules, as specific SIRT3 activators, will be developed soon as therapeutic approaches to promote inhibition and/or resolution of lung fibrosis, through the regulation of mitochondria quality control machinery, the antioxidant response, and metabolism. Overall, we propose that SIRT3 constitutes a new link between TGFβ1 activity and aging in the progression of pulmonary fibrosis.

5.4 Materials & Methods

Mice & Tissue Samples. All mice were obtained from the Jackson Laboratory (Bar Harbor, ME, USA). C57Bl/6 male mice, aged 6-8 weeks, were treated with 3×10^8 plaque-forming units (PFU) of replication-deficient adenovirus encoding either green fluorescent protein (GFP) (control group, AdGFP; n = 5) or active TGFβ1 (AdTGFβ1, n = 5). For age-dependent studies, C57Bl/6 male mice, aged young (2 months old, n = 5 per treatment) and old (22 months old, n = 5 per treatment), received 2 U/kg bleomycin (Teva Parenteral Medicines, Irvine, CA, USA) by oropharyngeal aspiration or vehicle only (phosphate buffered saline, PBS) for controls. 129S1/SvImJ (wild-type control) and 129-Sirt3$^{tm1.1Fwa/J}$ (knockout) male mice (4 months old) received 2 U/kg bleomycin (n = 7 per bleomycin treatment per knockout group, n = 5 per wild-type group) or PBS (n = 7 per PBS treatment per knockout group, n = 5 per wild-type group) as controls. Animals were anesthetized with 2% isoflurane vapor (VetOne, Meridian, ID, USA) in oxygen and all treatments were administered in 50 µl of sterile PBS by oropharyngeal aspiration. Upon completion of experiments, animals were anesthetized with an intraperitoneal injection of ketamine and xylazine, and lung tissue was collected as previously described[124]. All animal protocols were performed as approved by the Tulane University Institutional Animal Care and Use Committee.

Tissue microarray from patients with scleroderma and pulmonary fibrosis (SSc-PF) or IPF, and normal donor lung tissues as well as lung fibroblasts isolated from SSc patients and controls were provided by the National Scleroderma Core Center in collaboration with Dr. Carol Feghali-Bostwick at the Medical University of South Carolina. Isolated fibroblasts were cultured in high glucose DMEM (Mediatech, Inc.,

Manassas, VA, USA), supplemented with 10% fetal bovine serum (FBS, Gibco, Thermo Fisher Scientific, Waltham, MA, USA) and Penicillin-Streptomycin (Pen Strep, Gibco).

RNA Isolation & qRT-PCR. Isolation of total RNA was performed using Trizol® Reagent (Invitrogen) according to manufacturer's instructions. RNA concentration was measured using a NanoDrop spectrophotometer (Thermo Scientific NanoDrop, NanoDrop Technologies, Wilmington, DE, USA). For qRT-PCR analysis, 1 µg of total RNA was reverse transcribed using an iScript^{TM} cDNA Synthesis Kit (Bio-Rad) according to the manufacturer's protocol. Reactions were performed using iQ^{TM}SYBR® Green Supermix (Bio-Rad) and a Bio-Rad MyiQ iCycler. Relative expression levels were calculated using the $2^{-\Delta\Delta C(T)}$ method and normalized to 36b4 expression. All primer information given in Table 1.1.

Western Blots. Mouse lung tissue was flash-frozen, then homogenized in 1× radioimmunoprecipitation assay (RIPA) buffer purchased from Cell Signaling (Danvers, MA, USA) with an EDTA-free protease inhibitor cocktail (Roche Applied Science, Indianapolis, IN, USA), sonicated and quantified using the Bradford Method (Bio-Rad Laboratories Inc., Hercules, CA, USA). Protein samples combined with 4x NuPAGE LDS Sample Buffer and 10x NuPAGE Sample Reducing Agent (Invitrogen) for a final concentration of 1x for both buffers and boiled for 5 minutes. 20-25 micrograms of each protein sample was separated on NuPage SDS 4-12% Bis-Tris gradient gels (Invitrogen) and transferred onto PVDF membranes (Invitrogen). For time-dependent cell lysates, protein samples were separated on 15% Acrylamide 1.5M Tris/10% SDS gel. Membranes were blocked in 5% BSA in TBST or 5% nonfat dry milk (Blotting-Grade Blocker, Bio-

Rad) in TBST for 1 h at RT then probed with primary antibody overnight at 4°C while shaking.

Connective tissue growth factor (CTGF) antibody was purchased from Abcam (Cambridge, MA, USA) and used at a 1:1000 dilution. Antibodies to SIRT3 and β-actin were purchased from Cell Signaling (1:1000; Danvers, MA, USA). Antibody to heat shock protein 47 (Hsp47) (H300) was purchased from Santa Cruz Biotechnology (1:500; Dallas, TX, USA). Antibody to plasminogen activator inhibitor type 1 (Pai1) was purchased from PeproTech (1:10,000; Rocky Hill, NJ, USA). Antibody to alpha-smooth muscle actin (α-SMA) was purchased from Sigma-Aldrich (1:10,000; St. Louis, MO, USA). Antibody to type V collagen, alpha chain 1 (Col5A1) was purchased from Thermo Fisher Scientific (1:1000; Rockford, IL, USA). Anti-mouse immunoglobulin G (IgG), horseradish peroxidase (HRP)-linked and anti-rabbit IgG, HRP-linked (1:15,000; Cell Signaling) for chemiluminescence detection; and near-infrared dye 800CW (IRDye 800CW)-labeled goat anti-rabbit IgG or IRDye 680-labeled goat anti-mouse IgG (1:15,000) were purchased from LiCor, Lincoln, NE, USA) for fluorescence detection.

Histology and Immunostaining. Masson's trichrome staining and analysis was performed as previously described[31]. Hematoxylin and eosin (H&E) staining and analysis was performed as previously described[165]. VECTASTAIN Elite ABC Kit, Bloxal, Avidin/Biotin Blocking Kit, DAB Peroxidase Substrate Kit, and Vector Hematoxylin were obtained from Vector Laboratories (Burlingame, CA, USA). Buffer components Triton X-100 (TX-100) and Tween-20 were purchased from Sigma and glycine was purchased from Fisher Scientific (Pittsburgh, PA, USA).

For immunohistochemistry (IHC), tissue sections were deparaffinized, rehydrated, and stained using the VECTASTAIN Elite ABC Kit (VECTASTAIN). Antigen retrieval was performed using citrate buffer, pH 6.0 for 20 minutes in a microwave oven. Slides were permeabilized in 0.1% TX-100, 0.001% Tween-20, 0.3M Glycine, and 0.2% BSA in Tris-buffered saline (TBS) buffer. Endogenous peroxidase and biotin were blocked with the Bloxal and Avidin/Biotin Blocking Kit, respectively. Slides were washed and incubated with blocking buffer (5% normal goat serum plus 2% BSA, 0.1% TX-100 in TBS) for 30 min. Primary antibody for SIRT3 (1:100; Abgent, San Diego, CA, USA) was applied for 60 min at room temperature (RT) followed by staining with the VECTASTAIN Kit. Slides were washed in wash buffer, incubated with 3,3'-diaminobenzidine (DAB) Peroxidase Substrate Kit for 2 min then rinsed with water. Slides were counterstained for 2 min with hematoxylin (blue), rinsed with water, dehydrated, and cleared before applying coverslips.

For image analysis of IHC, images were captured using an Olympus BX60 microscope equipped with epifluorescence optics (Olympus, Melville, NY) and a charge-coupled device camera (MagnaFire 2.6, Olympus). All captured images were saved as 8-bit files and analyzed using Image J 1.48d (Wayne Rasband, NIH, Bethesda, MD, USA; http:imagei.nih.gov/ij). For histology analysis of Masson's trichrome staining, images were captured with a Scan Scope, Aperio version 10.2.0.0, Aperio Technologies (Leica Biosystems, Buffalo Grove, IL, USA) at the same magnification with similar contrast. Entire lung sections were analyzed using the Positive Pixel Algorithm, Aperio Image Scope (Aperio Technologies, Toronto, ON, Canada) to quantify the proportion of collagen (blue color) within the area analyzed. The amount of specific stain present in

each scanned slide image was assessed by the number of positive pixels per total number of positive and negative pixels × 100 (% positivity). One section from each mouse was analyzed.

Cell Culture and Reagents. Normal human lung fibroblasts (NHLF) from the American Type Culture Collection (ATCC, Manassas, VA, USA) were maintained in Fibroblast Growth Medium-2 (FGM-2, Lonza, Walkersville, MD, USA) before serum starving cells in Fibroblast Basal Medium (FBM, Lonza) supplemented with 0.2% bovine serum albumin (BSA, Gemini Bio-Products Inc., Woodland, CA, USA). NHLF were then cultured in FBM plus 0.2% BSA for various treatments. Recombinant human TGFβ1 (R&D Systems, Minneapolis, MN, USA) was used at various concentrations from 1-3 nanogram per milliliter (ng/ml). Resveratrol and NAD+ from Sigma (St. Louis, MO, USA) were used at concentrations of 100 μM and 500 μM respectively.

Transfections. For small interfering ribonucleic acid (siRNA) knockdown experiments, NHLF were transfected using the Neon Transfection System (Invitrogen, Carlsbad, CA, USA) with siGENOME SMARTpool SIRT3-targeted siRNA (Dharmacon RNAi Technologies Inc., Lafayette, CO, USA), control non-silencing siRNA (Qiagen, Valencia, CA, USA), or sterile water (mock transfection) for a final concentration of 50 nM siRNA. Cells were plated on 60-mm tissue culture dishes in FGM-2 medium for 48 h after electroporation, as previously described[124]. For SIRT3 over-expression experiments, adenoviruses encoding GFP (control virus, Cat. No. 1060) or human SIRT3 (Cat. No. 1499) were purchased from Vector Biolabs (Malvern, PA, USA). NHLF were transfected with 3 x 10^6 PFU/ml (MOI: 6) and cultured for 48 h with co-factor NAD+ to assure that transfected SIRT3 would be functional and/or 1 ng/ml TGFβ1.

Lactate Dehydrogenase Activity Assay. To measure lactate production in cells, the Lactate Dehydrogenase Activity Assay Kit (Sigma, St. Louis, MO, USA) was purchased and performed according to manufacturer's instructions.

Cellular Bioenergetics by Seahorse Analyzer. Extracellular acidification rate measurements were performed using the Seahorse XF^e24 instrument (Seahorse Biosciences, North Billerica, MA, USA). Cells were seeded into a XF^e24 cell culture microplate at a density of 20,000 cells per well and allowed to adhere overnight before treatment with TGFβ1 or resveratrol the next day. After 24 h, cells were washed and incubated in 525µl/well XF Glycolysis Stress Test Assay Medium (XF Base Medium supplemented with 2 mM L-Glutamine, pH 7.4) at 37^0C in a non-CO_2 incubator for 2 h prior to bioenergetics assessment. Three basal extracellular acidification rate (ECAR) measurements were performed using the Seahorse analyzer prior to triplicate measurements following injection of each chemical modifier. The first injection added glucose (10 mM), followed by oligomycin (1µM) and lastly 2-deoxyglucose (2-DG, 50mM) was added and last measurements were performed. For SIRT3 transfection experiments, ECAR was measured 48 h post transfections and 24 h post TGFβ1 treatment. To normalize data, immediately following assay completion cells were harvested in 20µl/well 1x RIPA buffer and protein quantified using the Bradford Method (Bio-Rad). Bioenergetic parameters were calculated and analyzed using Wave Software & Glycolytic Stress Test Report Generators provided by Seahorse Bioscience.

Statistical Analysis. All data are expressed as mean values ± standard error of the mean (SEM). Comparisons between two groups were made using the unpaired, two-tailed Student's t test. Analysis of variance (ANOVA) and Bonferroni's multiple

comparison test were used for multiple groups. Statistical significance was assigned at a value of $p < 0.05$. All experiments were repeated at least twice.

CONCLUSION

We demonstrated that the pro-fibrotic cytokine TGFβ1 represses autophagy and mitochondrial homeostasis in lung fibroblasts during the process of myofibroblast differentiation. We found that TGFβ1 inhibited PINK1 expression and the targeting of mitochondrial to autophagosomes for degradation. Additionally, mitochondrial metabolism and fusion/fission dynamics were altered by TGFβ1 resulting in increased reactive oxygen species. In our studies we have shown TGFβ1 represses mitochondrial biogenesis factors via downregulation of PGC-1α *in vitro* and *in vivo* which may also potentiate mitochondrial dyfunction. We found that the promotion of autophagy can reduce TGFβ1-induced fibrotic marker expression. Indeed, inhibition of autophagy alone resulted in increased fibrotic marker expression. In the future, stimulation of autophagy may offer therapeutic target against age-related fibrotic diseases.

We demonstrated for the first time an age-related decline in autophagy, mitophagy, and an increase in lipofuscin deposits correlate with susceptibility to pulmonary fibrosis. Our studies in an aging murine model confirmed older mice exposed to bleomycin expressed increased levels of fibrotic markers compared to young controls. Additionally, we found that PINK1 expression was reduced in two models of pulmonary fibrosis. Fibrotic foci in lung tissues from IPF patients expressed reduced levels of PINK1. An age-dependent decline in PINK1 expression was also noted in our murine model. This result was consistent with reduced sequestration of mitochondria in aging model after bleomycin-induced lung injury. Overall, this reduction in autophagy and the selective autophagic degradation of mitochondria (mitophagy) responses to lung injury may contribute to the promotion of pulmonary fibrosis.

We demonstrated that TGFβ1 reduced the expression of SIRT3. This downregulation has been shown to result in increased acetylation of major oxidative stress response regulators, including SOD2 and IDH2. Acetylation of antioxidant response enzymes results in their reduced activity potentially increasing oxidative stress and promoting myofibroblast differentiation. Indeed, we demonstrated that inhibition of SIRT3 promoted myofibroblast differentiation induced by TGFβ1 and that increased expression of SIRT3 attenuated TGFβ1 effects. Our studies illustrate a new protective role for SIRT3 in TGFβ1-induced myofibroblast differentiation.

We have shown an age-dependent decline in SIRT3 expression within the lung which may contribute to its predisposition for fibrosis. We demonstrated that lung tissues from patients with fibrotic diseases, systemic scleroderma and IPF, exhibited reduced levels of SIRT3 expression in fibrotic regions. Our studies in a murine model confirmed the role of SIRT3 in fibrosis, as SIRT3-deficient (*Sirt3*$^{-/-}$) mice showed increased expression of fibrotic markers and collagen deposition. We found that TGFβ1 induced the expression of glycolytic enzymes and overall glycolytic capacity of normal human lung fibroblasts, although, this function was SIRT3-independent. Overall, we have demonstrated that reduced SIRT3 expression during aging can promote the development of pulmonary fibrosis.

APPENDIX

Table 1.1. List of all primers employed in this study.

Gene	Species	Company & Catalog Number or Sequence
36B4		F 5'-CGACCTGGAAGTCCAACTAC -3' R 5'- ATCTGCTGCATCTGCTTG-3'
ASMA	Human	F 5'-GAAGAAGAGGACAGCACTG-3' R 5'-TCCCATTCCCACCATCAC-3'
ATG4C	Human	Real Time Primers, LLC— HATPL-I
ATG5	Human	F 5'-ATGCAGGGAACACTAAGCTG-3' R 5'-TCTAGGGCATTGTAGGCTTG-3'
ATG7	Human	F 5'-TTGAGCGGCGGCAAGAAATAATGG-3' R 5'-AGCTTCATCCAGCCGATACTCGTT-3'
ATG16L1	Human	Real Time Primers, LLC—HATPL-I
ATG16L2	Human	Real Time Primers, LLC— HATPL-I
BAD	Human	Real Time Primers, LLC—VHPS-733
BCL2	Human	F 5'-ATTTCCTGCATCTCATGCCAAGGG-3' R 5'-TGTGCTTTGCATTCTTGGACGAGG-3'
CASP8	Human	F 5'-ATTCCGCAAAGGAAGCAAGAACCC-3' R 5'-TGCCTGGTGTCTGAAGTTCCCTTT-3'
COL1	Human	F 5'-CGGAGGAGAGTCAGGAACG-3' R 5'-CACAAGGAACAGAACAGAACAG-3'
COL1	Mouse	F 5'-GCCAAGAAGACATCCCTGAAG-3' R 5'-TCATTGCATTGCACGTCATC-3'
CTGF	Mouse	Real Time Primers, LLC— VMPS-1447
CTSB	Human	F 5'-TATGCCACTGGTTTGCATTGCTGG-3' R 5'-TGTACCTTGGCAGGACAGTGGAAT-3'
DAPK1	Human	F 5'-AATGGAGTTGGCGATTTCAGCGTG-3' R 5'-AAGGGACTTCAGGAAACTGAGCCA-3'
GABARAP	Human	Real Time Primers, LLC— HATPL-I
HIF1A	Human	F 5'-TTGGCAGCAACGACACAGAAACTG-3' R 5'-TTGAGTGCAGGGTCAGCACTACTT-3'
HTT	Human	F 5'-CAGAACAGCACGGAAAAGTT-3' R 5'-AACAGTTGCCATCATTGGTT-3'
HXK2	Human	F 5'-TGCAGCGCATCAAGGAGAACAAAG-3'

		R 5’-ACGGTCTTATGTAGACGCTTGGCA-3’
IGF1	Human	F 5’-TGAAGATGCACACCATGTCCTCCT-3’ R 5’-AACTGAAGAGCATCCACCAGCTCA-3’
IL6	Mouse	Real Time Primers, LLC— VMPS-3096
LDHA	Human	F 5’-AATAGTTCTGCCACCTCTGACGCA-3’ R 5’-ACGGTAAACATCCACCTGGCTCAA-3’
MMP9	Mouse	F 5’-CCTGCAACTCACACGACATC-3’ R 5’-GGTGGTGGTGGTGGTCTC-3’
NRF1	Human	F 5’-ACGGAGTGACCCAAACCGAACATA-3’ R 5’-TCATCAGCTGTGGAGTTGAGT-3’
NRF2	Human	F 5’-AGCATGCCCTCACCTGCTACTTTA-3’ R 5’-ACTGAGTGTTCTGGTGATGCCACA-3’
PAI1	Human	F 5’-GGCTGGTGCTGGTGAATGC-3’ R 5’-AGTGCTGCCGTCTGATTTGTG-3’
PAI1	Mouse	Real Time Primers, LLC— VMPS-5797
PARK2	Human	F 5’-CACTGACAGCAGGAAGGACT-3’ R 5’-TCATCCGGTTTGGAATTAAA-3’
PGC1A	Human	F 5’-CCCTAGCTGAGGATGACAGA-3’ R 5’-TTCAGCAGCTGTGTTCATGT-3’
PGC1A	Mouse	Real Time Primers, LLC— CMPS-1
PINK1	Human	F 5’-AGAACATGGCATCTCTGTGTCGT-3’ R 5’-ACTAGACCAGCTTGGCCATTCACT-3’
PINK1	Mouse	Real Time Primers, LLC—VMPS-4763
SIRT3	Human	Integrated DNA Technologies— Hs.PT.58.40981592.g
SIRT3	Mouse	Integrated DNA Technologies— Mm.PT.58.6471148.gs
SMAD3	Human	F 5’-CCAGAACCAAACCTCAACAC-3’ R 5’-TCCTCTTGCGTACGTTTTTC-3’
SMAD3	Mouse	F 5’-TTCTCTGAAAGGGCACAGAC-3’ R 5’-TGACATAAACCCCTGCTGAT-3’
SNCA	Human	F 5’-ACAAGTGCTCAGTTCCAATGTGCC-3 R 5’-GTGAAAGGGAAGCACCGAAATGCT-3’
SOD2	Human	F 5’-GTTGCTGGAAGCCATCAAACGTGA-3’ R 5’-TAAGGCCTGTTGTTCCTTGCAGTG-3’
SQSTM1	Human	F 5’-ATCGGAGGATCCGAGTGT-3’ R 5’-TGGCTGTGAGCTGCTCTT-3’
TFAM	Human	F 5’-AAGATTCCAAGAAGCTAAGGGTGA-3’ R 5’-CAGAGTCAGACAGATTTTTCCAGTTT-3’
TNF	Human	Real Time Primers, LLC— VHPS-9415
TNFSF10	Human	Real Time Primers, LLC— VHPS-9439
TP73	Human	Real Time Primers, LLC— VHPS-9506
ULK2	Human	F 5’-AGATACGTGCCTTACGGTGCTTCA-3’ R 5’-AGATGGCGTAAGGTGTCTGTGTGT-3’

Table 1.1. List of all primers employed in this study.

Table 1.2

Gene Symbol	Fold Regulation of 1 ng/ml TGFβ1 treatment versus DMSO Control
AKT1	-1.5369
AMBRA1	-2.1735
APP	-2.1735
ARSA	-2.0279
ATG10	1.2142
ATG12	-1.0867
ATG16L1	-1.8921
ATG16L2	-2.6759
ATG3	1.1329
ATG4A	-1.2483
ATG4B	-2.0279
ATG4C	-1.6472
ATG4D	-1.1647
ATG5	-1.08867
ATG7	-3.2944
ATG9A	-1.0867
ATG9B	-2.1735
BAD	-4.3469
BAK1	-1.014
BAX	-2.0279
BCL2	-10.7034
BCL2L1	-6.1475
BECN1	-1.434
BID	-3.2944
BNIP3	1.3947
CASP3	1.057
CASP8	-1.1647
CDKN1B	-1.7654
CDKN2A	-1.8921
CLN3	-2.8679
CTSB	-4.0558
CTSS	-3.7842
CXCR4	-2.1735
DAPK1	-9.9866
DRAM1	-3.2944
EIF2AK3	1.1329
EIF4G1	-1.3379
ESR1	-2.1735

FADD	-1.014
FAS	-1.5369
GAA	-3.5308
GABARAP	-2.0279
GABARAPL1	-1.434
GABARAPL2	1.3947
HDAC1	-2.0279
HGS	-1.6472
HSP90AA1	-2.4967
HSPA8	-1.2483
HTT	-4.0558
IFNA2	-1.5369
IFNA4	-2.1735
IFNG	-2.1735
IGF1	41.6429
INS	-2.1735
IRGM	-2.1735
MAP1LC3A	-3.2944
MAP1LC3B	-1.0867
MAPK14	-1.6472
MAPK8	1.057
NFKB1	-1.5369
PIK3C3	-1.2483
PIK3CG	-2.1735
PIK3R4	-2.0279
PRKAA1	1.1329
PRKAA2	-1.5369
PTEN	-1.1647
RAB24	-1.5369
RB1	1.1329
RGS19	-1.3379
RPS6KB1	-1.2483
SNCA	-4.5489
SQSTM1	-4.0558
TGFB1	2.9897
TGM2	-1.1647
FAM176A	2.6027
TMEM74	-2.1735
DRAM2	-3.0738
TNF	-5.7358
TNFSF10	-5.7358
TP53	-1.8921
TP73	-2.1735
ULK1	-1.014

ULK2	-4.0558
UVRAG	-1.5369

Table 1.2. Autophagy related genes deregulated in NHLF by TGFB1. The list of genes fold changes between untreated and treated with 1 ng/ml TGFβ1.

REFERENCES

1. Coghlan MA, Shifren A, Huang HJ, Russell TD, Mitra RD, Zhang Q, Wegner DJ, Cole FS, Hamvas A: **Sequencing of idiopathic pulmonary fibrosis-related genes reveals independent single gene associations**. *BMJ Open Respir Res* 2014, **1**(1):e000057.
2. Leung J, Cho Y, Lockey RF, Kolliputi N: **The Role of Aging in Idiopathic Pulmonary Fibrosis**. *Lung* 2015, **193**(4):605-610.
3. Pardo A, Selman M: **Idiopathic pulmonary fibrosis: new insights in its pathogenesis**. *Int J Biochem Cell Biol* 2002, **34**(12):1534-1538.
4. Klingsberg RC, Mutsaers SE, Lasky JA: **Current clinical trials for the treatment of idiopathic pulmonary fibrosis**. *Respirology* 2010, **15**(1):19-31.
5. Wolters PJ, Collard HR, Jones KD: **Pathogenesis of idiopathic pulmonary fibrosis**. *Annu Rev Pathol* 2014, **9**:157-179.
6. Spagnolo P, Sverzellati N, Rossi G, Cavazza A, Tzouvelekis A, Crestani B, Vancheri C: **Idiopathic pulmonary fibrosis: an update**. *Ann Med* 2015, **47**(1):15-27.
7. Oikonomou A, Prassopoulos P: **Mimics in chest disease: interstitial opacities**. *Insights Imaging* 2013, **4**(1):9-27.
8. Raghu G, Weycker D, Edelsberg J, Bradford WZ, Oster G: **Incidence and prevalence of idiopathic pulmonary fibrosis**. *Am J Respir Crit Care Med* 2006, **174**(7):810-816.
9. Kaunisto J, Salomaa ER, Hodgson U, Kaarteenaho R, Myllarniemi M: **Idiopathic pulmonary fibrosis--a systematic review on methodology for the collection of epidemiological data**. *BMC Pulm Med* 2013, **13**:53.
10. Nalysnyk L, Cid-Ruzafa J, Rotella P, Esser D: **Incidence and prevalence of idiopathic pulmonary fibrosis: review of the literature**. *Eur Respir Rev* 2012, **21**(126):355-361.
11. Fernandez Perez ER, Daniels CE, Schroeder DR, St Sauver J, Hartman TE, Bartholmai BJ, Yi ES, Ryu JH: **Incidence, prevalence, and clinical course of idiopathic pulmonary fibrosis: a population-based study**. *Chest* 2010, **137**(1):129-137.
12. Iyer SN, Gurujeyalakshmi G, Giri SN: **Effects of pirfenidone on transforming growth factor-beta gene expression at the transcriptional level in bleomycin hamster model of lung fibrosis**. *J Pharmacol Exp Ther* 1999, **291**(1):367-373.
13. Gurujeyalakshmi G, Hollinger MA, Giri SN: **Pirfenidone inhibits PDGF isoforms in bleomycin hamster model of lung fibrosis at the translational level**. *Am J Physiol* 1999, **276**(2 Pt 1):L311-318.

14. Chaudhary NI, Roth GJ, Hilberg F, Muller-Quernheim J, Prasse A, Zissel G, Schnapp A, Park JE: **Inhibition of PDGF, VEGF and FGF signalling attenuates fibrosis**. *Eur Respir J* 2007, **29**(5):976-985.
15. Strieter RM, Mehrad B: **New mechanisms of pulmonary fibrosis**. *Chest* 2009, **136**(5):1364-1370.
16. Hinz B, Phan SH, Thannickal VJ, Galli A, Bochaton-Piallat ML, Gabbiani G: **The myofibroblast: one function, multiple origins**. *Am J Pathol* 2007, **170**(6):1807-1816.
17. van Moorsel CH, Hoffman TW, van Batenburg AA, Klay D, van der Vis JJ, Grutters JC: **Understanding Idiopathic Interstitial Pneumonia: A Gene-Based Review of Stressed Lungs**. *Biomed Res Int* 2015, **2015**:304186.
18. Renzoni E, Srihari V, Sestini P: **Pathogenesis of idiopathic pulmonary fibrosis: review of recent findings**. *F1000Prime Rep* 2014, **6**:69.
19. Brown MK, Naidoo N: **The endoplasmic reticulum stress response in aging and age-related diseases**. *Front Physiol* 2012, **3**:263.
20. Boucher RC: **Idiopathic pulmonary fibrosis--a sticky business**. *N Engl J Med* 2011, **364**(16):1560-1561.
21. Seibold MA, Wise AL, Speer MC, Steele MP, Brown KK, Loyd JE, Fingerlin TE, Zhang W, Gudmundsson G, Groshong SD *et al*: **A common MUC5B promoter polymorphism and pulmonary fibrosis**. *N Engl J Med* 2011, **364**(16):1503-1512.
22. Naik PK, Moore BB: **Viral infection and aging as cofactors for the development of pulmonary fibrosis**. *Expert Rev Respir Med* 2010, **4**(6):759-771.
23. Molyneaux PL, Maher TM: **The role of infection in the pathogenesis of idiopathic pulmonary fibrosis**. *Eur Respir Rev* 2013, **22**(129):376-381.
24. Tang YW, Johnson JE, Browning PJ, Cruz-Gervis RA, Davis A, Graham BS, Brigham KL, Oates JA, Jr., Loyd JE, Stecenko AA: **Herpesvirus DNA is consistently detected in lungs of patients with idiopathic pulmonary fibrosis**. *J Clin Microbiol* 2003, **41**(6):2633-2640.
25. Malizia AP, Keating DT, Smith SM, Walls D, Doran PP, Egan JJ: **Alveolar epithelial cell injury with Epstein-Barr virus upregulates TGFbeta1 expression**. *Am J Physiol Lung Cell Mol Physiol* 2008, **295**(3):L451-460.
26. Stowe RP, Kozlova EV, Yetman DL, Walling DM, Goodwin JS, Glaser R: **Chronic herpesvirus reactivation occurs in aging**. *Exp Gerontol* 2007, **42**(6):563-570.
27. B BM, Lawson WE, Oury TD, Sisson TH, Raghavendran K, Hogaboam CM: **Animal models of fibrotic lung disease**. *Am J Respir Cell Mol Biol* 2013, **49**(2):167-179.
28. Degryse AL, Lawson WE: **Progress toward improving animal models for idiopathic pulmonary fibrosis**. *Am J Med Sci* 2011, **341**(6):444-449.
29. Izbicki G, Segel MJ, Christensen TG, Conner MW, Breuer R: **Time course of bleomycin-induced lung fibrosis**. *Int J Exp Pathol* 2002, **83**(3):111-119.
30. Peng R, Sridhar S, Tyagi G, Phillips JE, Garrido R, Harris P, Burns L, Renteria L, Woods J, Chen L *et al*: **Bleomycin induces molecular changes directly relevant to idiopathic pulmonary fibrosis: a model for "active" disease**. *PLoS One* 2013, **8**(4):e59348.

31. Sueblinvong V, Neujahr DC, Mills ST, Roser-Page S, Ritzenthaler JD, Guidot D, Rojas M, Roman J: **Predisposition for disrepair in the aged lung**. *Am J Med Sci* 2012, **344**(1):41-51.
32. Sueblinvong V, Neveu WA, Neujahr DC, Mills ST, Rojas M, Roman J, Guidot DM: **Aging promotes pro-fibrotic matrix production and increases fibrocyte recruitment during acute lung injury**. *Adv Biosci Biotechnol* 2014, **5**(1):19-30.
33. Warshamana GS, Pociask DA, Fisher KJ, Liu JY, Sime PJ, Brody AR: **Titration of non-replicating adenovirus as a vector for transducing active TGF-beta1 gene expression causing inflammation and fibrogenesis in the lungs of C57BL/6 mice**. *Int J Exp Pathol* 2002, **83**(4):183-201.
34. Lomas NJ, Watts KL, Akram KM, Forsyth NR, Spiteri MA: **Idiopathic pulmonary fibrosis: immunohistochemical analysis provides fresh insights into lung tissue remodelling with implications for novel prognostic markers**. *International journal of clinical and experimental pathology* 2012, **5**(1):58-71.
35. Zhao J, Shi W, Wang YL, Chen H, Bringas P, Jr., Datto MB, Frederick JP, Wang XF, Warburton D: **Smad3 deficiency attenuates bleomycin-induced pulmonary fibrosis in mice**. *Am J Physiol Lung Cell Mol Physiol* 2002, **282**(3):L585-593.
36. Leask A, Abraham DJ: **TGF-beta signaling and the fibrotic response**. *FASEB J* 2004, **18**(7):816-827.
37. Pohlers D, Brenmoehl J, Loffler I, Muller CK, Leipner C, Schultze-Mosgau S, Stallmach A, Kinne RW, Wolf G: **TGF-beta and fibrosis in different organs - molecular pathway imprints**. *Biochim Biophys Acta* 2009, **1792**(8):746-756.
38. Hinz B: **The extracellular matrix and transforming growth factor-beta1: Tale of a strained relationship**. *Matrix Biol* 2015, **47**:54-65.
39. Fernandez IE, Eickelberg O: **The impact of TGF-beta on lung fibrosis: from targeting to biomarkers**. *Proc Am Thorac Soc* 2012, **9**(3):111-116.
40. Piersma B, Bank RA, Boersema M: **Signaling in Fibrosis: TGF-beta, WNT, and YAP/TAZ Converge**. *Front Med (Lausanne)* 2015, **2**:59.
41. Zhang YE: **Non-Smad pathways in TGF-beta signaling**. *Cell Res* 2009, **19**(1):128-139.
42. Shaw WM, Luo S, Landis J, Ashraf J, Murphy CT: **The C. elegans TGF-beta Dauer pathway regulates longevity via insulin signaling**. *Curr Biol* 2007, **17**(19):1635-1645.
43. Lapierre LR, Kumsta C, Sandri M, Ballabio A, Hansen M: **Transcriptional and epigenetic regulation of autophagy in aging**. *Autophagy* 2015, **11**(6):867-880.
44. Parzych KR, Klionsky DJ: **An overview of autophagy: morphology, mechanism, and regulation**. *Antioxid Redox Signal* 2014, **20**(3):460-473.
45. Yang Z, Klionsky DJ: **Mammalian autophagy: core molecular machinery and signaling regulation**. *Curr Opin Cell Biol* 2010, **22**(2):124-131.
46. Singh R, Cuervo AM: **Autophagy in the cellular energetic balance**. *Cell Metab* 2011, **13**(5):495-504.
47. Klionsky DJ, Abdalla FC, Abeliovich H, Abraham RT, Acevedo-Arozena A, Adeli K, Agholme L, Agnello M, Agostinis P, Aguirre-Ghiso JA *et al*: **Guidelines for the use and interpretation of assays for monitoring autophagy**. *Autophagy* 2012, **8**(4):445-544.

48. Araya J, Hara H, Kuwano K: **Autophagy in the pathogenesis of pulmonary disease**. *Intern Med* 2013, **52**(20):2295-2303.
49. Cuervo AM: **Autophagy and aging: keeping that old broom working**. *Trends Genet* 2008, **24**(12):604-612.
50. Vittorini S, Paradiso C, Donati A, Cavallini G, Masini M, Gori Z, Pollera M, Bergamini E: **The age-related accumulation of protein carbonyl in rat liver correlates with the age-related decline in liver proteolytic activities**. *The journals of gerontology Series A, Biological sciences and medical sciences* 1999, **54**(8):B318-323.
51. Chuang SY, Lin CH, Fang JY: **Natural compounds and aging: between autophagy and inflammasome**. *Biomed Res Int* 2014, **2014**:297293.
52. Levine B, Kroemer G: **Autophagy in the pathogenesis of disease**. *Cell* 2008, **132**(1):27-42.
53. Tukaj C: **The significance of macroautophagy in health and disease**. *Folia Morphol (Warsz)* 2013, **72**(2):87-93.
54. Yang DL, Zhang HG, Xu YL, Gao YH, Yang XJ, Hao XQ, Li XH: **Resveratrol inhibits right ventricular hypertrophy induced by monocrotaline in rats**. *Clin Exp Pharmacol Physiol* 2010, **37**(2):150-155.
55. Ding WX, Yin XM: **Mitophagy: mechanisms, pathophysiological roles, and analysis**. *Biol Chem* 2012, **393**(7):547-564.
56. Pyo JO, Yoo SM, Jung YK: **The Interplay between Autophagy and Aging**. *Diabetes Metab J* 2013, **37**(5):333-339.
57. Hamacher-Brady A, Brady NR: **Mitophagy programs: mechanisms and physiological implications of mitochondrial targeting by autophagy**. *Cell Mol Life Sci* 2016, **73**(4):775-795.
58. Chan DC: **Mitochondria: dynamic organelles in disease, aging, and development**. *Cell* 2006, **125**(7):1241-1252.
59. Eiyama A, Okamoto K: **PINK1/Parkin-mediated mitophagy in mammalian cells**. *Curr Opin Cell Biol* 2015, **33**:95-101.
60. Durcan TM, Fon EA: **The three 'P's of mitophagy: PARKIN, PINK1, and post-translational modifications**. *Genes Dev* 2015, **29**(10):989-999.
61. Kelly G: **A review of the sirtuin system, its clinical implications, and the potential role of dietary activators like resveratrol: part 1**. *Altern Med Rev* 2010, **15**(3):245-263.
62. Pillai VB, Sundaresan NR, Gupta MP: **Regulation of Akt signaling by sirtuins: its implication in cardiac hypertrophy and aging**. *Circ Res* 2014, **114**(2):368-378.
63. Giralt A, Villarroya F: **SIRT3, a pivotal actor in mitochondrial functions: metabolism, cell death and aging**. *Biochem J* 2012, **444**(1):1-10.
64. Hirschey MD, Shimazu T, Huang JY, Schwer B, Verdin E: **SIRT3 regulates mitochondrial protein acetylation and intermediary metabolism**. *Cold Spring Harb Symp Quant Biol* 2011, **76**:267-277.
65. Chen Y, Fu LL, Wen X, Wang XY, Liu J, Cheng Y, Huang J: **Sirtuin-3 (SIRT3), a therapeutic target with oncogenic and tumor-suppressive function in cancer**. *Cell Death Dis* 2014, **5**:e1047.

66. Webster BR, Scott I, Han K, Li JH, Lu Z, Stevens MV, Malide D, Chen Y, Samsel L, Connelly PS *et al*: **Restricted mitochondrial protein acetylation initiates mitochondrial autophagy**. *J Cell Sci* 2013, **126**(Pt 21):4843-4849.
67. Bellizzi D, Rose G, Cavalcante P, Covello G, Dato S, De Rango F, Greco V, Maggiolini M, Feraco E, Mari V *et al*: **A novel VNTR enhancer within the SIRT3 gene, a human homologue of SIR2, is associated with survival at oldest ages**. *Genomics* 2005, **85**(2):258-263.
68. Rose G, Dato S, Altomare K, Bellizzi D, Garasto S, Greco V, Passarino G, Feraco E, Mari V, Barbi C *et al*: **Variability of the SIRT3 gene, human silent information regulator Sir2 homologue, and survivorship in the elderly**. *Exp Gerontol* 2003, **38**(10):1065-1070.
69. Sundaresan NR, Gupta M, Kim G, Rajamohan SB, Isbatan A, Gupta MP: **Sirt3 blocks the cardiac hypertrophic response by augmenting Foxo3a-dependent antioxidant defense mechanisms in mice**. *J Clin Invest* 2009, **119**(9):2758-2771.
70. Zhu L, Barrett EC, Xu Y, Liu Z, Manoharan A, Chen Y: **Regulation of Cigarette Smoke (CS)-Induced Autophagy by Nrf2**. *PLoS One* 2013, **8**(4):e55695.
71. Ryter SW, Choi AM: **Autophagy in the lung**. *Proc Am Thorac Soc* 2010, **7**(1):13-21.
72. Ryter SW, Lee SJ, Choi AM: **Autophagy in cigarette smoke-induced chronic obstructive pulmonary disease**. *Expert Rev Respir Med* 2010, **4**(5):573-584.
73. Morse D, Rosas IO: **Tobacco smoke-induced lung fibrosis and emphysema**. *Annu Rev Physiol* 2014, **76**:493-513.
74. Patel AS, Lin L, Geyer A, Haspel JA, An CH, Cao J, Rosas IO, Morse D: **Autophagy in idiopathic pulmonary fibrosis**. *PLoS One* 2012, **7**(7):e41394.
75. Bratic A, Larsson NG: **The role of mitochondria in aging**. *J Clin Invest* 2013, **123**(3):951-957.
76. Schiavi A, Ventura N: **The interplay between mitochondria and autophagy and its role in the aging process**. *Exp Gerontol* 2014, **56**:147-153.
77. Casalena G, Daehn I, Bottinger E: **Transforming growth factor-beta, bioenergetics, and mitochondria in renal disease**. *Semin Nephrol* 2012, **32**(3):295-303.
78. Sohn EJ, Kim J, Hwang Y, Im S, Moon Y, Kang DM: **TGF-beta suppresses the expression of genes related to mitochondrial function in lung A549 cells**. *Cell Mol Biol (Noisy-le-grand)* 2012, **Suppl.58**:OL1763-1767.
79. Aguirre A, Lopez-Alonso I, Gonzalez-Lopez A, Amado-Rodriguez L, Batalla-Solis E, Astudillo A, Blazquez-Prieto J, Fernandez AF, Galvan JA, dos Santos CC *et al*: **Defective autophagy impairs ATF3 activity and worsens lung injury during endotoxemia**. *J Mol Med (Berl)* 2014, **92**(6):665-676.
80. Chang AL, Ulrich A, Suliman HB, Piantadosi CA: **Redox regulation of mitophagy in the lung during murine Staphylococcus aureus sepsis**. *Free Radic Biol Med* 2015, **78**:179-189.
81. Ichimura Y, Waguri S, Sou YS, Kageyama S, Hasegawa J, Ishimura R, Saito T, Yang Y, Kouno T, Fukutomi T *et al*: **Phosphorylation of p62 activates the Keap1-Nrf2 pathway during selective autophagy**. *Mol Cell* 2013, **51**(5):618-631.

82. Calderilla-Barbosa L, Seibenhener ML, Du Y, Diaz-Meco MT, Moscat J, Yan J, Wooten MW, Wooten MC: **Interaction of SQSTM1 with the motor protein dynein--SQSTM1 is required for normal dynein function and trafficking**. *J Cell Sci* 2014, **127**(Pt 18):4052-4063.
83. Hecker L, Logsdon NJ, Kurundkar D, Kurundkar A, Bernard K, Hock T, Meldrum E, Sanders YY, Thannickal VJ: **Reversal of persistent fibrosis in aging by targeting Nox4-Nrf2 redox imbalance**. *Sci Transl Med* 2014, **6**(231):231ra247.
84. Bitto A, Lerner CA, Nacarelli T, Crowe E, Torres C, Sell C: **P62/SQSTM1 at the interface of aging, autophagy, and disease**. *Age (Dordr)* 2014, **36**(3):9626.
85. Jain M, Rivera S, Monclus EA, Synenki L, Zirk A, Eisenbart J, Feghali-Bostwick C, Mutlu GM, Budinger GR, Chandel NS: **Mitochondrial reactive oxygen species regulate transforming growth factor-beta signaling**. *J Biol Chem* 2013, **288**(2):770-777.
86. Vestergaard PF, Hansen M, Frystyk J, Espelund U, Christiansen JS, Jorgensen JO, Fisker S: **Serum levels of bioactive IGF1 and physiological markers of ageing in healthy adults**. *Eur J Endocrinol* 2014, **170**(2):229-236.
87. Feng Z, Levine AJ: **The regulation of energy metabolism and the IGF-1/mTOR pathways by the p53 protein**. *Trends Cell Biol* 2010, **20**(7):427-434.
88. Honeyman L, Bazett M, Tomko TG, Haston CK: **MicroRNA profiling implicates the insulin-like growth factor pathway in bleomycin-induced pulmonary fibrosis in mice**. *Fibrogenesis Tissue Repair* 2013, **6**(1):16.
89. Chistiakov DA, Sobenin IA, Revin VV, Orekhov AN, Bobryshev YV: **Mitochondrial aging and age-related dysfunction of mitochondria**. *Biomed Res Int* 2014, **2014**:238463.
90. Ryter SW, Choi AM: **Autophagy in lung disease pathogenesis and therapeutics**. *Redox Biol* 2015, **4**:215-225.
91. Chen ZH, Kim HP, Sciurba FC, Lee SJ, Feghali-Bostwick C, Stolz DB, Dhir R, Landreneau RJ, Schuchert MJ, Yousem SA *et al*: **Egr-1 regulates autophagy in cigarette smoke-induced chronic obstructive pulmonary disease**. *PLoS One* 2008, **3**(10):e3316.
92. Chow JY, Cabral JA, Chang J, Carethers JM: **TGFbeta modulates PTEN expression independently of SMAD signaling for growth proliferation in colon cancer cells**. *Cancer Biol Ther* 2008, **7**(10):1694-1699.
93. He Z, Deng Y, Li W, Chen Y, Xing S, Zhao X, Ding J, Gao Y, Wang X: **Overexpression of PTEN suppresses lipopolysaccharide-induced lung fibroblast proliferation, differentiation and collagen secretion through inhibition of the PI3-K-Akt-GSK3beta pathway**. *Cell Biosci* 2014, **4**(1):2.
94. Roe ND, Xu X, Kandadi MR, Hu N, Pang J, Weiser-Evans MC, Ren J: **Targeted deletion of PTEN in cardiomyocytes renders cardiac contractile dysfunction through interruption of Pink1-AMPK signaling and autophagy**. *Biochim Biophys Acta* 2015, **1852**(2):290-298.
95. Bueno M, Lai YC, Romero Y, Brands J, St Croix CM, Kamga C, Corey C, Herazo-Maya JD, Sembrat J, Lee JS *et al*: **PINK1 deficiency impairs mitochondrial homeostasis and promotes lung fibrosis**. *J Clin Invest* 2015, **125**(2):521-538.

96. Knight DA, Ernst M, Anderson GP, Moodley YP, Mutsaers SE: **The role of gp130/IL-6 cytokines in the development of pulmonary fibrosis: critical determinants of disease susceptibility and progression?** *Pharmacol Ther* 2003, **99**(3):327-338.
97. Hirose T, Nakano Y, Nagamatsu Y, Misumi T, Ohta H, Ohshima Y: **Cyclic GMP-dependent protein kinase EGL-4 controls body size and lifespan in C elegans**. *Development* 2003, **130**(6):1089-1099.
98. Carrieri G, Marzi E, Olivieri F, Marchegiani F, Cavallone L, Cardelli M, Giovagnetti S, Stecconi R, Molendini C, Trapassi C *et al*: **The G/C915 polymorphism of transforming growth factor beta1 is associated with human longevity: a study in Italian centenarians**. *Aging Cell* 2004, **3**(6):443-448.
99. Doyle KP, Cekanaviciute E, Mamer LE, Buckwalter MS: **TGFbeta signaling in the brain increases with aging and signals to astrocytes and innate immune cells in the weeks after stroke**. *J Neuroinflammation* 2010, **7**:62.
100. van der Kraan PM, Goumans MJ, Blaney Davidson E, ten Dijke P: **Age-dependent alteration of TGF-beta signalling in osteoarthritis**. *Cell Tissue Res* 2012, **347**(1):257-265.
101. Hawkins A, Guttentag SH, Deterding R, Funkhouser WK, Goralski JL, Chatterjee S, Mulugeta S, Beers MF: **A non-BRICHOS SFTPC mutant (SP-CI73T) linked to interstitial lung disease promotes a late block in macroautophagy disrupting cellular proteostasis and mitophagy**. *Am J Physiol Lung Cell Mol Physiol* 2015, **308**(1):L33-47.
102. Sener G, Topaloglu N, Sehirli AO, Ercan F, Gedik N: **Resveratrol alleviates bleomycin-induced lung injury in rats**. *Pulm Pharmacol Ther* 2007, **20**(6):642-649.
103. Akgedik R, Akgedik S, Karamanli H, Uysal S, Bozkurt B, Ozol D, Armutcu F, Yildirim Z: **Effect of resveratrol on treatment of bleomycin-induced pulmonary fibrosis in rats**. *Inflammation* 2012, **35**(5):1732-1741.
104. Georgakopoulou EA, Tsimaratou K, Evangelou K, Fernandez Marcos PJ, Zoumpourlis V, Trougakos IP, Kletsas D, Bartek J, Serrano M, Gorgoulis VG: **Specific lipofuscin staining as a novel biomarker to detect replicative and stress-induced senescence. A method applicable in cryo-preserved and archival tissues**. *Aging (Albany NY)* 2013, **5**(1):37-50.
105. Chakraborty C, Doss CG: **Sirtuins family--recent development as a drug target for aging, metabolism, and age related diseases**. *Curr Drug Targets* 2013, **14**(6):666-675.
106. Guarente L: **Sirtuins, aging, and metabolism**. *Cold Spring Harb Symp Quant Biol* 2011, **76**:81-90.
107. Yao Y, Yang Y, Zhu WG: **Sirtuins: nodes connecting aging, metabolism and tumorigenesis**. *Curr Pharm Des* 2014, **20**(11):1614-1624.
108. Hurst LD, Williams EJ, Pal C: **Natural selection promotes the conservation of linkage of co-expressed genes**. *Trends Genet* 2002, **18**(12):604-606.
109. Brown K, Xie S, Qiu X, Mohrin M, Shin J, Liu Y, Zhang D, Scadden DT, Chen D: **SIRT3 reverses aging-associated degeneration**. *Cell Rep* 2013, **3**(2):319-327.

110. Kincaid B, Bossy-Wetzel E: **Forever young: SIRT3 a shield against mitochondrial meltdown, aging, and neurodegeneration**. *Front Aging Neurosci* 2013, **5**:48.
111. Sadoshima J: **Sirt3 targets mPTP and prevents aging in the heart**. *Aging (Albany NY)* 2011, **3**(1):12-13.
112. Zeng L, Yang Y, Hu Y, Sun Y, Du Z, Xie Z, Zhou T, Kong W: **Age-related decrease in the mitochondrial sirtuin deacetylase Sirt3 expression associated with ROS accumulation in the auditory cortex of the mimetic aging rat model**. *PLoS One* 2014, **9**(2):e88019.
113. Jacobs KM, Pennington JD, Bisht KS, Aykin-Burns N, Kim HS, Mishra M, Sun L, Nguyen P, Ahn BH, Leclerc J *et al*: **SIRT3 interacts with the daf-16 homolog FOXO3a in the mitochondria, as well as increases FOXO3a dependent gene expression**. *Int J Biol Sci* 2008, **4**(5):291-299.
114. Cheung KG, Cole LK, Xiang B, Chen K, Ma X, Myal Y, Hatch GM, Tong Q, Dolinsky VW: **Sirtuin-3 (SIRT3) Protein Attenuates Doxorubicin-induced Oxidative Stress and Improves Mitochondrial Respiration in H9c2 Cardiomyocytes**. *J Biol Chem* 2015, **290**(17):10981-10993.
115. Han C, Someya S: **Maintaining good hearing: calorie restriction, Sirt3, and glutathione**. *Exp Gerontol* 2013, **48**(10):1091-1095.
116. Qiu X, Brown K, Hirschey MD, Verdin E, Chen D: **Calorie restriction reduces oxidative stress by SIRT3-mediated SOD2 activation**. *Cell Metab* 2010, **12**(6):662-667.
117. Vassilopoulos A, Pennington JD, Andresson T, Rees DM, Bosley AD, Fearnley IM, Ham A, Flynn CR, Hill S, Rose KL *et al*: **SIRT3 deacetylates ATP synthase F1 complex proteins in response to nutrient- and exercise-induced stress**. *Antioxid Redox Signal* 2014, **21**(4):551-564.
118. Yu W, Dittenhafer-Reed KE, Denu JM: **SIRT3 protein deacetylates isocitrate dehydrogenase 2 (IDH2) and regulates mitochondrial redox status**. *J Biol Chem* 2012, **287**(17):14078-14086.
119. Schumacker PT: **SIRT3 controls cancer metabolic reprogramming by regulating ROS and HIF**. *Cancer Cell* 2011, **19**(3):299-300.
120. Samant SA, Zhang HJ, Hong Z, Pillai VB, Sundaresan NR, Wolfgeher D, Archer SL, Chan DC, Gupta MP: **SIRT3 deacetylates and activates OPA1 to regulate mitochondrial dynamics during stress**. *Mol Cell Biol* 2014, **34**(5):807-819.
121. Chen T, Li J, Liu J, Li N, Wang S, Liu H, Zeng M, Zhang Y, Bu P: **Activation of SIRT3 by resveratrol ameliorates cardiac fibrosis and improves cardiac function via the TGF-beta/Smad3 pathway**. *Am J Physiol Heart Circ Physiol* 2015, **308**(5):H424-434.
122. Olson ER, Naugle JE, Zhang X, Bomser JA, Meszaros JG: **Inhibition of cardiac fibroblast proliferation and myofibroblast differentiation by resveratrol**. *Am J Physiol Heart Circ Physiol* 2005, **288**(3):H1131-1138.
123. Zhou X, Chen M, Zeng X, Yang J, Deng H, Yi L, Mi MT: **Resveratrol regulates mitochondrial reactive oxygen species homeostasis through Sirt3 signaling pathway in human vascular endothelial cells**. *Cell Death Dis* 2014, **5**:e1576.

124. Sosulski ML, Gongora R, Danchuk S, Dong C, Luo F, Sanchez CG: **Deregulation of selective autophagy during aging and pulmonary fibrosis: the role of TGFbeta1**. *Aging Cell* 2015, **14**(5):774-783.
125. Desai LP, Zhou Y, Estrada AV, Ding Q, Cheng G, Collawn JF, Thannickal VJ: **Negative regulation of NADPH oxidase 4 by hydrogen peroxide-inducible clone 5 (Hic-5) protein**. *J Biol Chem* 2014, **289**(26):18270-18278.
126. Hecker L, Vittal R, Jones T, Jagirdar R, Luckhardt TR, Horowitz JC, Pennathur S, Martinez FJ, Thannickal VJ: **NADPH oxidase-4 mediates myofibroblast activation and fibrogenic responses to lung injury**. *Nat Med* 2009, **15**(9):1077-1081.
127. Thannickal VJ, Lee DY, White ES, Cui Z, Larios JM, Chacon R, Horowitz JC, Day RM, Thomas PE: **Myofibroblast differentiation by transforming growth factor-beta1 is dependent on cell adhesion and integrin signaling via focal adhesion kinase**. *J Biol Chem* 2003, **278**(14):12384-12389.
128. Bondi CD, Manickam N, Lee DY, Block K, Gorin Y, Abboud HE, Barnes JL: **NAD(P)H oxidase mediates TGF-beta1-induced activation of kidney myofibroblasts**. *J Am Soc Nephrol* 2010, **21**(1):93-102.
129. Sampson N, Berger P, Zenzmaier C: **Therapeutic targeting of redox signaling in myofibroblast differentiation and age-related fibrotic disease**. *Oxid Med Cell Longev* 2012, **2012**:458276.
130. Kim HS, Patel K, Muldoon-Jacobs K, Bisht KS, Aykin-Burns N, Pennington JD, van der Meer R, Nguyen P, Savage J, Owens KM *et al*: **SIRT3 is a mitochondria-localized tumor suppressor required for maintenance of mitochondrial integrity and metabolism during stress**. *Cancer Cell* 2010, **17**(1):41-52.
131. Tao R, Coleman MC, Pennington JD, Ozden O, Park SH, Jiang H, Kim HS, Flynn CR, Hill S, Hayes McDonald W *et al*: **Sirt3-mediated deacetylation of evolutionarily conserved lysine 122 regulates MnSOD activity in response to stress**. *Mol Cell* 2010, **40**(6):893-904.
132. Ozden O, Park SH, Kim HS, Jiang H, Coleman MC, Spitz DR, Gius D: **Acetylation of MnSOD directs enzymatic activity responding to cellular nutrient status or oxidative stress**. *Aging (Albany NY)* 2011, **3**(2):102-107.
133. Scheurmann J, Treiber N, Weber C, Renkl AC, Frenzel D, Trenz-Buback F, Ruess A, Schulz G, Scharffetter-Kochanek K, Weiss JM: **Mice with heterozygous deficiency of manganese superoxide dismutase (SOD2) have a skin immune system with features of "inflamm-aging"**. *Arch Dermatol Res* 2014, **306**(2):143-155.
134. Weyemi U, Parekh PR, Redon CE, Bonner WM: **SOD2 deficiency promotes aging phenotypes in mouse skin**. *Aging (Albany NY)* 2012, **4**(2):116-118.
135. Luckhardt TR, Thannickal VJ: **Systemic sclerosis-associated fibrosis: an accelerated aging phenotype?** *Curr Opin Rheumatol* 2015, **27**(6):571-576.
136. McDonnell E, Peterson BS, Bomze HM, Hirschey MD: **SIRT3 regulates progression and development of diseases of aging**. *Trends Endocrinol Metab* 2015, **26**(9):486-492.

137. Nepal S, Park PH: **Activation of autophagy by globular adiponectin attenuates ethanol-induced apoptosis in HepG2 cells: involvement of AMPK/FoxO3A axis**. *Biochim Biophys Acta* 2013, **1833**(10):2111-2125.
138. Sanchez AM, Csibi A, Raibon A, Cornille K, Gay S, Bernardi H, Candau R: **AMPK promotes skeletal muscle autophagy through activation of forkhead FoxO3a and interaction with Ulk1**. *J Cell Biochem* 2012, **113**(2):695-710.
139. Warr MR, Binnewies M, Flach J, Reynaud D, Garg T, Malhotra R, Debnath J, Passegue E: **FOXO3A directs a protective autophagy program in haematopoietic stem cells**. *Nature* 2013, **494**(7437):323-327.
140. Nho RS, Hergert P, Kahm J, Jessurun J, Henke C: **Pathological alteration of FoxO3a activity promotes idiopathic pulmonary fibrosis fibroblast proliferation on type i collagen matrix**. *Am J Pathol* 2011, **179**(5):2420-2430.
141. Nho RS, Peterson M, Hergert P, Henke CA: **FoxO3a (Forkhead Box O3a) deficiency protects Idiopathic Pulmonary Fibrosis (IPF) fibroblasts from type I polymerized collagen matrix-induced apoptosis via caveolin-1 (cav-1) and Fas**. *PLoS One* 2013, **8**(4):e61017.
142. Im J, Hergert P, Nho RS: **Reduced FoxO3a expression causes low autophagy in idiopathic pulmonary fibrosis fibroblasts on collagen matrices**. *Am J Physiol Lung Cell Mol Physiol* 2015, **309**(6):L552-561.
143. Payne BA, Chinnery PF: **Mitochondrial dysfunction in aging: Much progress but many unresolved questions**. *Biochim Biophys Acta* 2015, **1847**(11):1347-1353.
144. Chilosi M, Carloni A, Rossi A, Poletti V: **Premature lung aging and cellular senescence in the pathogenesis of idiopathic pulmonary fibrosis and COPD/emphysema**. *Transl Res* 2013, **162**(3):156-173.
145. Homer RJ, Herzog EL: **Recent advances in pulmonary fibrosis: implications for scleroderma**. *Curr Opin Rheumatol* 2010, **22**(6):683-689.
146. Leslie KO: **Idiopathic pulmonary fibrosis may be a disease of recurrent, tractional injury to the periphery of the aging lung: a unifying hypothesis regarding etiology and pathogenesis**. *Arch Pathol Lab Med* 2012, **136**(6):591-600.
147. Thannickal VJ: **Mechanistic links between aging and lung fibrosis**. *Biogerontology* 2013, **14**(6):609-615.
148. Yamane K, Ihn H, Kubo M, Tamaki K: **Increased transcriptional activities of transforming growth factor beta receptors in scleroderma fibroblasts**. *Arthritis Rheum* 2002, **46**(9):2421-2428.
149. Cho EH: **SIRT3 as a Regulator of Non-alcoholic Fatty Liver Disease**. *J Lifestyle Med* 2014, **4**(2):80-85.
150. Yang W, Zou Y, Zhang M, Zhao N, Tian Q, Gu M, Liu W, Shi R, Lu Y, Yu W: **Mitochondrial Sirt3 Expression is Decreased in APP/PS1 Double Transgenic Mouse Model of Alzheimer's Disease**. *Neurochem Res* 2015, **40**(8):1576-1582.
151. Liu Y, Zhang D, Chen D: **SIRT3: Striking at the heart of aging**. *Aging (Albany NY)* 2011, **3**(1):1-2.
152. Zeng H, Vaka VR, He X, Booz GW, Chen JX: **High-fat diet induces cardiac remodelling and dysfunction: assessment of the role played by SIRT3 loss**. *J Cell Mol Med* 2015, **19**(8):1847-1856.

153. Calabresi C, Arosio B, Galimberti L, Scanziani E, Bergottini R, Annoni G, Vergani C: **Natural aging, expression of fibrosis-related genes and collagen deposition in rat lung**. *Exp Gerontol* 2007, **42**(10):1003-1011.
154. Bernard K, Logsdon NJ, Ravi S, Xie N, Persons BP, Rangarajan S, Zmijewski JW, Mitra K, Liu G, Darley-Usmar VM *et al*: **Metabolic Reprogramming Is Required for Myofibroblast Contractility and Differentiation**. *J Biol Chem* 2015, **290**(42):25427-25438.
155. Xie N, Tan Z, Banerjee S, Cui H, Ge J, Liu RM, Bernard K, Thannickal VJ, Liu G: **Glycolytic Reprogramming in Myofibroblast Differentiation and Lung Fibrosis**. *Am J Respir Crit Care Med* 2015, **192**(12):1462-1474.
156. Courtnay R, Ngo DC, Malik N, Ververis K, Tortorella SM, Karagiannis TC: **Cancer metabolism and the Warburg effect: the role of HIF-1 and PI3K**. *Mol Biol Rep* 2015, **42**(4):841-851.
157. Darnell JE, Jr.: **STAT3, HIF-1, glucose addiction and Warburg effect**. *Aging (Albany NY)* 2010, **2**(12):890-891.
158. Paulin R, Dromparis P, Sutendra G, Gurtu V, Zervopoulos S, Bowers L, Haromy A, Webster L, Provencher S, Bonnet S *et al*: **Sirtuin 3 deficiency is associated with inhibited mitochondrial function and pulmonary arterial hypertension in rodents and humans**. *Cell Metab* 2014, **20**(5):827-839.
159. Lettieri CJ, Nathan SD, Barnett SD, Ahmad S, Shorr AF: **Prevalence and outcomes of pulmonary arterial hypertension in advanced idiopathic pulmonary fibrosis**. *Chest* 2006, **129**(3):746-752.
160. Chicoine LG, Stewart JA, Jr., Lucchesi PA: **Is resveratrol the magic bullet for pulmonary hypertension?** *Hypertension* 2009, **54**(3):473-474.
161. Fagone E, Conte E, Gili E, Fruciano M, Pistorio MP, Lo Furno D, Giuffrida R, Crimi N, Vancheri C: **Resveratrol inhibits transforming growth factor-beta-induced proliferation and differentiation of ex vivo human lung fibroblasts into myofibroblasts through ERK/Akt inhibition and PTEN restoration**. *Exp Lung Res* 2011, **37**(3):162-174.
162. Impellizzeri D, Talero E, Siracusa R, Alcaide A, Cordaro M, Maria Zubelia J, Bruschetta G, Crupi R, Esposito E, Cuzzocrea S *et al*: **Protective effect of polyphenols in an inflammatory process associated with experimental pulmonary fibrosis in mice**. *Br J Nutr* 2015, **114**(6):853-865.
163. Liu B, Luo XJ, Yang ZB, Zhang JJ, Li TB, Zhang XJ, Ma QL, Zhang GG, Hu CP, Peng J: **Inhibition of NOX/VPO1 pathway and inflammatory reaction by trimethoxystilbene in prevention of cardiovascular remodeling in hypoxia-induced pulmonary hypertensive rats**. *J Cardiovasc Pharmacol* 2014, **63**(6):567-576.
164. Zhou S, Li MT, Jia YY, Liu JJ, Wang Q, Tian Z, Liu YT, Chen HZ, Liu DP, Zeng XF: **Regulation of Cell Cycle Regulators by SIRT1 Contributes to Resveratrol-Mediated Prevention of Pulmonary Arterial Hypertension**. *Biomed Res Int* 2015, **2015**:762349.
165. Fischer AH, Jacobson KA, Rose J, Zeller R: **Hematoxylin and eosin staining of tissue and cell sections**. *CSH Protoc* 2008, **2008**:pdb prot4986.

BIOGRAPHY

Meredith L. Sosulski was born the fourth of five children to her parents Elizabeth and Richard Sosulski on October 22, 1988 in Stony Brook, New York. She gained an early interest in the sciences after attending many field trips to the American Museum of Natural History in Manhattan. She attended the State University of New York at Binghamton in upstate New York where she double majored. While an undergraduate, Meredith worked in the laboratory of Dr. Alexander Rickard studying the development of bacterial biofilms in the oral cavity. This research earned her departmental honors in Biochemistry. Meredith graduated from Binghamton with a B.S. in Biochemistry and B.A. in Anthropology in May 2010 and moved to New Orleans in August of the same year to pursue a Ph.D. at the Tulane University School of Medicine. She began working in Dr. Sanchez's laboratory in 2011 where she completed her dissertation work investigating the role of mitochondria in pulmonary fibrosis. In May 2016 Meredith will graduate with a Ph.D. in Biomedical Sciences and continue her postdoctoral work.